

Measurements of 5G New Radio Spectral and Spatial Power Emissions for Radar Altimeter Interference Analysis

Frank H. Sanders
Kenneth R. Calahan
Geoffrey A. Sanders
Savio M. Tran



Technical Report

Measurements of 5G New Radio Spectral and Spatial Power Emissions for Radar Altimeter Interference Analysis

**Frank H. Sanders
Kenneth R. Calahan
Geoffrey A. Sanders
Savio M. Tran**



U.S. DEPARTMENT OF COMMERCE

Alan Davidson
Assistant Secretary of Commerce for Communications and Information
National Telecommunications and Information Administration

October 2022

DISCLAIMER

Certain commercial equipment and materials are identified in this report to specify adequately the technical aspects of the reported results. In no case does such identification imply recommendation or endorsement by the National Telecommunications and Information Administration, nor does it imply that the material or equipment identified is the best available for this purpose.

CONTENTS

Figures.....	viii
Tables.....	xiii
Abbreviations/Acronyms	xiv
Executive Summary	xvii
1. Introduction.....	1
1.1 Background.....	1
1.2 JI-FRAI Membership and Work Program	2
1.2.1 Radalt Interference Bench Test Phase of the JI-FRAI QRT Work Program	3
1.2.2 In-Flight Radalt Performance Test Phase of the JI-FRAI QRT Work Program	4
1.2.3 Radalt On-the-Ground Emission Measurement Phase of the JI-FRAI QRT Work Program	4
1.3 JI-FRAI QRT Sub-Tasking and Results Presented in This Report	4
1.4 Measured Airborne 5G EIRP Data	5
1.5 Measured 5G Base Station Emission Spectra.....	5
1.6 Integration of These Data with the Overall JI-FRAI QRT Work Program	6
1.7 Significant Conclusions Presented in This Report	6
1.8 Report Outline.....	7
2. History of US Radio Band Occupancy of 3700–4200 and 4200–4400 mhz	9
2.1 Radalt Development and Use in WW II	9
2.2 Post-War Radalt Spectrum-Related Development	11
2.3 The 3700–4200 MHz Spectrum Band Was Historically Quiet	11
2.4 Implications for Radalt Receiver Designs and Overall Spectrum EMC Issues.....	12
3. High-level Description of Radalts.....	14
3.1 Radalt Spectrum Band 3700–4200 MHz and Safety-of-Life Status.....	14
3.2 Radalt Basic Description	14
3.3 Two Basic Radalt Flavors: Pulsed and FMCW	16
3.4 Radalt Functions	17
3.5 Overview of Radalt Characteristics	18
3.6 Basic Radalt Design Architectures	19
3.7 Radalt Receiver RF Bandpass Filtering.....	21
3.8 Echo-Return Power Management in Radalt Receivers.....	21
3.9 Overview of Radalt Detection, Acquisition and Tracking	22
3.10 Loop Sensitivity as a Radalt Performance Criterion	23
3.11 Radalt Antenna Radiation Patterns	23
4. RF-level Description of 5G Signals in the US n77 Band	26
4.1 Sketch of 5G US n77 Band RF Signals at a Glance	27
4.2 Spectrum Domain Characteristics of US n77 Band 5G in Finer Detail	28
4.2.1 Channel Physical Resource Blocks and Sub-Carrier Spacings	28
4.2.2 Available Channel Bandwidths in the US n77 Band	28
4.2.3 Maximum Power Spectrum Density and Maximum Total EIRP in 5G Base Station Transmitter Channels	29

4.2.4 Selection of Measurement Bandwidths for 5G RF Signals.....	31
4.3 Time Domain Characteristics and Peak versus Average Power of 5G in Finer Detail	32
4.3.1 Time Base and Periodicity of 5G TDD.....	32
4.3.2 Maximum Base Station Duty Cycle versus Channel Loading by Numbers of UEs	34
4.3.3 Base Station Channel Loading Tools for 5G: Are the Generated Loads “Real”?	34
4.4 Peak versus Average Statistics and Measurement for 5G Signals.....	35
4.4.1 RMS Averaging Applied to 5G RF Signals	35
4.4.2 Peak Detection Applied to 5G RF Signals	36
4.4.3 Average 5G Signal Power Derived from a Peak Detected Measurement.....	37
4.5 Antenna Radiation Patterns for 5G MIMO Arrays.....	38
4.5.1 64T64R MIMO Array Designs, Briefly	39
4.5.2 5G MIMO Beam Elevation Angle Range and Control for the US n77 Band.....	40
4.5.3 JI-FRAI Consideration of US n77 Band UE Operation Onboard Aircraft in Flight	42
4.5.4 Base Station Beam Elevations and Beam Control for the JI-FRAI QRT Work Program	43
4.6 Examples of Computed 5G MIMO Antenna Patterns for 3 GHz Spectrum	44
5. Potential Interference Mechanisms for coexisting 5g Transmitters and Radalt Receivers.....	49
5.1 Co-Channel (to Radalt Receivers) RF Interference from 5G Unwanted Emissions	49
5.2 Out-of-Band (to Radalt Receivers) RF Interference from 5G Intentional Emissions	50
5.3 Avoidance of Both Potential Interference Mechanisms	51
5.4 Dependence of Harmful Interference Mitigation on the Interference Mechanism.....	52
5.5 Note on OOBE and Spurious Mask Limits for Unwanted Emissions from Transmitters.....	52
6. Base Station and UE Setup for Measuring 5g Emissions.....	53
6.1 Table Mountain Measurement Location Description	53
6.2 Base Station 5G Radios Operated at Table Mountain for the JI-FRAI Program	54
6.2.1 5G MIMO Base Station Radio 1, Lower C-band.....	54
6.2.2 Base Station and UE Geometry for Radios 2 through 4, Upper C-band.....	55
6.3 Table Mountain Geometry and Configuration of 5G Radio Models 2–4.....	55
6.3.1 Downtilt Angles from Base Stations to UEs for 5G MIMO Radios 2–4.....	57
6.3.2 Base Station to UE Communication (DL/UL) Quality During Table Mountain Measurements	59
6.4 Table Mountain Geometry and Configuration of 5G Radio Model 1	59
6.4.1 Radio 1 5G Base Station Setup and Operation at Table Mountain.....	61
6.5 March 2022 Hill AFB Setup and Measurements.....	61
6.6 Schedule and Completed Measurements at Table Mountain and Hill AFB for 5G Base Station Radios 1 Through 4	62
6.7 Summary Table of 5G Base Station Radio Model Characteristics.....	63
7. Measuring 5G MIMO Base Station Emission Spectra	66
7.1 Approach for Measuring 5G MIMO Base Station Emission Spectra.....	66

7.1.1 RSMS-5G Hardware	66
7.1.2 RSMS-5G Measurement Software Including Stepped-Frequency Algorithm.....	69
7.1.3 Stored Emission Spectra and Supporting Associated Data	73
7.2 Monitoring 5G Transmitter Emissions on the Ground During Airborne Measurements.....	73
8. Measuring 5G MIMO Base Airborne Radiation Patterns.....	74
8.1 The JI-FRAI Need for Three-Dimensional Antenna Radiation Pattern Measurements Around 5G MIMO Arrays	74
8.2 Outdoor Airborne versus Indoor Chamber Antenna Pattern Measurements	75
8.2.1 Multipath Considerations for Airborne Measurements	76
8.3 Airborne 5G MIMO Antenna Pattern Measurement Methodology.....	77
8.3.1 Airborne Flight Slices Taken Through 5G MIMO Hemispheres.....	77
8.3.2 Airborne Antennas	78
8.3.3 Airborne Spectrum Analyzer Settings and Data Collection.....	84
8.3.4 Airborne Data Analysis and Reduction to a Usable Product	85
8.3.5 Notes on the Final Data Products	86
8.3.6 Access to the 5G Airborne EIRP Data Files	87
9. 5G MIMO Base station transmitter emission spectrum measurement results	88
9.1 Structure of 5G Base Station Transmitter Emission Spectra.....	90
9.1.1 Wideband Plateau Structure of the 5G Base Station Transmitters.....	90
9.1.2 Channelized Desired-Signal Emission of the 5G Base Station Transmitters.....	90
9.1.3 Steep Band-Edge Roll-Offs of the 5G Base Station Transmitters	90
9.2 Measurement Dynamic Ranges	91
9.2.1 Dynamic Range Relative to Measurement System Noise Floor	91
9.2.2 Measurement-Based Maximum Possible 5G Unwanted Power in the Radalt Band.....	92
10. Three Dimensional 5G Radiation Pattern Measurement Results	94
10.1 The Four Airborne 5G Radiation Pattern EIRP-Measurement Graph Types.....	97
10.2 Reading the Graphs.....	97
10.3 Note on Isolated Data Points in the Airborne Data	98
10.4 Airborne Radiation Levels Compared to Main Beam Levels.....	98
10.5 Airborne Radiation Patterns at Zenith Angles Above 5G MIMO Arrays	99
10.6 Near-Far Effect for Radiation from Pairs of CoWs and CoLTs.....	100
11. Applying the Data in this Report	101
11.1 Applicable EMC Equations	101
11.1.1 Propagation Assumption	102
11.1.2 Out-of-Band, Off-Axis Radalt Antenna Gains.....	103
11.2 Types of Applications.....	103
12. Summary and Conclusions	106
12.1 Summary.....	106
12.2 Conclusions.....	106
13. References.....	109
Acknowledgements.....	112

Appendix A : Flight Cards for Airborne Sorties Around 5G Base Station Radios 2 Through 4 at Table Mountain	114
Appendix B : Flight Cards for Airborne Sorties Around 5G Radio 1 Base Stations at Table Mountain and Hill AFB	114
Appendix C : Measured Emission Spectra of Lower C-band Base Stations (Radio 1).....	121
Appendix D : Solutions for Example Applications from Section 11.....	125
D.1 Example 1 Solution.....	125
D.2 Example 2 Solution.....	126
D.3 Example 3 Solution.....	127
D.4 Example 4 Solution.....	127

FIGURES

Figure 1. Tasking overview and flow diagram of the JI-FRAI QRT work program.....	3
Figure 2. Propeller of a WW II aircraft that flew, under control, into Mt. Moffett (inset), Adak, Alaska in low visibility conditions where height-above-ground information was lacking (no radalt), according to records of the 1990 Adak Naval Air Station historian. Photos by F. Sanders.	9
Figure 3. APN-1 radalt, deployed by the US Army Air Force from 1943 (from [8]).....	10
Figure 4. Mid-1990s spectrum occupancy scans of the 3700–4200 MHz band in four major US metropolitan areas, showing the historically quiet environment of that band in the US.....	12
Figure 5. Line drawing, from an installation and maintenance manual, of a typical radalt.	15
Figure 6. A typical radalt installation. <i>Left</i> : radalt transmitter-receiver in an avionics bay. <i>Right</i> : a pair of conformally mounted radalt transmit and receive antennas. Photos by F. Sanders.....	15
Figure 7. Radar (transmitted waveform with echo return) operational principle of radalts.....	16
Figure 8. The beat-frequency operational principle of FMCW radalts. The radalt receiver mixes (beats) the transmitted waveform (blue chirp, frequency modulated around, for example, 4300 MHz) against the identical but time-delayed ground-bounce echo (purple chirp) to produce a delta-frequency (beat) output at about 100 kHz. The output beat frequency is proportional to the time delay and hence height above ground.....	17
Figure 9. Homodyne (no LO) radalt architecture; no mixed-down IF stage.	20
Figure 10. Noncoherent (dual independent LOs) heterodyne radalt architecture.....	20
Figure 11. Coherent (single, unitary LO) heterodyne radalt architecture.....	21
Figure 12. Example of a measured radalt antenna pattern in the center of the radalt band (4300 MHz). Data and graph courtesy and permission of The MITRE Corporation.	24
Figure 13. Example of some measured radalt antenna realized-gain patterns across 3700–4000 MHz. Data and graph courtesy and permission of The MITRE Corporation.	25

Figure 14. A 5G NR 60 MHz RF channel with time-varying PRB structure (yellow). Graphic is adapted from data provided courtesy of the NOAA-sponsored Radio Frequency Interference Monitoring System Project at NTIA/ITS.....	29
Figure 15. 5G time domain capture (at 3928 MHz) for a 3880–3980 MHz channel showing 70 per cent TDD duty cycle at 3.5 milliseconds ON and 1.5 milliseconds OFF, repeating.	33
Figure 16. Measured peak and average detection offset for a 5G signal at 70 percent TDD duty cycle.	38
Figure 17. Diagram of 64T64R MIMO array architecture and beam-directing capability.....	39
Figure 18. A MIMO 64T64R transmitter-receiver box for a US n77 band 5G base station. It is an integrated, weather-sealed unit with connectors on the lower edge for power and data.	40
Figure 19. Azimuthal computed pattern for a 3 GHz band MIMO array antenna. Courtesy and permission of MITRE.	45
Figure 20. Elevation computed pattern for a 3 GHz band MIMO array antenna. Courtesy and permission of MITRE.	46
Figure 21. Azimuthal computed pattern for a 3 GHz band MIMO array antenna, from a manufacturer’s specification.	46
Figure 22. Elevation computed pattern for a 3 GHz band MIMO array antenna, from a manufacturer’s specification.	47
Figure 23. Azimuthal computed pattern for a 3 GHz band MIMO array antenna, from a manufacturer’s specification.	47
Figure 24. Elevation computed pattern for a 3 GHz band MIMO array antenna, from a manufacturer’s specification.	48
Figure 25. Schematic representation of 5G unwanted emissions within the radalt receivers’ band.	49
Figure 26. Schematic representation of 5G desired (intentional) emissions producing harmful interference to radalt receivers due to insufficient radalt receiver RF filtering.	50
Figure 27. Ideal spectrum filtering and roll-off for avoiding <i>both</i> potential interference mechanisms between adjacent-band 5G transmitters and radalt receivers.	51

Figure 28. Overview of Table Mountain with the northeastern area where upper C-band 5G MIMO transmitter emissions were measured. Imagery data ©2021 Google.....	53
Figure 29. Detailed overview geometry of locations of 5G base stations; 5G UEs; and spectrum measurement and signal monitoring (RSMS-5G) at Table Mountain for the JI-FRAI project. Imagery data ©2021 Google.....	55
Figure 30. An upper C-band (3700–3980 MHz) CoLT deployed at Table Mtn. The US 5G n77 band MIMO array is at right. Support links are a Ku-band (14 GHz) satellite dish and a UHF (700 MHz) LTE panel (upper left).....	56
Figure 31. Example of a 5G-capable UE with an external power supply deployed on a plastic table top while supporting 5G base station measurements at Table Mountain.....	57
Figure 32. Overhead view of Table Mountain measurement geometry for 5G base station Radios 2–4.....	58
Figure 33. Side view and ¾ view of the Table Mountain setup geometry for 5G base station Radios 2–4.....	58
Figure 34. One of the pair of Radio 1 CoWs at Table Mountain, with a set of three lower C-band (3300–3600 MHz) MIMO panels at the “normal” 12 m (40 ft) height.....	60
Figure 35. Lower C-band CoW locations at Table Mountain. This siting replicates the dual-CoLT siting at Hill AFB and Majors Field, with the Table Mountain N-S gravel road being in the same relative position as the runways at the airfields. Imagery data ©2021 Google.....	60
Figure 36. Layout of two CoLTs and UEs at Hill AFB, earlier replicated at Table Mountain. Imagery data ©Google	62
Figure 37. Schematic of the critical hardware core of the NTIA/ITS RSMS-5G.....	67
Figure 38. RSMS-5G measurement antenna (front & back) with a target 5G MIMO CoLT in the background, at 161 m distance. RSMS antenna heights were between 4 m (13 ft) and 5.8 m (19 ft) AGL, depending on circumstances. MIMO arrays were at ~10 m (33 ft) AGL. (A UE is on the rear platform at the base of the mast.).....	67
Figure 39. The four types of flight slices taken through the hemisphere around a MIMO array: orbital (circles), lateral (flyby), traverse (straight overhead) and vertical sections.....	77
Figure 40. Dual low-gain antenna solution for the airborne 5G field strength collection challenge.	79

Figure 41. Measurement antenna configuration on UH-60 Blackhawk for 5G airborne field strength measurements on Radio 1 (lower C-band MIMO arrays).....	80
Figure 42. Measurement antenna configuration on Raven R-44 for 5G airborne field strength measurements on Radios 2–4 (upper C-band MIMO arrays).....	80
Figure 43. Details of boom-mounted antenna array (see Figure 42) used for airborne field strength measurements of upper C-band 5G MIMO Radios 2 through 4 on Raven R-44.....	81
Figure 44. The 2.4 m (8 ft) square metal-screen plate used for calibration of the omni antenna gain at UH-60 ventral (belly) mount banked angles. Plate width matches center-fuselage width.....	81
Figure 45. Airborne field strength measurement in progress with a 5G CoLT base station.....	82
Figure 46. Measured emission spectrum of 5G base station transmitter Radio 2.....	88
Figure 47. Measured emission spectrum of 5G base station transmitter Radio 3.....	89
Figure 48. Measured emission spectrum of 5G base station transmitter Radio 4.....	89
Figure 49. Decibel-math addition graph (from [30], pg. 9).....	92
Figure 50. An ascending-hover section through Radio 4 radiation pattern.	94
Figure 51. Corresponding ascending-hover heat map of Radio 4. Imagery data ©2021 Google.....	94
Figure 52. NE to SW overhead traverse at 200 ft AGL radiation pattern for Radio 2.....	95
Figure 53. Corresponding NE to SW traverse heat map of Radio 2. Imagery data ©2021 Google.....	95
Figure 54. Orbital (circle-around) radiation pattern around Radio 2 at 200 ft AGL.	96
Figure 55. Corresponding orbital heat map of Radio 2. Imagery data ©2021 Google.....	96
Figure 56. Overhead section of a 5G MIMO array, west-to-east. Note that power is in the full 100 MHz of the 5G channel (which was itself at +77.5 dBm EIRP in its main beam).....	99
Figure C-1. Measured emission spectrum of lower C-band 5G base station transmitter Radio 1 running with a 20 MHz channel bandwidth. Note that power	

is plotted in 1 MHz measurement bandwidth, relative to the center-frequency emission level, which was itself at +77.5 dBm EIRP in its main beam.123

Figure C-2. Measured emission spectrum of lower C-band 5G base station transmitter Radio 1 running with a 100 MHz channel bandwidth. Power is plotted in 1 MHz measurement bandwidth, relative to the center-frequency emission level, which was itself at +77.5 dBm EIRP in its main beam.....124

Figure D-1. Example graph of spatial field strength as a function of distance from a 5G transmitter antenna.125

TABLES

Table 1. Typical radalt performance characteristics	18
Table 2. Typical radalt antenna characteristics.....	19
Table 3. Typical radalt transceiver characteristics.....	19
Table 4. Overview of typical US n77 band 5G base station RF characteristics.	26
Table 5. Power spectrum density as a function of channel bandwidth for tested US n77 band base station transmitters for +77.5 dBm total EIRP.....	31
Table 6. Manufacturer-specified electronic elevation beam scanning limits for 5G MIMO arrays in the US n77 band, relative to the MIMO broadside axis.	41
Table 7. 5G MIMO base station radios deployed at Table Mountain for the JI-FRAI program.	54
Table 8. Schedule and completed measurements for 5G base stations at Table Mountain and Hill AFB for JI-FRAI.	63
Table 9. Specified technical characteristics of 5G base station transmitters 1 through 4.	63
Table 10. Antennas used for airborne 5G field strength measurements.	82
Table 11. Received-power offsets for UH-60 helicopter plate-section bank angles. Receiver-power offsets for helicopter plate-section bank angles.	83
Table 12. Minimum suppression of measured 5G base station power in the radalt band of 4200–4400 MHz.	93
Table 13. Maximum 5G base station power in the radalt band of 4200–4400 MHz.....	93
Table 14. 5G MIMO base station main-beam power during the airborne measurements.....	98

ABBREVIATIONS/ACRONYMS

3D	three dimensional
3GPP	Third Generation Partnership Project
5G NR	Fifth Generation New Radio
64T64R	64 transmit and 64 receive elements (each element having two dipoles)
AAS	active antenna system
AGC	automatic gain control
AGL	height above (relative to) local ground level
AILG	air interface load generator
AN	Army-Navy (DoD designator code)
APN-x	airborne radar navigation (DoD designator code) w. model number x or Avionics Part Number for Honeywell
ARA	Antenna Research Associates
AVSI	Aerospace Vehicle Systems Institute
bit	binary digit
CBS	cavity backed spiral (antenna)
CFIT	controlled flight into terrain
chirp(ed)	frequency modulated (linear or non-linear) carrier wave
CoLT	cellular (base station) on light truck
CoW	cellular (base station) on wheels (trailer)
CTIA	Cellular Telecommunications and Internet Association
dB	decibel
dB_i	decibels relative to isotropic
dB_m	decibels relative to a milliwatt
dB_{μV/m}	decibels relative to a microvolt per meter
dBW	decibels relative to a watt
DL	downlink (base station to user equipment)
DHS	Department of Homeland Security
DoD	Department of Defense
DoT	Department of Transportation
EIRP	effective isotropic radiated power
EMC	electromagnetic compatibility
E-plane	electric field oscillatory plane
ERP	effective radiated power
ETSI	European Telecommunications Standards Institute
FAA	Federal Aviation Administration
FCC	Federal Communications Commission
FMCW	frequency modulated continuous wave

G7D	modulation designator for a digital QPSK waveform
GPWS	ground proximity warning system(s)
high C-band	3700–3980 MHz (also known as the US n77 band)
H-plane	magnetic field oscillatory plane
IF	intermediate frequency
ITS	Institute for Telecommunication Sciences
JI-FRAI	Joint Interagency — 5G Radar Altimeter Interference (Group)
JT&E	Joint Test and Evaluation
kW	kilowatt(s)
LFM	linear frequency modulation
low C-band	3300–3600 MHz
LNA	low noise amplifier
LO	local oscillator
MHz	megahertz
MIMO	multiple input multiple output (phased array antenna)
MSa/sec	megasamples per second
MSL	height (altitude) above (relative to) mean sea level
NIST	National Institute of Standards and Technology
NTIA	National Telecommunications and Information Administration
OCNS	orthogonal channel noise simulator
ON	Active portion (transmitting) of a TDD duty cycle
OFF	Non-active (non-transmitting) portion of a TDD duty cycle
P0N	modulation designator for a pulsed waveform
PA	power amplifier (in a transmitter)
PIM	passive intermodulation
PRB	physical resource block
PSK	phase shift keyed
Q3N	modulation designator for a chirped pulsed waveform, usually radar
QAM	quadrature amplitude modulation (16, 64 or 256 available phase states)
QPSK	quadrature phase shift keyed modulation with 4 available phase states
QRT	quick reaction test
radalt	radar (or radio) altimeter, carried by an airborne platform
RF	radio frequency
RMS	root mean square (averaging)
RRE	risk reduction event
RSMS	NTIA’s radio spectrum measurement system
RTCA	formerly the Radio-Technical Commission for Aeronautics; now a company name
Rx or rx	radio receiver

SSB	5G signal synchronization block (for new UE connections to base stations)
SNR	signal to noise power ratio in a receiver
STC	sensitivity time control
Table Mountain	Table Mountain Radio Quiet Zone (north of Boulder, Colorado)
TAWS	terrain awareness warning system(s)
TCAS	traffic collision avoidance system(s)
TDD	time division duplex
TWG-3	Technical Working Group 3
Tx or tx	radio transmitter
UE	user equipment (e.g., wireless mobile phone)
UL	uplink (user equipment to base station)
USCG	US Coast Guard
US n77 band	3700–3980 MHz
W7D	modulation designator for a digital QAM-OFDM waveform
YIG	yttrium iron garnet electronically tuned radiofrequency bandpass filter

EXECUTIVE SUMMARY

The Federal Communications Commission (FCC) has authorized the frequency band 3700–3980 MHz¹ for use by Fifth Generation New Radio (5G NR, simply called 5G in this report) base stations (technically gNodeBs) and associated user equipment (UEs, colloquially “cellphones”) in the United States. This authorization has raised technical concerns about whether 5G transmitters can or will cause harmful² radio interference to airborne radar (or radio) altimeter (radalt) receivers which operate in the band 4200–4400 MHz. This overarching concern can be broken down into two engineering sub-component questions:

- When or if harmful interference occurs from 5G signals to radalt receivers, what is the physical interference mechanism?
- At what limiting (coordination) distances, and in what directions, can harmful interference occur to radalt receivers from 5G transmitters?

The Joint Interagency Fifth Generation (5G) Radar Altimeter Interference (JI-FRAI) Quick Reaction Test (QRT) was formed to gain a better understanding of potential 5G interference issues, develop methods for testing 5G interference, and to provide answers to questions from government and industry communities. While most of the radalts tested under JI-FRAI are unique to the military, a subset of models tested are also used in civilian aircraft. JI-FRAI QRT was a Department of Defense led project chartered by the Director, Operational Test and Evaluation under the Joint Test and Evaluation (JT&E) Program. The QRT was sponsored by the Office of the Under Secretary of Defense for Acquisition and Sustainment (OUSD [A&S]) and the United States Transportation Command (USTRANSCOM). The project has been conducted with government-industry support and cooperation that includes membership from: the Department of Defense (DoD, including US Air Force, US Army and US Navy); Department of Homeland Security (DHS, specifically US Coast Guard (USCG)); FCC; National Telecommunications and Information Administration (NTIA; specifically the Office of Spectrum Management (OSM) and Institute for Telecommunication Sciences (ITS)); The MITRE Corporation; the National Institute of Standards and Technology (NIST); the National Advanced Spectrum and Communications Test Network (NASCTN); Department of Transportation (DoT, specifically the Federal Aviation Administration (FAA)); Customs and Border Patrol (CBP); the Department of Justice Drug Enforcement Agency; the Cellular Telecommunications and Internet Association (CTIA, also known as the Wireless Association); AT&T; T-Mobile; Verizon; Ericsson; Nokia; the Boeing Company; American Airlines; Jet Blue; United Airlines; RTCA (formerly the Radio-Technical Commission for Aeronautics); Aerospace Vehicle Systems

¹ Called, interchangeably, high C-band and US n77 band in this report in recognition of differing aviation and wireless community terminology, respectively.

² As defined in the Code of Federal Regulations (CFR) Part 47 § 15.3, harmful interference is: “Any emission, radiation or induction that endangers the functioning of a radio navigation service or of other safety services or seriously degrades, obstructs or repeatedly interrupts a radiocommunications service operating in accordance with this chapter [of the CFR].”

Institute (AVSI); Collins Aerospace; Honeywell; Garmin; Johns Hopkins Applied Physics Laboratory; and the Georgia Institute of Technology (Georgia Tech).

The JI-FRAI QRT work program had four major phases of testing. One of these was bench testing of radalt receivers, in which radalt units were configured to operate in a laboratory setting. The radalts were set up to operate with nominal transmissions and ground-bounce echo returns, all in hardline (closed) loops. Then, 5G radio interference was introduced into those loops, and its power was adjusted to cause harmful interference into the radalt receivers. The bench testing, performed by MITRE for JI-FRAI, indicated interference-power thresholds within the radalt receiver circuits. It also provided information on the underlying physical interference mechanisms. The procedures and results of closed-loop-conditions bench testing and radiated-conditions will be reported separately from this report.

A second major JI-FRAI effort was in-flight Joint Test and Evaluation (JT&E) of radalt performance in the presence of radiated high C-band 5G signals under controlled conditions. Selected aircraft carrying representative examples of a wide variety of radalts were used for JT&E at Hill AFB in Utah (outside Salt Lake City) and at Majors Airfield at Greenville, Texas (near Dallas). Radalt performance, determined via qualitative pilot reports and quantitative measurements of comparative radalt outputs with 5G signals radiating versus not radiating, will be reported separately from this report.

The third JI-FRAI task was collection of measured power levels emitted by radalts from taxiing aircraft at two airfields, military and civilian. These power levels can be compared to theoretically estimated power levels for such aircraft, which figure in previous work by other groups. That work attempts to gauge the extent to which power radiated from radalts on the ground causes radiofrequency interference to aircraft performing landing approaches at such airfields. The results of those measurements will be published in an NTIA Technical Memorandum that will follow this report's publication.

This report describes the procedures and results of the fourth phase of the JI-FRAI QRT effort. This phase was the characterization, via carefully calibrated radiated measurements, of (a) the three-dimensional aerial radiation patterns and (b) the emission spectra of 5G base station transmitters that are being built and sold by the three known manufacturers of US n77 band equipment now being deployed in the United States.

This work has been led and accomplished for JI-FRAI³ by NTIA's Boulder, Colorado laboratory, ITS. Between January and June 2022, and working with the support of the US Army, Verizon and AT&T, ITS engineers performed detailed, precision measurements of aerial radiation patterns of low C-band (3300–3600 MHz) and high C-band (3700–3980 MHz) multiple input multiple output (MIMO) transmitter arrays incorporated in four radio models produced by the three known manufacturers of C-band (3300–3980 MHz) 5G equipment deployed in the United States. All of the measurements in this report have been performed via radiated 5G

³ Funding for the ITS portion of the JI-FRAI tasking described in this report was provided by the US Air Force (USAF) under the Hill AFB 5G Project, via an Interagency Agreement between ITS and USAF.

emissions at the US Department of Commerce (DoC) Table Mountain Radio Quiet Zone (TMRQZ) north of Boulder, Colorado.

As described in this report, these measurements substantially characterize the effective isotropic radiated power (EIRP) from these arrays in three dimensions in the skyward-looking (horizon to zenith) hemispheres of these arrays. These measurements have been performed with calibrated, helicopter-borne, computer-controlled ITS measurement and data-recording systems using specially fabricated (by ITS), calibrated antenna arrays extending from the ventral and lateral surfaces (bellies and sides) of helicopters.

The raw airborne EIRP data, taken as described in this report's main body, have been converted by ITS engineers into a variety of processed radiation patterns that are more understandable than the raw data. While NTIA/ITS has made the raw data available to researchers (see Section 8.3.6), the majority of readers and users of the collected EIRP pattern data will likely find the processed plots to be the most useful for their purposes. Examples of those plots are provided in this report. All of the processed plots are available electronically as described in Section 8.3.6.

Emission spectrum measurements of those same 5G transmitters, performed on the ground at the TMRQZ with the NTIA/ITS Radio Spectrum Measurement System (RSMS), show radiated 5G base station emission spectra across a wide frequency range (3500–4400 MHz) and with wide dynamic range (i.e., with 80 to 95 decibels of total spectrum dynamic range, depending on the 5G radio model).

This report includes descriptions of exactly *how* the data collected at TMRQZ by ITS under the JI-FRAI tasking, both the EIRP data from the air and the spectrum data from the ground, may be used to resolve the outstanding technical questions surrounding coexistence between high C-band 5G operations and adjacent-band airborne radalt receivers. Following this report's publication, the remaining pieces of the entire 5G/radalt engineering picture will be filled in by the MITRE-collected bench-testing data and the airborne flight data from Hill AFB and Majors Field.

Two substantial stand-alone results are presented in this report. The first is that the measured, airborne EIRP data for the 5G MIMO arrays are consistent with (albeit more voluminous and arguably more complicated than) numerical simulation data and manufacturers' engineering specification sheets for the same, or similar, MIMO radiating arrays. This similarity between measured and modeled radiation patterns gives us confidence that future radiation-pattern modeling should provide credible supporting results in additional, future 5G/radalt engineering studies, without needing to necessarily perform additional airborne measurements on future 5G MIMO arrays, at least in the C-band part of the spectrum.

The second substantial stand-alone result is found in the emission spectra of the three high C-band 5G radio models. These spectra show that all three of these 5G base station transmitters incorporate effective bandpass filtering in their output stages.

We offer the following conclusions from the results we have published in this report.

The first conclusion regards the amount of suppression of 5G unwanted emissions within the allocated radalt spectrum band. As just noted, three models of 5G base station that are being deployed in the US 5G n77 band show distinctly visible, effective RF bandpass filtering in their emission spectra. The 5G transmitter high-frequency filter cut-offs are all at 4 GHz; above 4 GHz (i.e., within the radalt band of 4200–4400 MHz) these radios' spectrum emissions are as much as 106 decibels lower than their on-tuned intentional-radiation power in the 5G frequency band 3700–3980 MHz.

As described in more detail in Table 13 of the main report, the 5G unwanted-emission power levels in the radalt band are upper-bounded by our results as being between -37.5 dBm/MHz (for the radio on which we achieved the smallest measurement dynamic range) to -48.5 dBm/MHz (for the radio model for which we achieved the largest measurement dynamic range). These being upper bounds, the actual unwanted emission levels may have been lower than these numbers—how much lower, we do not know. This low level of unwanted 5G emissions within the radalt spectrum band reduces the potential for a 5G-to-radalt harmful interference scenario which would be due to 5G unwanted emissions on radalt receiver frequencies. The FCC might seek to examine unwanted emissions from future 5G base station radios to see if they remain similarly low.

This measurement-based observation increases the likelihood that, to the extent that any EMC problem exists between 5G transmitters and adjacent-band radalt receivers, the technical solution to such a problem might be the installation or retrofitting of more-effective RF power-rejection filters on radalt receivers for frequencies below 4200 MHz.

The second conclusion is that airborne radiation patterns show measurably, significantly less power than is found in 5G base station main antenna beams directed toward UEs at ground level. The amount of power reduction in the sky is variable and needs to be examined by researchers in detail, using the collected data that we have made available.

We note however that our airborne field strength data show that all the 5G MIMO arrays have distinct nulls (not zero power, but significantly reduced power relative to the main antenna-beam levels) at the skyward zeniths above the arrays. These radiated-power nulls will reduce vertical height separations between 5G towers and aircraft where any given power level will be encountered by radalt receivers passing through the sky above the 5G MIMO arrays. This observation, and the data that we have collected that show this effect, should be addressed for the EMC cases of radalt receivers whose flight paths carry them directly above 5G base station transmitter arrays.

A third conclusion is that we have observed a distinct near-far effect in our airborne measurements on pairs of transportable 5G base stations, called Cells on Wheels (CoWs). This effect causes the nearer base station transmitters' emissions to be dominant in a receiver, with more-distant transmitters' contributions rapidly fading to insignificance. This effect implies that aggregates of 5G base station transmitters might be most usefully analyzed for EMC cases in which there are *no* individual, nearby transmitters. Otherwise, when a single 5G transmitter is near a receiver, that single transmitter's emitted power will tend to be dominant over the cumulative, aggregated emissions from more-distant groupings of 5G transmitters.

This report is one of three that will be produced as a result of the JI-FRAI QRT efforts. The other two reports from the JI-FRAI QRT efforts will describe the approaches and results of radalt receiver 5G interference-effects bench testing and 5G-versus-radalt flight measurement and observation results. A second report from ITS will describe in situ measured radalt emission power levels emitted by aircraft that are sitting and taxiing on the ground. The combined materials in all of these reports will provide a thorough description of the extent, if any, to which EMC problems exist between high 3700–3980 MHz 5G emissions and radalt receivers, and will point the way toward practical and effective technical solutions of any such potential problems.

MEASUREMENTS OF 5G NEW RADIO SPECTRAL AND SPATIAL POWER EMISSIONS FOR RADAR ALTIMETER INTERFERENCE ANALYSIS

Frank Sanders, Kenneth R. Calahan, Geoffrey A. Sanders, and Savio Tran⁴

Introduction of Fifth Generation New Radio (5G NR) systems in the US between 3700 and 3980 MHz has raised concerns about electromagnetic compatibility with airborne radar altimeter (radalt) receivers operating between 4200 and 4400 MHz. This report describes work performed by the Department of Commerce's Institute for Telecommunication Sciences (ITS) for the Joint Interagency 5G Radar Altimeter Interference (JI-FRAI) Quick Reaction Testing (QRT) program to address these concerns. Two collected data sets are described: radiated wideband, wide dynamic range 5G base station emission spectra; and three-dimensional radiation patterns around 5G base station antennas. The emission spectra show effective filtering that reduces out-of-band (OoB) 5G emissions in the radalt band by as much as -106 dB below the 5G fundamental, for an upper-bounded OoB 5G power density not exceeding -48.5 dBm/MHz when maximum measurement range was achieved. The 5G radiation patterns show significantly less power in the sky than in 5G main beams directed groundward, especially at array zeniths. These data can be used for receivers whose flight paths carry them laterally past, and even directly above, 5G base stations. Finally, we have documented a near-far effect in airborne measurements on pairs of 5G transmitters. This causes the nearer transmitters' emissions to be dominant in receivers. When a single 5G transmitter is near a receiver, that single transmitter's emitted power will tend to dominate over the cumulative, aggregated emissions from more-distant, aggregated 5G transmitters.

Keywords: 5G; 5G NR; 5G emissions; 5G electromagnetic compatibility; 5G EMC; 5G emission spectrum; 5G radiation; 5G spectrum; airborne radar altimeter interference; airborne radio altimeter interference; JI-FRAI; MIMO antenna radiation patterns; radar altimeters; radio altimeters; radalts; radalt electromagnetic compatibility; radalt EMC; radalt interference; radalt receiver interference; radalt spectrum

1. INTRODUCTION

1.1 Background

The Federal Communications Commission (FCC) has authorized [1] the frequency band 3700–3980 MHz (interchangeably called “high C-band” and “US n77 band” in this report⁵) for

⁴ The authors are with the Institute for Telecommunication Sciences (ITS), National Telecommunications and Information Administration (NTIA), U.S. Department of Commerce, Boulder, Colorado 80305-3337.

⁵ This report focuses on concerns of two stakeholder communities: aviation and wireless. The aviation community uses the name “high C-band,” derived from terminology of the Second World War when band designations of P, L,

use by Fifth Generation New Radio (5G NR, called simply 5G in this report) base stations and associated user equipment (UEs, colloquially “cellphones”) in the United States. This authorization has raised technical concerns, as expressed in studies [2]–[5], about whether 5G transmitters can or will cause harmful⁶ radio interference to airborne radar (or radio) altimeter (radalt) receivers which operate in the band 4200–4400 MHz. This overall concern can be broken down into engineering sub-component questions:

- At what limiting (coordination) distances, and in what directions relative to 5G main-beam vectors, can 5G base station transmitters cause harmful interference to radalt receivers?
- When or if harmful interference occurs from transmitted 5G base station signals to radalt receivers, what is the physical interference mechanism?

1.2 JI-FRAI Membership and Work Program

The Joint Interagency Fifth Generation (5G) Radar Altimeter Interference (JI-FRAI) Quick Reaction Test (QRT) was formed to gain a better understanding of potential 5G interference issues, develop methods for testing 5G interference, and provide answers to questions from government and industry communities. While most of the radalts tested under JI-FRAI are unique to the military, a subset of models tested are also used in civilian aircraft. JI-FRAI QRT was a Department of Defense led project chartered by the Director, Operational Test and Evaluation under the Joint Test and Evaluation (JT&E) Program. The QRT was sponsored by the Office of the Under Secretary of Defense for Acquisition and Sustainment (OUSD [A&S]) and the United States Transportation Command (USTRANSCOM). The project has been conducted with government-industry support and cooperation that includes membership from the Department of Defense (DoD, including US Air Force, US Army and US Navy); Department of Homeland Security (DHS, specifically US Coast Guard (USCG)); FCC; National Telecommunications and Information Administration (NTIA; specifically the Office of Spectrum Management (OSM) and Institute for Telecommunication Sciences (ITS)); The MITRE Corporation; the National Institute of Standards and Technology (NIST); the National Advanced Spectrum and Communications Test Network (NASCTN); Department of Transportation (DoT, specifically the Federal Aviation Administration (FAA)); Customs and Border Patrol (CBP); the Department of Justice Drug Enforcement Agency; the Cellular Telecommunications and Internet Association (CTIA, also known as the Wireless Association); AT&T; T-Mobile; Verizon; Ericsson; Nokia; the Boeing Company; American Airlines; Jet Blue; United Airlines; RTCA (formerly the Radio-Technical Commission for Aeronautics); Aerospace Vehicle Systems

S, C, X and K were intended to confound the enemy (and are now an established terminology). The wireless community uses the 3GPP band designation of n77, with the modifier “US” added because the US n77 band of 3700–3980 MHz differs from the international n77 band of 3300–4200 MHz. The FCC has also referred to 3700–3980 MHz as being in the “mid-band” spectrum of 3700–4200 MHz.

⁶ As defined in the Code of Federal Regulations (CFR) Part 47 § 15.3, harmful interference is: “Any emission, radiation or induction that endangers the functioning of a radio navigation service or of other safety services or seriously degrades, obstructs or repeatedly interrupts a radiocommunications service operating in accordance with this chapter [of the CFR].”

Institute (AVSI); Collins Aerospace; Honeywell; Garmin; Johns Hopkins Applied Physics Laboratory; and the Georgia Institute of Technology (Georgia Tech).

The JI-FRAI QRT work program is diagrammed in Figure 1. Although much of the JI-FRAI focus was on radalts used in military aircraft, some of the radalts examined in the JI-FRAI QRT work program were either civilian or had dual deployment in military, government, and civilian aircraft.

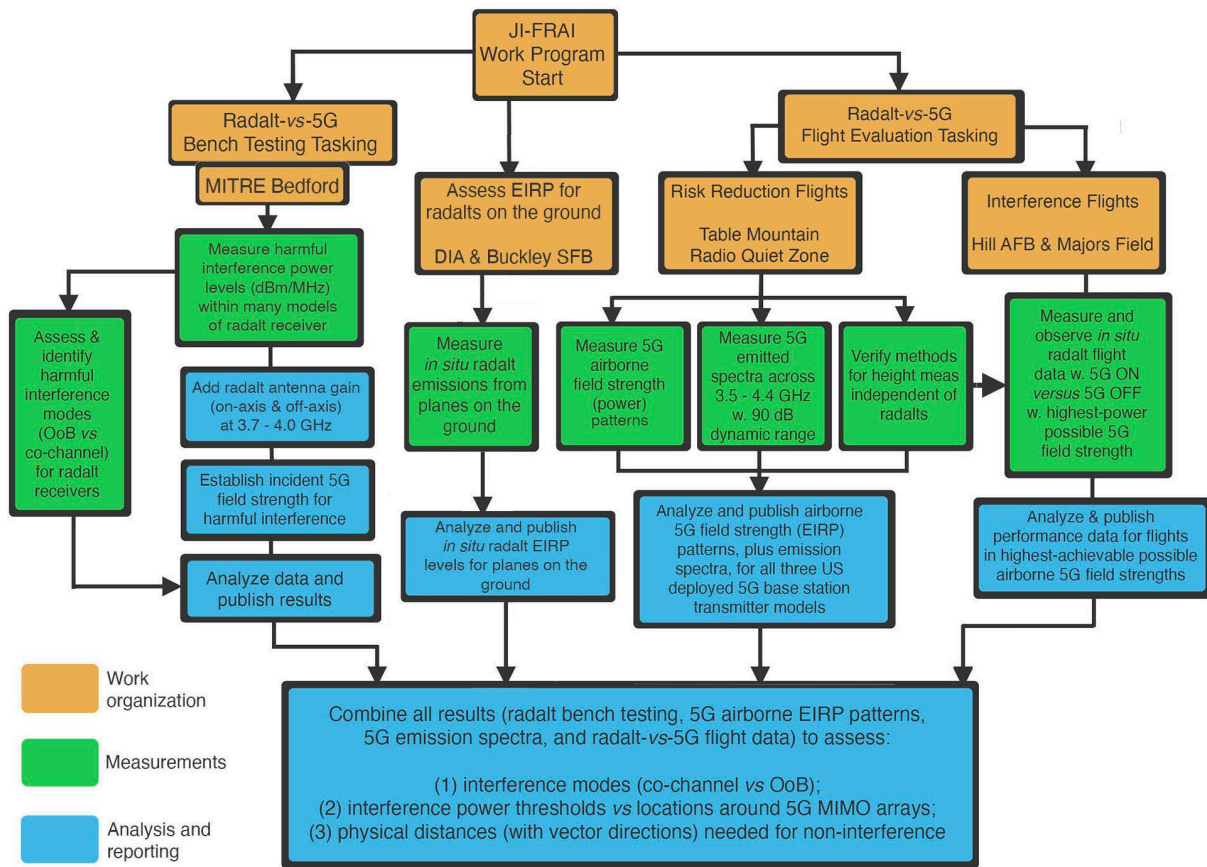


Figure 1. Tasking overview and flow diagram of the JI-FRAI QRT work program.

The JI-FRAI QRT program had four major phases of testing. These were: (1) bench testing with hardline-injected 5G interference signals; (2) in-flight radalt performance testing in the presence of 5G radiated signals; (3) EIRP measurements of on-the-ground radalt emissions from taxiing aircraft at civilian and military airfields; and (4) controlled, calibrated measurements of emission spectra and three-dimensional radiated field strength patterns around 5G base station transmitters being deployed in 3700–3980 MHz in the US.

1.2.1 Radalt Interference Bench Test Phase of the JI-FRAI QRT Work Program

In bench testing, radalt units were operated in a laboratory setting with nominal transmissions and ground-bounce echo returns running in hardline (closed) loops between the transmitter and

receiver sections. Then 5G radio interference was introduced into those loops, its power level being adjusted to cause degradation to the radalt receivers. The JI-FRAI QRT bench testing, performed by MITRE, identified power thresholds for interference within radalt receiver circuits. It also provided information on underlying physical interference mechanisms (which are themselves described later in this report). The MITRE bench testing results are to be published separately from this report.

1.2.2 In-Flight Radalt Performance Test Phase of the JI-FRAI QRT Work Program

The second major JI-FRAI QRT tasking effort was in-flight Joint Test and Evaluation (JT&E) of radalt performance in the presence of radiated high C-band 5G base station signals under controlled conditions. Selected aircraft carrying representative examples of a wide variety of radalts (mostly military but some civilian and some dual-use) were used for JT&E at Hill AFB in Utah (near Salt Lake City) and at Majors Airfield at Greenville, Texas (near Dallas). In these flight tests, aircraft with radalts were repetitively flown in closed-loop routes, such as traffic patterns. Each route was flown while nearby 5G base station transmitters were turned on and then flown again with them turned off. Comparative radalt performance was assessed for when 5G base station signals were in transmitter-on versus transmitter-off conditions. The JT&E results are to be published separately from this report.

1.2.3 Radalt On-the-Ground Emission Measurement Phase of the JI-FRAI QRT Work Program

The third JI-FRAI QRT tasking effort was to measure emitted radalt power being radiated from aircraft on the ground while they were sitting in gate areas and taxiing at a major airport (for civilian airliners) and at a military airfield (for military aircraft). These emissions were needed for comparison to predictions of such emissions that have been produced in separate work projects by other groups. The reason is that some predictions of radalt interference thresholds have tried to take into account stray or background radalt-to-radalt radiation emanating from planes on the ground and coupled into nearby planes that are in-flight, landing at airports. For this tasking, the authors of this report measured on-the-ground emissions from airliners at Denver International Airport (DIA) and from F-16 jet fighters at Buckley Space Force Base (SFB). The raw data taken in those environments have been converted to effective isotropic radiated power (EIRP) levels radiating from underneath the on-the-ground aircraft bellies. We will report those results in a separate report.

1.3 JI-FRAI QRT Sub-Tasking and Results Presented in This Report

This report describes the procedures and results of the RF over-the-air phase of the JI-FRAI QRT. It is complementary to reports on the other phases of the QRT project. This work-program component is the characterization, via carefully calibrated radiated measurements, of (a) the three-dimensional aerial radiation patterns; and (b) the emission spectra of 5G base station transmitters that are being built and sold by the three known manufacturers of US 5G n77 band equipment now under deployment in the United States.

The tasking of measuring spatial radiation patterns and emission spectra and establishing the validity of independent height-above-ground equipment⁷ has been led and accomplished for JI-FRAI⁸ by NTIA's Boulder, Colorado laboratory, ITS. Between January and June 2022, and working with the support of the US Army, Verizon and AT&T, ITS engineers have performed detailed, precision measurements of aerial radiation patterns of low C-band (3300–3600 MHz) and high C-band (3700–3980 MHz) multiple input multiple output (MIMO) transmitter arrays incorporated four radio models produced by the three known manufacturers of US n77 band (3300–3980 MHz) 5G transmitter equipment being deployed in the United States. All the measurements done for this tasking and described in this report have been performed via radiated 5G base station emissions at the US Department of Commerce (DoC) Table Mountain Radio Quiet Zone (Table Mountain) north of Boulder, Colorado.

1.4 Measured Airborne 5G EIRP Data

As described in this report, these measurements characterize the effective isotropic radiated power (EIRP) from the subject 5G MIMO arrays in three dimensions in the skyward-looking (horizon to zenith) hemispheres of these arrays. These measurements have been performed with calibrated, helicopter-borne, computer-controlled ITS measurement and data-recording systems using specially fabricated (by ITS), calibrated antenna arrays extending from the ventral and lateral surfaces (bellies and sides) of helicopters.

The raw airborne EIRP data, taken as described in this report, have been converted by ITS engineers into a variety of processed radiation patterns that are more understandable than the raw data. While NTIA/ITS will make the raw data available to researchers upon request, the majority of readers and users of the collected EIRP pattern data will most likely find the processed plots to be the most useful for their purposes. Examples of those plots are provided in this report. All of the processed plots are available electronically as described in Section 8.2.6.

1.5 Measured 5G Base Station Emission Spectra

Emission spectrum measurements of those same 5G transmitters, were performed on the ground at the Table Mountain with the NTIA/ITS Radio Spectrum Measurement System (RSMS) . These data show radiated 5G base station emission spectra across a wide frequency range (3500–4400 MHz) and with wide dynamic range (i.e., with 80 to 95 decibels of total spectrum dynamic range, depending on the 5G radio model).

⁷ Performed with a laser altimeter on a UH-60 helicopter from the Redstone Arsenal.

⁸ The funding sponsorship for ITS for the JI-FRAI tasking described in this report has been from the US Air Force (USAF) under the Hill AFB 5G Project, via an Interagency Agreement between ITS and USAF Force.

1.6 Integration of These Data with the Overall JI-FRAI QRT Work Program

This report includes descriptions of exactly *how* the data collected at Table Mountain by ITS under the JI-FRAI tasking, both the EIRP data from the air and the spectrum data from the ground, may be used to resolve the outstanding technical questions surrounding coexistence of 3700–3980 MHz 5G operations and airborne radalt receivers. Following this report’s publication, the remaining pieces of the entire 5G/radalt engineering picture will be filled in by the MITRE-collected bench-testing data and the airborne flight data from Hill AFB and Majors Field.

1.7 Significant Conclusions Presented in This Report

The first conclusion regards the amount of suppression of 5G unwanted emissions within the allocated radalt spectrum band. As just noted, three models of 5G base station that are being deployed in the US 5G n77 band show distinctly visible, effective RF bandpass filtering in their emission spectra. The 5G transmitter high-frequency filter cut-offs are all at 4 GHz; above 4 GHz (i.e., within the radalt band of 4200–4400 MHz) these radios’ spectrum emissions are as much as 106 decibels lower than their on-tuned intentional-radiation power in the 5G frequency band 3700–3980 MHz.

As described in more detail in Table 13, the 5G unwanted-emission power levels in the radalt band are upper-bounded by our results as being between -37.5 dBm/MHz (for the radio on which we achieved the smallest measurement dynamic range) to -48.5 dBm/MHz (for the radio model for which we achieved the largest measurement dynamic range). These being upper bounds, the actual unwanted emission levels may have been lower than these numbers—how much lower, we do not know. This low level of unwanted 5G emissions within the radalt spectrum band reduces the potential for a 5G-to-radalt harmful interference scenario which would be due to 5G unwanted emissions on radalt receiver frequencies. The FCC might seek to examine unwanted emissions from future 5G base station radios to see if they remain similarly low.

This measurement-based observation increases the likelihood that, to the extent that any EMC problem exists between 5G transmitters and adjacent-band radalt receivers, the technical solution to such a problem might be the installation or retrofitting of more-effective RF power-rejection filters on radalt receivers for frequencies below 4200 MHz.

The second conclusion is that airborne radiation patterns show measurably, significantly less power than is found in 5G base station main antenna beams directed toward UEs at ground level. The amount of power reduction in the sky is variable and needs to be examined by researchers in detail, using the collected data that we have made available.

We note however that our airborne field strength data show that all the 5G MIMO arrays have distinct nulls (not zero power, but significantly reduced power relative to the main antenna-beam levels) at the skyward zeniths above the arrays. These radiated-power nulls will reduce vertical height separations between 5G towers and aircraft where any given power level will be encountered by radalt receivers passing through the sky above the 5G MIMO arrays. This observation, and the data that we have collected that show this effect, should be addressed for the

EMC cases of radalt receivers whose flight paths carry them directly above 5G base station transmitter arrays.

A third conclusion is that we have observed a distinct near-far effect in our airborne measurements on pairs of CoWs. This effect causes the nearer base station transmitters' emissions to be dominant in a receiver, with more-distant transmitters' contributions rapidly fading to insignificance. This effect implies that aggregates of 5G base station transmitters might be most usefully analyzed for EMC cases in which there are *no* individual, nearby transmitters. Otherwise, when a single 5G transmitter is near a receiver, that single transmitter's emitted power will tend to be dominant over the cumulative, aggregated emissions from more-distant groupings of 5G transmitters.

1.8 Report Outline

Because this report stands alone in reporting one phase of the JI-FRAI QRT, it is organized as follows:

- 1) Introduction and description of the JI-FRAI QRT work program, and how the work described in this report fits within that work program's overall framework.
- 2) Historical introduction to the radio spectrum band occupancy of 3700–4200 MHz and 4200–4400 MHz, and how that history has contributed to the current technical electromagnetic compatibility (EMC) questions for coexistence between 5G transmitters in the lower-frequency band and radalt receivers in the higher-frequency band.
- 3) Introduction and description of radalts.
- 4) Introduction and description of 5G radio signals in the US n77 band.
- 5) Description of the two potential interference modes for 5G transmitters operating between 3700 and 3980 MHz and coexisting radalt receivers operating within 4200–4400 MHz.
- 6) Description of how we set up 5G MIMO base stations and associated UEs for emission measurements.
- 7) Description of our approach for measuring radiated 5G transmitter emission spectra with wide frequency range (3500–4400 MHz) and wide dynamic range (at least 90 dB), to determine the power levels of unwanted 5G spectrum emissions within 4200–4400 MHz.
- 8) Description of our approach for measuring 5G MIMO transmitter antenna radiation patterns in three dimensions (3D) in spatial hemispheres around the antennas.
- 9) Wideband, wide dynamic range radiated emission spectrum measurement results for the same three 5G base station transmitters, showing that unwanted 5G transmitter emissions from these radios within 4200–4400 MHz have less than one-billionth of the power in the transmitters' on-tuned (desired, licensed) emissions.

- 10) 3D radiation pattern measurement results for all three models of US n77 band 5G base station transmitters that are being deployed in the US.
- 11) A brief description of how the results shown in this report can (and will) be integrated into the larger EMC coexistence picture for 5G transmitters and radalt receivers.
- 12) Summary and conclusions

As noted above, this report is one of three that will be produced as a result of the JI-FRAI QRT efforts. The other two reports from the JI-FRAI QRT efforts will describe the approaches and results of radalt receiver 5G interference-effects bench testing and 5G-versus-radalt flight measurement and observation results. The combined materials in all of these reports will provide a thorough description of the extent, if any, to which EMC problems exist between US n77 band 5G emissions and radalt receivers, and will point the way toward practical and effective technical solutions of such potential problems. The ultimate goal of these efforts is to determine the best way for 5G transmitters and radalt receivers to safely and effectively coexist in adjacent spectrum bands.

2. HISTORY OF US RADIO BAND OCCUPANCY OF 3700–4200 AND 4200–4400 MHZ

To fully understand the potential technical problem at hand between 5G transmissions and radalt receivers, it is necessary to examine the histories of the two subject bands (3700–4200 MHz for 5G and 4200–4400 MHz for radalts). We present this history here because the 5G/radalt coexistence issue is only one of a number of current, similar adjacent-band technical coexistence problems facing spectrum managers, engineers, and policy makers. Understanding this particular technical problem, and how it has arisen, can be helpful in more fully understanding the larger adjacent-band technical problem as it currently pertains to other radio bands and services.

2.1 Radalt Development and Use in WW II

Radalts were first manufactured and deployed in large numbers by the United States during the Second World War. They were needed partly due to substantial terrain-related aircraft-accident losses (see Figure 2) in theaters such as the Aleutians and New Guinea [6], [7].^{9, 10}



Figure 2. Propeller of a WW II aircraft that flew, under control, into Mt. Moffett (inset), Adak, Alaska in low visibility conditions where height-above-ground information was lacking (no radalt), according to records of the 1990 Adak Naval Air Station historian. Photos by F. Sanders.

⁹ [6] chronicles aviation difficulties in the Aleutian theater, including aircraft losses due to flight into terrain and difficulties with knowing height-above-ground. See for example p. 189, describing a flight of B-17s flying a raid across open water between Adak and Kiska: “Every few minutes they [the pilots] reset their [barometric] altimeters to compensate for strange variations in sea-level atmospheric pressure.”

¹⁰ [7] describes accident-related losses of about 350 Allied aircraft that disappeared in the New Guinea theater. Many of the aircraft are thought to have crashed into mountainous terrain in low-visibility conditions where pilots lacked height-above-ground information (no radalts) on the flight decks.

The first radalts introduced by the US Army Air Force circa 1943 were the Army-Navy Airborne Radar Navigation Model 1 (AN/APN-1 [8], also known as the RT-7, Figure 3), and the Signal Corps Radio model 718C (SCR-718C, [9]).

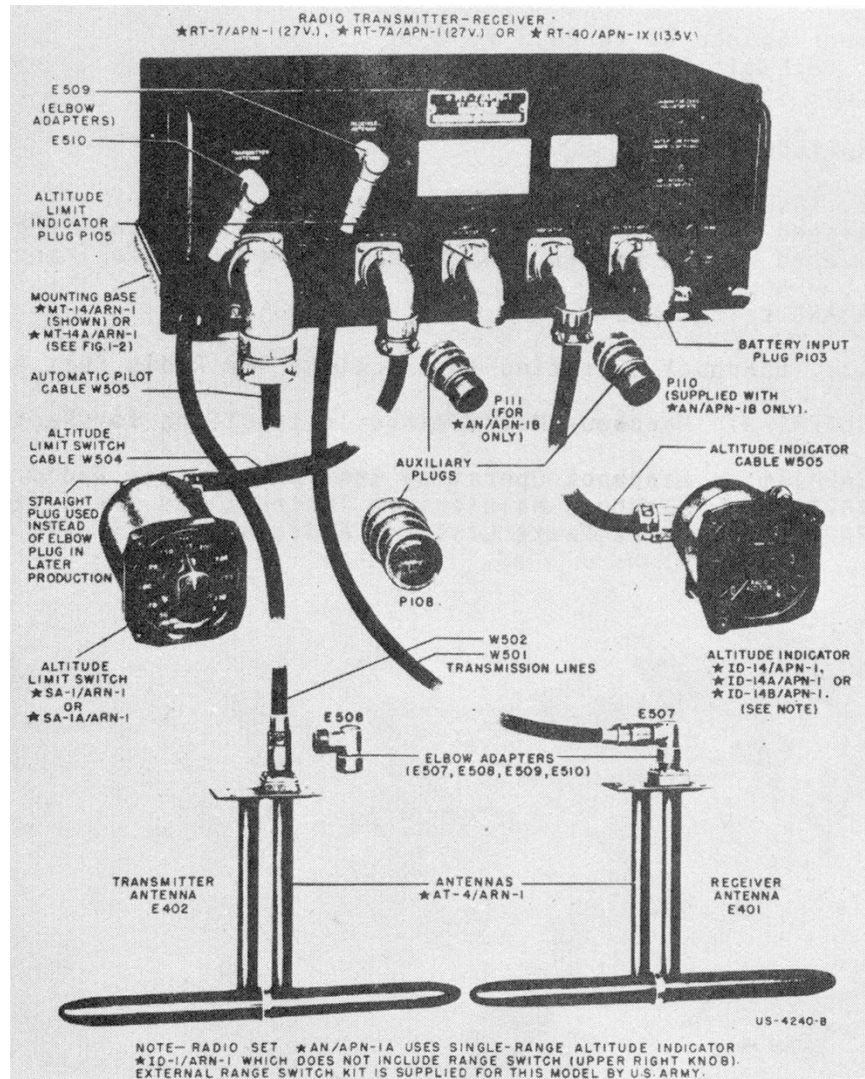


Figure 3. APN-1 radalt, deployed by the US Army Air Force from 1943 (from [8]).

As described in [9], the SCR-718C was a conventional pulsed-waveform outbound-and-return-echo radar. It operated at 440 MHz, with a pulse width of 200 to 300 nanoseconds and a pulse repetition rate of 98,356 pulses per second. It used a pair of external (protruding) dipole antennas, essentially identical to those shown in Figure 3, for its transmitter and receiver sections. Height above ground was determined by the time delay between the transmitted and echo-returned pulse edges.

As described in [8] and [9], the APN-1 transmitter used an RCA model 955 (= VT212) “acorn” triode vacuum tube to produce a linear frequency modulated (LFM) continuous wave (FMCW)

sawtooth¹¹ (“chirp”) on frequencies between 418 to 462 MHz. Its receiver processed the beat frequency difference between the transmitted and echo-returned chirped waveform to derive height above ground. The APN-1 operated throughout heights above ground of zero to 4000 feet (0–1200 m).

2.2 Post-War Radalt Spectrum-Related Development

The advent of high-speed (high subsonic to supersonic) military jet aircraft that required maximal streamlining and minimal radar cross section echo returns led to the need to bring radalt antennas, or at least their external apertures, inside the aircraft bodies. The first radalt design that accomplished this goal was the AN/APN-22 [10].¹² This model was introduced in the 1950s in A-3 and B-66 aircraft models. It used FMCW beat-frequency differences between transmitted and echo-returned power to indicate height above ground. It worked at altitudes of zero to 10,000 ft (0–3000 m) over land and up to 20,000 ft (6,000 m) over water.

Importantly for spectrum engineering considerations, the APN-22 operational frequency range was transitioned from the earlier-used ultrahigh frequency (UHF) band of 418–462 MHz to a new band of ten times higher frequency, 4200–4400 MHz. This 4.3 GHz band eventually became the engineering default for all radalts worldwide. Today the 4200–4400 MHz band has an exclusive service allocation for radalts worldwide, as a protected safety-of-life service (see for example Section 4.3.1¹³ of [11]).

With a wavelength at 4300 MHz of just 7 cm, radalt antenna sizes for this microwave band were small enough to be kept within airframes, meeting the streamlining needs of both military and civilian high-speed jet aircraft. The frequency width of the new band, two and a half times the original band’s width (200 MHz for the new microwave band versus 40 MHz for the original UHF band), allowed for wider-frequency chirps for FMCW radalts and for shorter pulses for pulsed radalts. It also allowed enough bandwidth for installation of *multiple* radalts (two or even three units, called multi-ship installations) in individual airframes, an important back-up (redundancy) improvement for these safety-of-life systems in large aircraft such as commercial airliners.

2.3 The 3700–4200 MHz Spectrum Band Was Historically Quiet

The spectrum adjacent to (just below, that is) the 4.3 GHz band was historically quiet, as demonstrated in Figure 4 (taken from [16]–[17]).

The scans in Figure 4 were performed with a 1 m diameter (+25 dBi gain) dish 30 ft (10 m) above ground level on hilltop locations. The dish was slowly scanned 360 degrees around the

¹¹ “Sawtooth” is taken here to be either a periodically repeating, linear, one-way FM ramp that re-sets to zero at the end of each period, or else periodically repeating FM triangles of linear up-and-down ramps.

¹² Honeywell uses APN as Avionics Part Number.

¹³ Table of Allocations, Note 5.438.

horizon, once with vertical polarization and once with horizontal polarization, while a fast-sweeping maximum-hold mode was used on a spectrum analyzer to retain the highest power level observed on any frequency and on all azimuths. Thus the Figure 4 scans show the spectrum in each metropolitan area with 360 degree coverage and the gain of a dish antenna.

Until recent changes [1] in 3700–4200 MHz allocations, the band was mostly used in the US for fixed-service point-to-point microwave links (notably cross-country telephone networks)¹⁴ and fixed space-to-earth satellite downlinks. In Figure 4, the only visible signals are generated by sidelobes of point-to-point horns when the measurement antenna’s beam was pointed at them.¹⁵

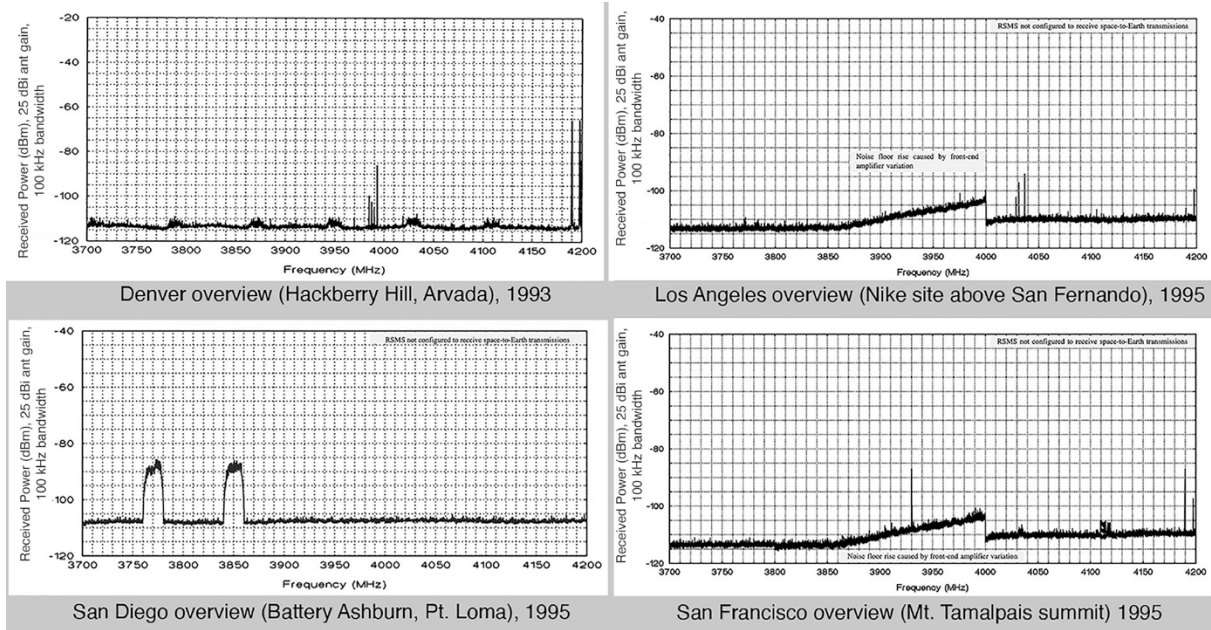


Figure 4. Mid-1990s spectrum occupancy scans of the 3700–4200 MHz band in four major US metropolitan areas, showing the historically quiet environment of that band in the US.

2.4 Implications for Radalt Receiver Designs and Overall Spectrum EMC Issues

In even lower-frequency spectrum bands of 2700–2900 MHz, 2900–3000 MHz, 3000–3100 MHz and 3100–3700 MHz, a variety of high-powered radars were (and are) operated for airport traffic control; weather surveillance; maritime navigation and surface search; and

¹⁴ In 1964, A. A. Penzias and R. W. Wilson were studying noise levels in this radio band, at 4.08 GHz, when they discovered the Big Bang cosmic microwave background radiation. The antenna they used for scanning the sky was a large AT&T horn designed for point-to-point microwave links. These large horns were very high-performance with very low sidelobes, contributing to the overall quietness of the band even when they were used in workaday cross-country telephone networks.

¹⁵ As demonstrated in other data scans of [14]–[17] spectrum has been similarly quiet across 4400–4800 MHz, just above the radalt band; that spectrum has likewise historically been allocated for point-to-point fixed-service and satellite downlinks.

tactical military applications; respectively. Radalt receivers were designed from early periods with receiver front-end filtering designed to de-couple them from radar transmitters operating in the allocated radar bands between 2900 MHz and 3700 MHz.¹⁶ However, although such filtering was (and is) ordinarily intended to be effective at radar frequencies below 3700 MHz, the filtering in radalt receiver front ends was not historically understood to need much effectiveness in the higher 3700 MHz to 4200 MHz frequency range where there were (and are) no radars.

The quietness (Figure 4) of the 3700–4200 MHz spectrum just below the radalt band, combined with the fact that some radalt receivers, at least, can perform better when they have relatively slow rates of frequency-dependent roll-off in their RF front end filtering, has led to some radalt models having only slow roll-offs across 3700–4200 MHz in their front-end filters.¹⁷

Although a slow frequency-dependent roll-off rate of some radalt receiver filters was well-adapted to the earlier, quiet band conditions between 3700–4200 MHz, the introduction of new, relatively high-powered 5G base station transmitted signals within 3700–3980 MHz does introduce the possibility of a type of harmful interference to radalt receivers, as will be explained in Section 5. This potential should be considered even though an unoccupied gap of 220 MHz has been provided between the upper edge (3980 MHz) of the US n77 band and the lower edge (4200 MHz) of the radalt band. We note here that some radalt receivers do already have effective filtering across 3700–4200 MHz, and that such filtering is thought to generally be feasible for future radalt designs and retrofits to existing radalts.¹⁸

A historical (now eliminated) harmful interference situation documented in [18] demonstrates a case in which such interference did occur in the 1990s, at frequency separations exceeding 300 MHz between naval and airborne radars below 3700 MHz and television receive-only 3700–4200 MHz (TVRO) satellite downlinks. Similar adjacent-band receiver-transmitter coexistence problems have occurred in recent years between other services, in which one band is occupied by sensitive receivers (often incorporating minimal RF front-end filtering because they have heretofore operated in quiet spectrum conditions) and an adjacent band is occupied by newly introduced high-power transmitters. The situation between 5G transmitters and radalt receivers in adjacent spectrum is thus *only one of a larger set of such receiver-band and adjacent transmitter-band electromagnetic coexistence EMC situations currently being addressed by spectrum engineers.*

¹⁶ As early as the 1960s, Bendix radio altimeter engineers recognized the presence of high-power emitters outside the radalt band: “The received signal is then passed through rf filter (14) to eliminate possible interference from ground radars, and other interference sources,” from *ALA-51A Radio Altimeter Overhaul Manual*, The Bendix Corporation, November 1, 1966.

¹⁷ Faster (steeper) frequency roll-off rates can introduce radalt receiver complications due to the filters’ frequency-dependent phase dispersion characteristics, according to private communications with radalt manufacturing engineers. This is not understood to preclude tighter filtering, but it is an engineering consideration for filters.

¹⁸ Private communication with engineering staff of a US radalt manufacturer.

3. HIGH-LEVEL DESCRIPTION OF RADALTS

3.1 Radalt Spectrum Band 3700–4200 MHz and Safety-of-Life Status

As noted above, radalts are given the status of safety-of-life systems within an internationally recognized service-exclusive radio band allocation [11] of 4200–4400 MHz. This section describes radalts more fully. The description is intended as a high-level introduction to radalts, suitable for providing an engineering-level understanding of their radio-frequency characteristics, especially for their receiver sections. Material in this section is largely drawn from [21]-[21].¹⁹

Radalts were first operated on an experimental or near-experimental basis as early as the 1930s [19]. First manufactured and introduced into military aircraft in large numbers beginning in the 1940s, their use and criticality to civilian air travel and overall air safety became large in succeeding decades. By 1969 for instance, radalts were being used to queue aircraft landing-flare maneuvers and even to perform fully automatically-controlled landings of commercial airliners [22].

3.2 Radalt Basic Description

Basic radalt operational functionality has had constancy even as the systems themselves have been continuously improved and upgraded through time. Figure 5 shows an external view of a radalt that is typical of those found in commercial airliners. Most radalts conform roughly to this physical size and configuration. Figure 6 shows a typical radalt *in situ* in an airframe avionics bay with its associated conformal-patch pair (transmit and receive) of radalt antennas on the airframe surface. Figure 7 shows the operational out-and-back radar principle of radalts.

¹⁹ The presentation [21] by the Honeywell Company's Senior Radar Systems Engineer, Mr. Seth Frick, has been especially informative. Particular data drawn from the Honeywell document are explicitly noted throughout this section.

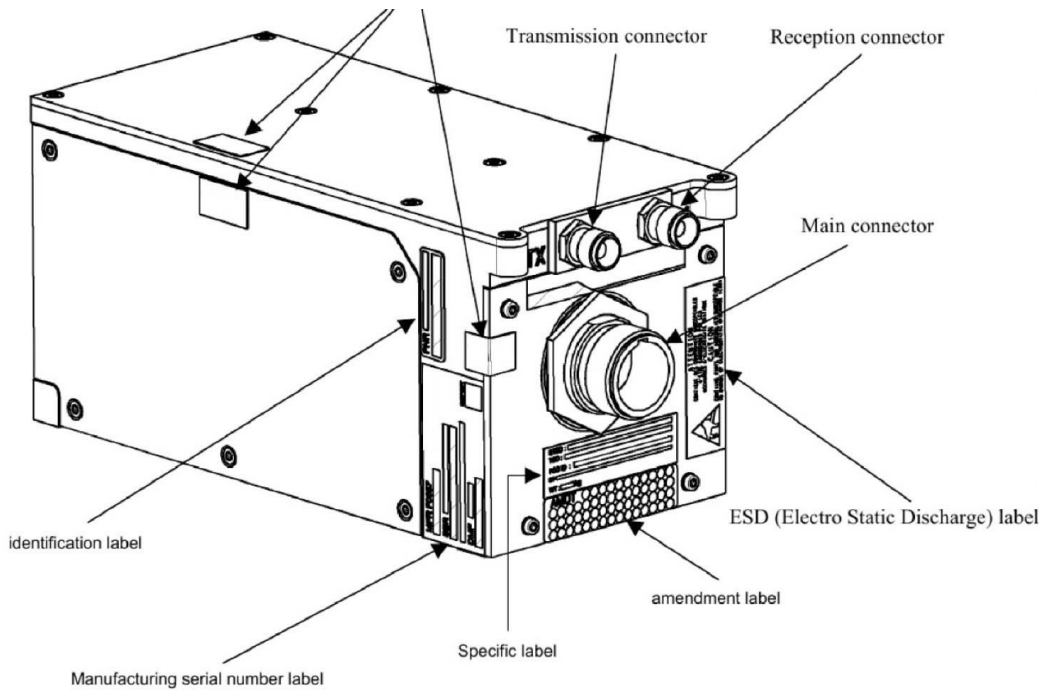


Figure 5. Line drawing, from an installation and maintenance manual, of a typical radalt.

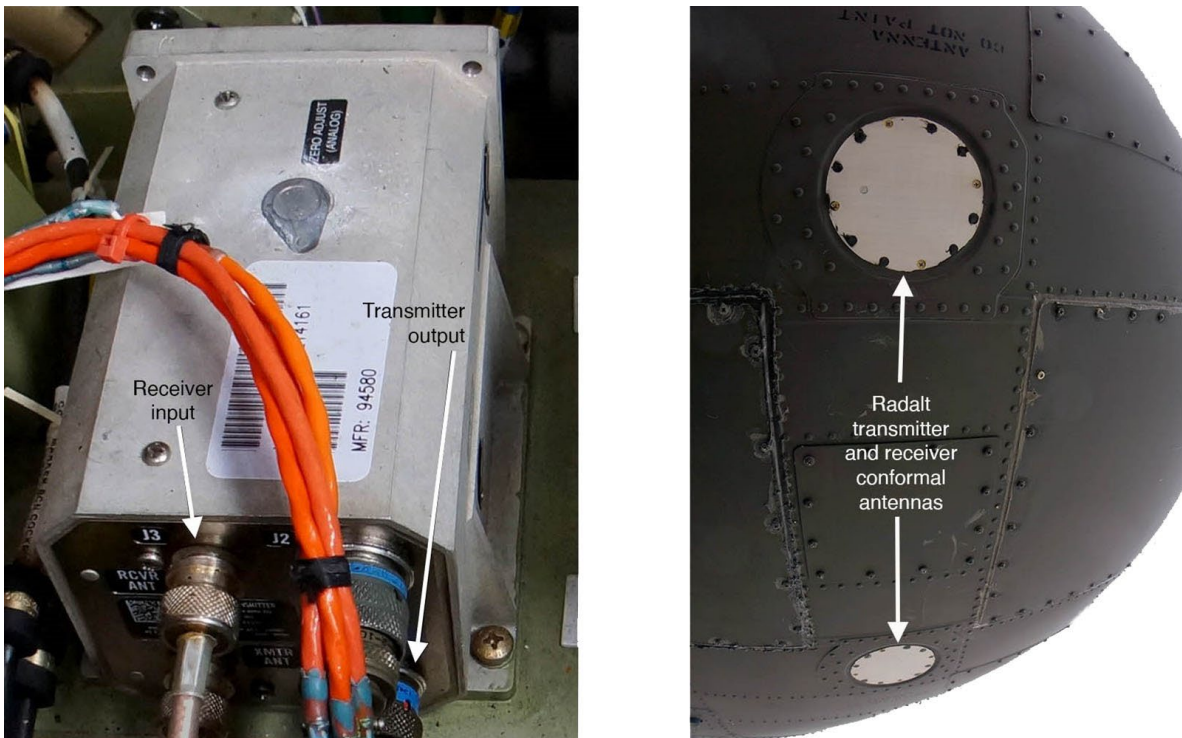


Figure 6. A typical radalt installation. *Left*: radalt transmitter-receiver in an avionics bay. *Right*: a pair of conformally mounted radalt transmit and receive antennas. Photos by F. Sanders.

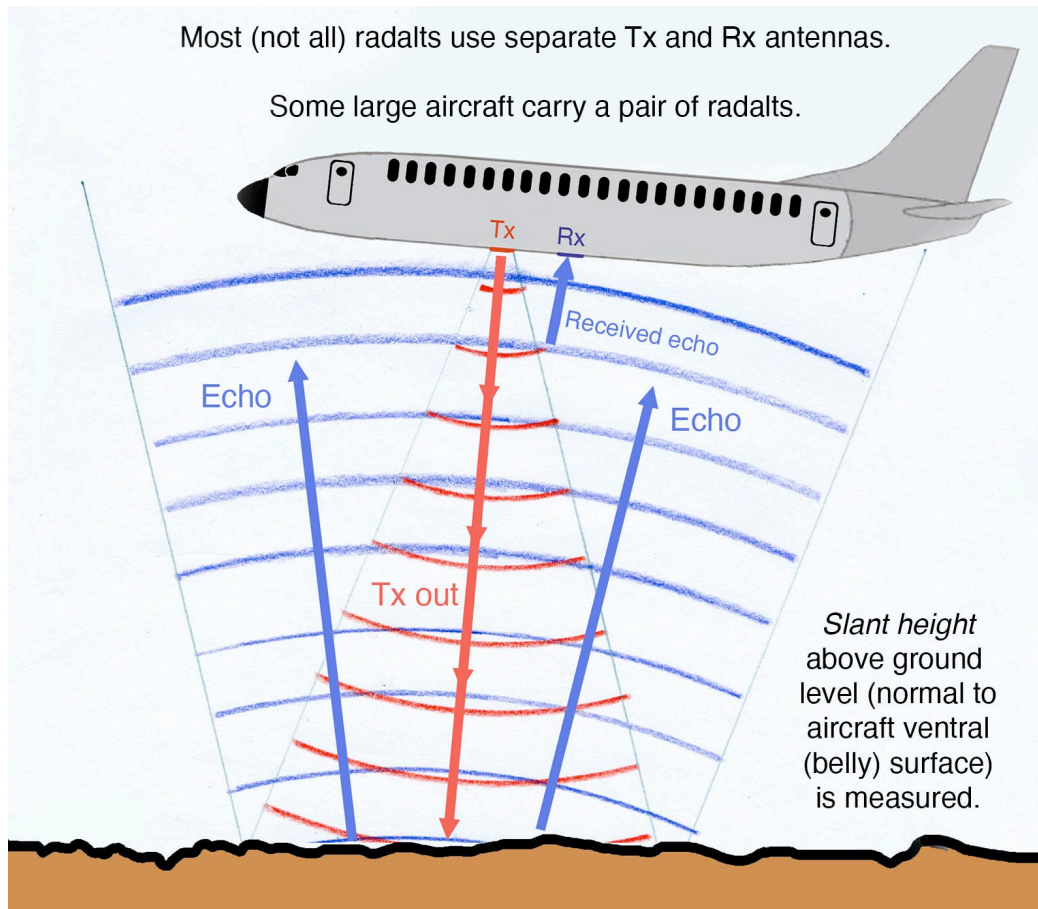


Figure 7. Radar (transmitted waveform with echo return) operational principle of radalts.

3.3 Two Basic Radalt Flavors: Pulsed and FMCW

As noted in the previous section, radalts are found in two flavors: pulsed and FMCW. Pulsed radalts operate on conventional principles of out-and-back translation of transmitted-pulse and echo-return travel time that translates into the distance the pulses have traveled.²⁰ Pulsed radalts are found more often (but not entirely) in military aircraft, which some sources attribute to an ostensibly lower likelihood of pulsed emissions being externally observed or intercepted (relative to FMCW emissions) [23].

²⁰ Strictly, the radalt-indicated “height” is the slant range, normal to the airframe’s ventral surface where the radalt antennas are mounted, from the strongest echo-return zone on the underlying ground, within the radalt antenna beam pattern. This particularly is to be noted for rough, uneven underlying terrain and for moments when aircraft are in high (large) bank angles.

FMCW radalts are found more often (but not always) in civilian aircraft.²¹ They operate on the principle of beating, within the receiver circuitry, the transmitted waveform's chirped waveform against the identical (but time-shifted) echo bounce-return sawtooth, as diagrammed in Figure 8.

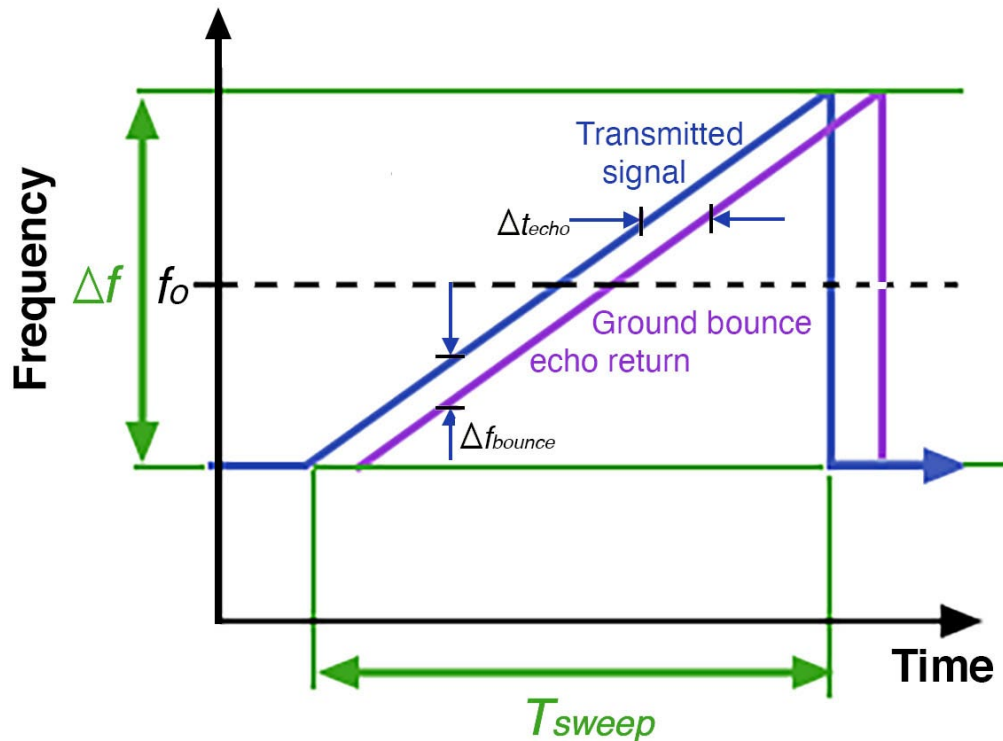


Figure 8. The beat-frequency operational principle of FMCW radalts. The radalt receiver mixes (beats) the transmitted waveform (blue chirp, frequency modulated around, for example, 4300 MHz) against the identical but time-delayed ground-bounce echo (purple chirp) to produce a delta-frequency (beat) output at about 100 kHz. The output beat frequency is proportional to the time delay and hence height above ground.

3.4 Radalt Functions

Radalts are deployed in a very wide range of platforms. These include all types of civilian and military aircraft, both fixed-wing and rotary-wing (helicopters); missiles including cruise missiles; and unmanned aerial vehicles (UAVs, colloquially drones). Radalt in-flight functions include [21]:

- Cockpit situational awareness (visual cockpit display) of height above ground

²¹ Some radalt models are found in military, government, and civilian aircraft, but usually with separate model designations.

- Terrain awareness for Ground Proximity Warning Systems (TAWS/GPWS) to prevent controlled flight into terrain (CFIT)
- Automated flight control support including auto-throttle, automated landing flares, and pitch-roll authority
- Landing vertical guidance with aural call-outs for instrument and visual landings
- Traffic collision avoidance systems support (TCAS)
- Mode controls and inhibiting for systems such as predictive windshear in weather radars
- Terrain-following flight control for some military applications
- Terrain-aided navigation for some military applications

3.5 Overview of Radalt Characteristics

As noted briefly above, some platforms use single radalts while others use redundant, multi-radalt installations. Table 1, adapted from [21], shows typical physical performance characteristics of many radalts.

Table 1. Typical radalt performance characteristics.

Parameter	Civilian/Commercial Value	Military Value
Max. Reported Altitude	2500–7500 ft (760–2300 m)	1500–50,000 ft (460–15,000 m)
Altitude Accuracy Relative to Ground Level (AGL)	±1.5 ft to ±3 ft up to 100 ft ±2% to ±3% from 100 to 500 ft ±2% to ±5% above 500 ft	±2 ft to ±4 ft up to 100 ft ±2% to ±4% above 100 ft
Pitch and Roll Angle Range	±20° to ±40°	±20° to ±60°
Operating Environment Specifications	DO-160 (ENV and EMI/EMC)	MIL-STD-8 (ENV) and MIL-STD-46 (EMI/EMC)

Radalt “loop sensitivity” (the radar’s out-and-back echo-return performance) depends on radalt antenna patterns; pitch-and-roll requirements and conditions; RF installation cable losses; and the reflection (backscattering) characteristics of the terrain beneath the radalt. Backscattering depends on the coefficient of reflectivity of the terrain (e.g., water versus soil and bare rock or concrete versus vegetative cover) and the terrain’s roughness.

Radalt antenna characteristics are important to the JI-FRAI study. Table 2 shows typical radalt antenna characteristics. Table 3 shows typical radalt transceiver characteristics. Both tables are adapted from [21].

Table 2. Typical radalt antenna characteristics.

Radalt Antenna Parameter	Typical Value
Size	4" × 4" (100 mm × 100 mm) squares or 6" (150 mm) diameter circles
Gain Relative to Isotropic at 4.3 GHz	7–13 dBi; most commonly 10–11 dBi
Polarization	Linear
3-dB (half-power) angular beam width at 4.3 GHz	±20° to ±45°
Tx–Rx Separation Distance	3–4 ft (0.9 m–1.2 m)
Tx–Rx Power Isolation	75–100 dB (typically 85–90 dB)
Cross-System Power Isolation in Multi-Radalt Installations	60–90 dB
Tx–Rx Installation Orientation	Tx–Rx pairs are H-plane coupled. Tx–Rx pairs are more commonly (but not always) installed on a fore-and-aft line with the E-plane aligned with the aircraft lateral axis.

Table 3. Typical radalt transceiver characteristics.

Radalt Tx–Rx Parameter	Typical FMCW Radalt Value	Typical Pulsed Radalt Value
Tx Peak Power	0.05 W to 2 W (+17 to +33 Bm)	1 W to 10 W (+30 to +40 dBm)
Tx Pulse Width	n/a	20 ns to 20 ms
Tx Pulse Repetition Interval	n/a	10 ms to 200 ms
Tx Sweep Bandwidth	100 MHz to 180 MHz	n/a
Tx Sweep Period	0.2 ms to 10 ms	n/a
Rx IF Frequency	n/a	20 MHz to 80 MHz
Rx IF Bandwidth	200 kHz to 2 MHz (single sided)	10 MHz to 50 MHz
Rx Detection Bandwidth	100 Hz to 10 kHz	100 Hz to 50 kHz

3.6 Basic Radalt Design Architectures

Radalt transmitter-receiver designs fall into three broad architectural categories:

- 1) Homodyne (no mixed-down intermediate frequency (IF) stage) for FMCW models;
- 2) Noncoherent (using two independent local oscillators (LO) heterodyne (mixed-down IF) for some pulsed radalts;
- 3) Coherent (using a single, common LO) heterodyne (mixed-down IF) for some pulsed and phase-shift-keyed (PSK) radalt models.

Figures 9–11 show schematic block diagrams for these three model architectures, as adapted from [21], [20] and especially [21].

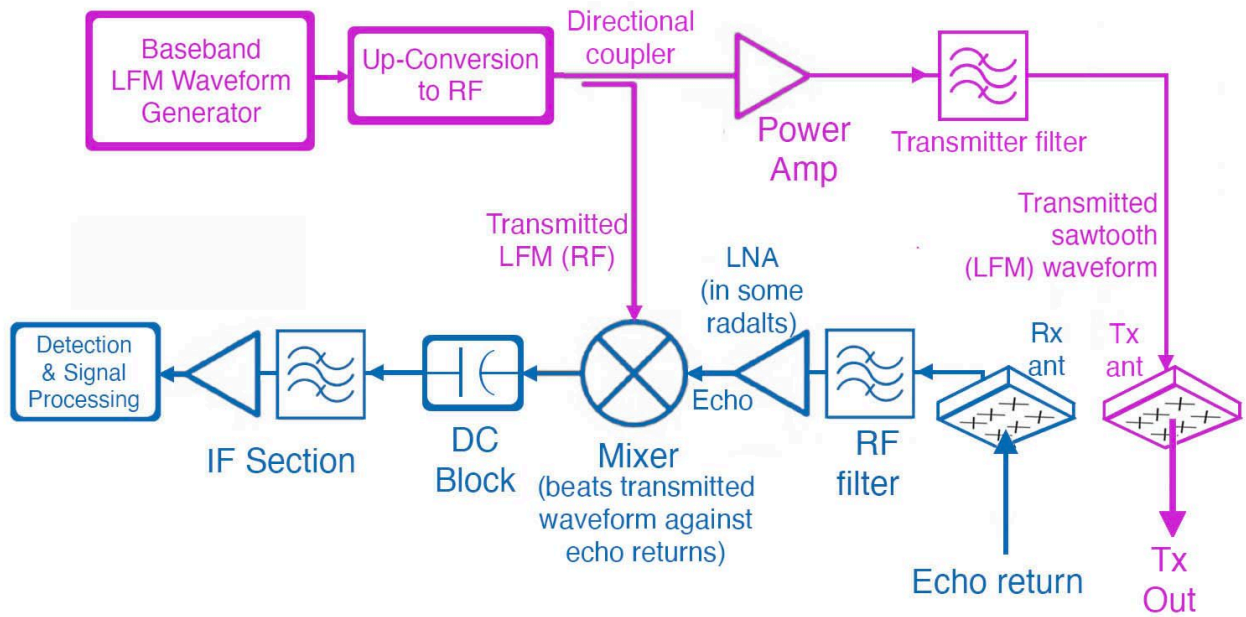


Figure 9. Homodyne (no LO) radalt architecture; no mixed-down IF stage.

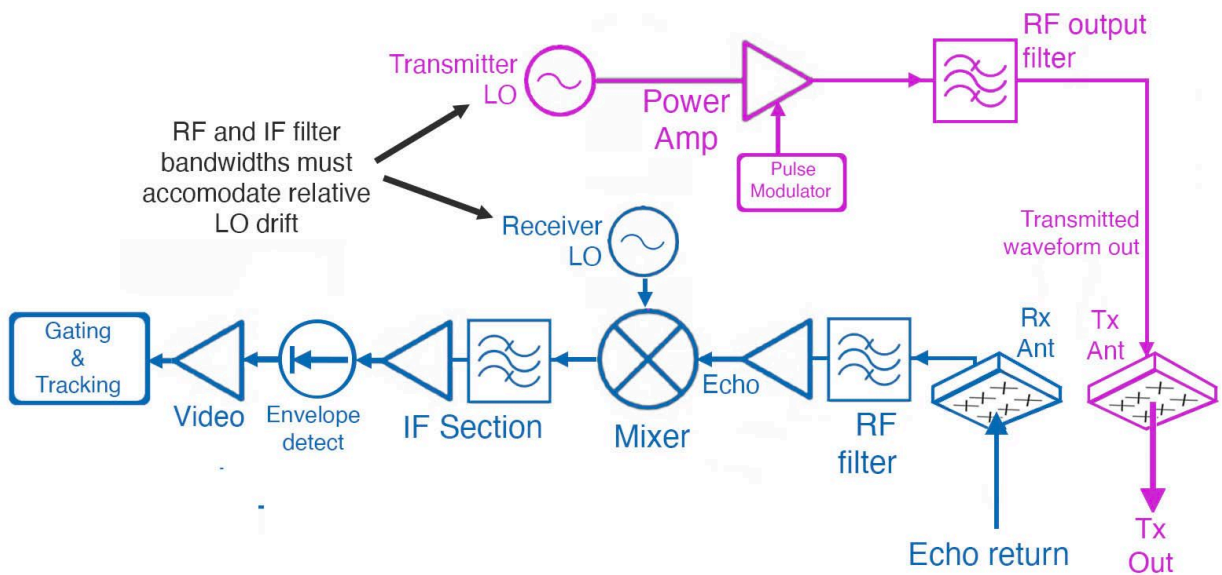


Figure 10. Noncoherent (dual independent LOs) heterodyne radalt architecture.

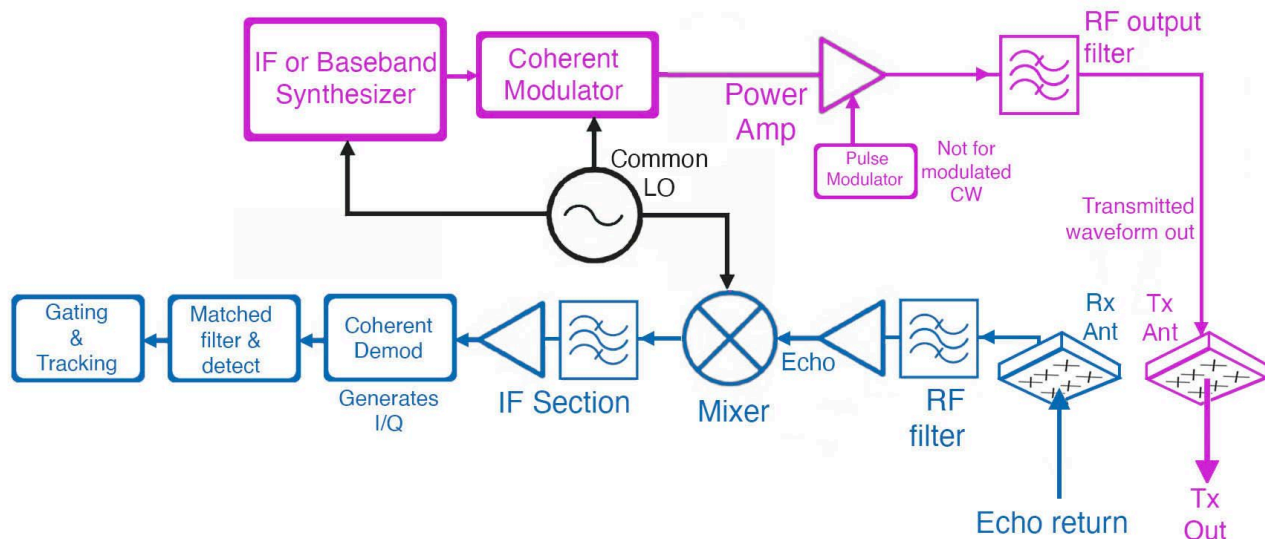


Figure 11. Coherent (single, unitary LO) heterodyne radar architecture.

3.7 Radar Receiver RF Bandpass Filtering

In Figures 9–11, note that RF bandpass filtering on the front ends of the receiver stages is a standard design feature across all architectures. The *widths* and *roll-off rates* of the bandpass filters do, however, vary from one radar model to the next. Some models utilize relatively tight bandpass widths (close to 4200–4400 MHz) with relatively fast roll-offs, while others employ filters that are wider with relatively slow roll-offs (e.g., perhaps only 10 dB of rejection at a relatively low frequency such as 3700 MHz). This variation reflects design trade-offs that involve such engineering factors as frequency-dependent phase responses of tight filters with fast roll-offs; filter insertion losses; and design complexity. We will return to consideration of radar receiver RF filtering as an EMC topic in Section 5.

3.8 Echo-Return Power Management in Radar Receivers

A particular design challenge for radar receivers is dynamic ranging across wide variations in echo input-power. The classical out-and-back $(r^2)^2 = r^4$ power versus range dependence of radar echo returns introduces, for an available radar operational height range of, for instance, 20 ft to 2,500 ft, an echo-return power variation of $(2500/20)^4 \sim 244,000,000 = 84$ dB over that range, if transmitter output power is held constant. Overall variation in loop loss, including additional factors of varying terrains, signal fading, aircraft maneuvering, and varying propagation loss, may ultimately call for at least 100 dB of total available dynamic range for a radar receiver [21].

Noting that the largest portion of this range, perhaps 84 dB out of a total of 100 dB, is, however, due to height variation alone, it is apparent that the total of needed dynamic range does *not* need to be available *at any one moment in time*. Rather, a radar's dynamic range can be adjusted through time as the height above ground varies, like a window with a height that is adjusted upward and downward above the floor.

For FMCW radalts, higher-power returns from lower heights will correspond to lower beat frequencies in the receiver, and vice versa. FMCW radalt sensitivity (effective gain) versus altitude is adjusted by providing more gain at higher frequencies, equivalent to having more sensitivity at higher altitudes.

For pulsed radalts, the ordinary (for radar receivers) features of sensitivity time control (STC) and automatic gain control (AGC) are implemented [21]. STC uses time-varying attenuation in the receiver, with more loss (more power attenuation in the receiver’s input stage) used for higher-power (lower-height) echo returns, and less (or zero) attenuation used for lower-power (higher-height) returns. AGC implements time-varying receiver gain factors or stages in an analogous but inverse manner to STC.

The use of dynamic power-control features of variable gain, STC, and AGC in radalt receiver designs means that the echo signal-to-receiver-noise (SNR) ratios of terrain returns are in fact held within a restricted range of power levels in any given receiver model, regardless of height above ground. Although some echo-return power variation will occur with height above ground, the *maximum amount of such variation* will be much more limited than the wide-ranging numbers of 84–100 dB noted above; it will be held within a fixed dynamic-range “window” of relatively few decibels. Overall, to the extent that built-in dynamic ranging features are effective, radalt loop-loss SNR levels should not change appreciably due solely to height. *This means that it cannot be assumed that radalts will be more or less susceptible to a given level of harmful interference power solely as a function of radalt height above the ground.*

References such as [2] call out issues with the echo-reflectivity of terrain, and this topic was a source of considerable discussion in the JI-FRAI effort. The central concern with ground reflectivity is the strength of the echo returns from relatively weakly reflecting surfaces. We note here, however, that the dynamic range control features of radalts should tend to compensate for relatively weak ground-echo returns. Overall, dynamic range is a solved technical problem for radalts. Blocking dynamic range (the amount above the radalt noise floor of an out-of-band signal, such as an intentional 3900 MHz 5G emission) that degrades the detection of a desired in-band radalt signal (within 4200–4400 MHz) needs to be understood. This is briefly discussed below in Section 3.10.

3.9 Overview of Radalt Detection, Acquisition and Tracking

Radars detect, acquire, and track “targets.” For radalts, the “target” is the ground beneath an airframe. Radalt target detection is based on a power threshold within the receiver section, that threshold often being between 7 to 13 dB of SNR [21]. Statistically, detection might not (usually will not) occur for every single out-and-back pulse echo or FMCW chirp period. To accommodate this reality, target validation may be performed over a *percentage* of pulse or chirp intervals; or else *averaging* of the radalt’s baseband (output) signal may be performed over time (through many pulses or chirp cycles). Such validation may require a few milliseconds to tens of milliseconds [21]. This condition is termed *acquisition*.

With the acquisition condition established, the target (the “ground”) is then tracked for its range (height). If the ground presents multiple ranges, the smallest (lowest) equivalent height is

tracked, obviously. During height tracking, a *maximum* step-time interval of 1/10 second (100 milliseconds) is typically needed and implemented for civilian aircraft; height update rates on external radalt data buses are between 1/10 second and 1/60 second (10 Hz to 60 Hz) [21].

3.10 Loop Sensitivity as a Radalt Performance Criterion

Loop sensitivity and loop loss, critically important for understanding and implementing bench testing of radalts, and for understanding criteria for harmful interference to radalt receivers, are briefly summarized here for the purpose of introducing EMC assessments of radalt performance in the presence of potentially harmful radio interference.²²

Loop sensitivity is the *maximum* loop loss at which a radalt can meet its operational requirements [21]. It is perhaps the single most important, individually identifiable, high-level performance criterion for radalt receiver performance in the presence of harmfully interfering signals. Loop sensitivity can be regarded as a power threshold criterion for performance in the presence of harmful radio interference.

The maximum loop loss, or loop sensitivity (equating to the weakest possible receiver echo-power level) at which a radalt can acquire the ground from a non-tracking initial state, at a given height, is called *make-track sensitivity*. Similarly, the maximum loop loss at which a radalt can *continue* to track at a given height *after* acquisition is called *break-track sensitivity*. Break-track sensitivity is typically a few decibels higher than make-track sensitivity—meaning that acquisition is more difficult than maintenance of a track [21]. Put another way, acquisition is the weakest link in the radalt’s loop loss performance, in interference analyses.

We will return later (in Section 10) to how to apply the airborne 5G EIRP data presented in this report to bench-testing radalt loop sensitivity results. The time varying dynamic echo return power management features of radalt receivers described above (Section 3.8), should, ideally, be understood in the context of time varying ground reflection in flight as compared to steady-state ground reflection values in bench testing.

3.11 Radalt Antenna Radiation Patterns

Radalt antennas couple power in space (377 ohms impedance) to power in a circuit (50 ohms). Radalt antennas need wide angular beamwidths (Figure 12). Radalt antenna beams have a typical gain factor of 10 relative to spherical isotropic distribution, or +10 dBi. The antennas are designed for proper beam forming and space-to-circuit impedance matching across their operational band. Figure 12 shows an example of such a chamber-measured pattern at 4300 MHz.

²² General minimum-performance criteria for radalts are provided in [24].

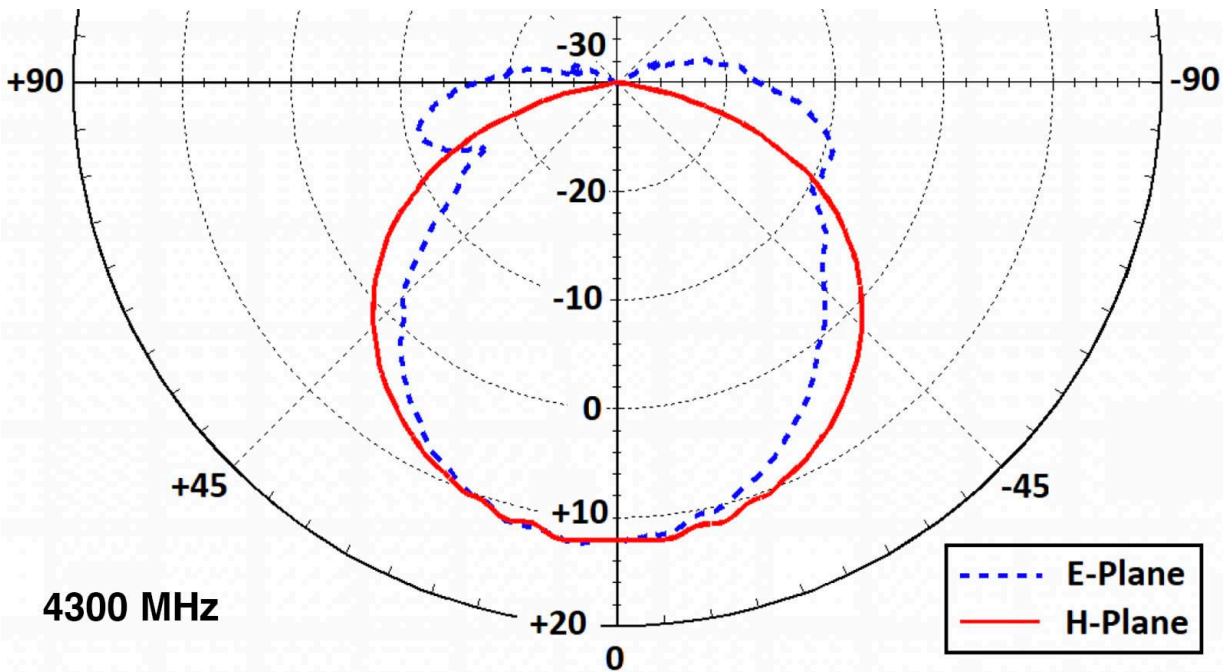


Figure 12. Example of a measured radalt antenna pattern in the center of the radalt band (4300 MHz). Data and graph courtesy and permission of The MITRE Corporation.

As discussed in Section 5, 5G RF interference may occur to radalt receivers via two possible mechanisms. One of these is due to 5G unwanted emissions within the radalt band of 4200–4400 MHz. The other possible mechanism is due to coupling of 5G power into radalt receivers on the licensed, intentional frequencies of the 5G transmitters between 3700 and 3980 MHz. For EMC analyses of the first possible mechanism, the radalt antenna patterns at about 4300 MHz, as shown for example in Figure 12, are needed.

For EMC analyses of the second possible mechanism, radalt antenna patterns within the 3700–3980 MHz band need to be known and used. Radalt antennas are not, of course, designed to operate within this frequency range. Data about their gain patterns and impedance-matching characteristics will not ordinarily be expected to be available for this range. Such characteristics need to be specifically measured for studies such as this JI-FRAI project. An example of such an out-of-band radalt antenna pattern measurement, by The MITRE Corporation, is shown in Figure 13. In this example, note that the radalt antenna gain characteristics between 3700 and 4000 MHz differ substantially from the pattern measured at 4300 MHz.

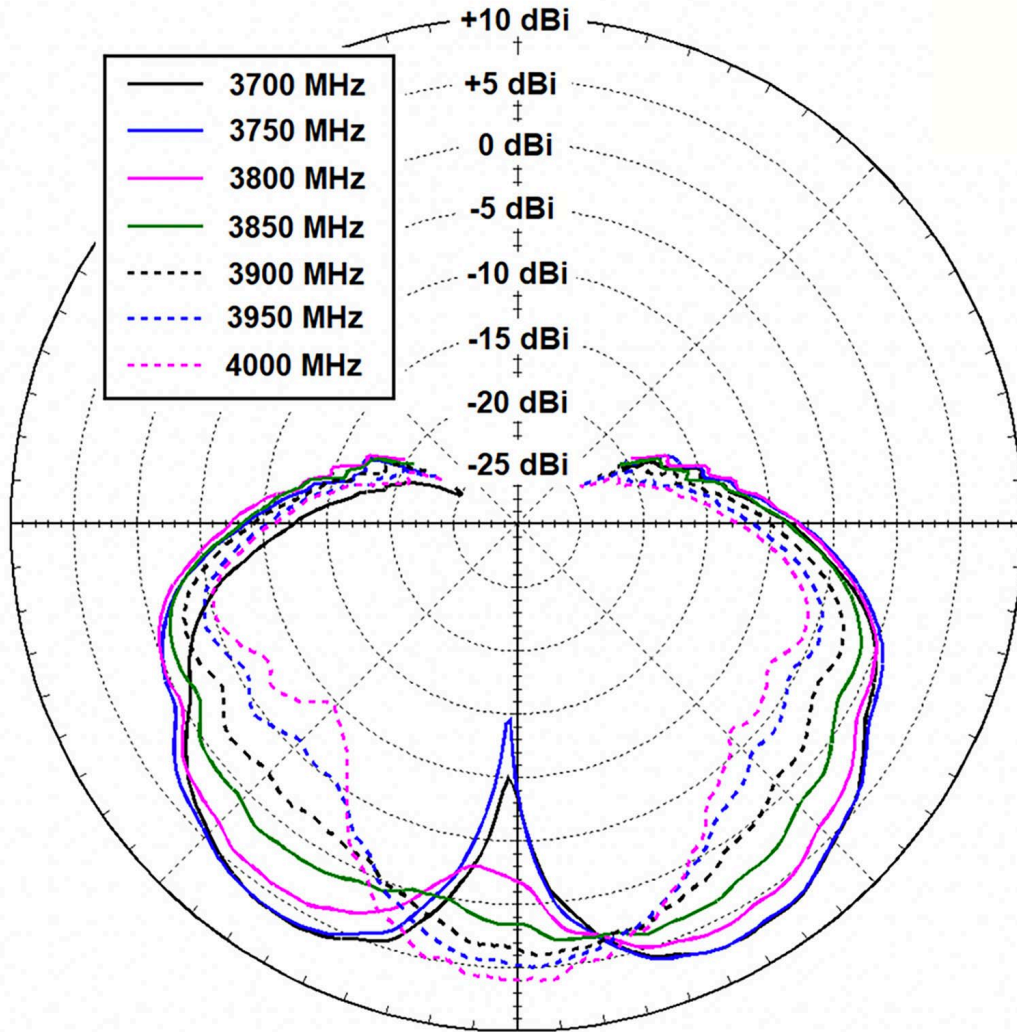


Figure 13. Example of some measured radalt antenna realized-gain patterns across 3700–4000 MHz. Data and graph courtesy and permission of The MITRE Corporation.

4. RF-LEVEL DESCRIPTION OF 5G SIGNALS IN THE US N77 BAND

This section describes 5G signals in the US n77 band (3700–3980 MHz) at the physical level of RF radiation. The 5G signals are described in three RF domains: spectrum, time, and spatial radiation patterns. The focus is on the 5G emissions, as tested, that will be “seen” by radalt receivers. Table 4 provides a brief, generic overview of US n77 band 5G base station²³ RF emissions.²⁴

Table 4. Overview of typical US n77 band 5G base station RF characteristics.

5G Base Station Parameter	Parameter Value
Compliance Standard	3GPP ²⁵ New Radio (3GPP NR)
Spectrum Band	US Band n77 (3700–3980 MHz) ²⁶
RF Transmitter Architecture	Multiple input multiple output (MIMO) solid state array
Radio Head Ports	64-port MIMO arrays (64T64R) with 128 crossed-dipole elements
Max Power per Port	3.125 watts (+35 dBm) per port
Nominal Total Max Output Power	200 total watts (+53 dBm) applied to the radiating elements
Available Channel Bandwidths ²⁷	20 MHz; 40 MHz; 60 MHz; 100 MHz (60 MHz and 100 MHz are preferred by the carriers)
Allowed Modulations	QPSK; 16 QAM; 64 QAM; 256 QAM
Channel Occupancy Mode	Time division duplex (TDD) with orthogonal frequency division multiplexing (OFDM) ²⁸
Typical Loaded Channel Duplexing (DL/UL) Duty Cycle	70 percent, typically 3.5 ms base station transmitter ON condition for DL, with 1.5 ms base station transmitter OFF condition for UL, repeating, when fully loaded with traffic
Antenna Design	128 crossed-dipole antenna elements (128AE), in 64 pairs, for digital beam forming with up to four spatial MIMO streams
Antenna Gain	+24.5 dBi
Antenna Height Above Ground	Variable; but excessive height is undesirable if it produces overly large antenna coverage areas

²³ 5G base station emissions for downlinks (DLs) have EIRPs on the order of 50,000 watts (+77 dBm), compared to user equipment (UE) uplink (UL) EIRPs that are restricted to not exceed 1 watts (+30 dBm), from [1]. With 50,000 times more power in the DLs than the ULs, 5G base station signals are taken to be the limiting factor in radalt harmful-interference analyses. The emissions of even an aggregated number of UEs associated with a base station will be insignificant compared to the impact of the base station itself on a radalt receiver.

²⁴ Detailed parameter descriptions of the particular 5G base station transmitters that have been measured for this report are provided in Table 9 in Section 6.

²⁵ Third Generation Partnership Project.

²⁶ Internationally, the n77 band is 3300–4200 MHz [25]. The US n77 band is a subset of that, 3700–3980 MHz.

²⁷ Standards such as 3GPP [25] allow bandwidths of 10, 15, 20, 40, 50, 60, 80, 90 and 100 MHz. However, the radio manufacturers do not build their transmitters to incorporate all of these allowed choices.

²⁸ TDD is required due to: 1) lack of available spectrum bandwidth at 3 GHz; 2) TDD is preferable to frequency division duplex (FDD) because UL/DL ratios are tunable; and 3) TDD systems can utilize reciprocity efficiently for power control situations including MIMO operations.

5G Base Station Parameter	Parameter Value
Maximum Available EIRP ²⁹	+77.5 dBm = 56.2 kilowatts (kW)
Polarization	±45° (slant) generated by pairs of crossed dipoles
Antenna Beam Forming	Electronic via MIMO technology as described below
Antenna Beam Steering	Some steering control is available for focusing on UEs and following UE positions, as described below, but there are limits to 5G MIMO beam steering ranges
Antenna Beam Azimuths	Typically three MIMO physical sectors, up to 120° per MIMO sector, for 360° of azimuth coverage (if needed; fewer physical sectors can be operated)
Antenna Beam Elevation Angles	Variable; down-tilt of -1° to a few degrees below local horizontal is often desirable, although MIMO arrays can physically form beams slightly above the local horizon

4.1 Sketch of 5G US n77 Band RF Signals at a Glance³⁰

5G RF signals are formed as follows. Baseband input information (audio, video, digital) is organized as a time-domain stream of binary digits (bits). This baseband (source) bit stream will probably have some organized structure and will thus have relatively low entropy. (In addition to encryption there is a 1-for-1 randomization of the data performed specifically for entropy reasons called “scrambling” within the standard.) The bit stream is run through a 256-bit encryption stage, which intentionally disorders the structure in a way that is hard to reverse without special, supplemental information. This encrypted bit stream has maximal entropy; it looks noise-like without separate, supplemental decryption knowledge.

The encrypted, high-entropy bit stream is then run through a phase modulator that has 4, 16, 64 or 256 available amplitude-phase states. The output is called quadrature phase-shift keyed (QPSK) or else 2ⁿ-quadrature amplitude modulated (QAM), e.g., 16-QAM, 64-QAM, or 256-QAM. The transmitted 5G bit stream will appear like random Gaussian noise to any receiver (like a radalt receiver, for instance) that is “dumb” to the underlying encryption and QAM modulation (QAMing) that have been performed on the originally-organized, low-entropy input bits.³¹

Channel bandwidths are: 20 MHz (QPSK only), 40 MHz, 60 MHz, or 100 MHz.³² However this bandwidth-limited Gaussian noise, transmitted by base stations as downlinks (DLs) to phones (user equipment, UEs) must be interrupted periodically so that the base stations can listen for uplink (UL) transmissions from local UEs. This *time division duplexing* (TDD) is needed

²⁹ EIRP is *defined* as the maximum root mean square (RMS) average power that the base station radiates in a given beam direction *during the transmitter-ON period of any TDD cycle* ([25], Section 9.2.1).

³⁰ This sub-section is a very brief overview of the bare essentials of 5G RF signals; it is intended for readers who need to understand the bare minimum about 5G signals in an expeditious manner.

³¹ 5G transmitted bit streams should have maximal unpredictability from one bit to the next, which corresponds to maximal information being contained by each bit.

³² Channels of 60 MHz and 100 MHz have been observed as frequently-used by 5G base stations.

because the entire n77 band (3300–4200 MHz) is not wide enough to separate the DL and UL traffic into two independent radio bands.³³ Running fully loaded at their informational capacity, the 5G base stations in the US n77 band typically transmit their DL signals to the UEs for 3.5 milliseconds, and then turn off for 1.5 milliseconds to listen to the UL signals coming back from the UEs. This means that the percentage of time (duty cycle) of the 5G base stations' transmissions is usually about $3.5/(3.5 + 1.5) = 3.5/5 = 70$ percent.

In summary, fully information-loaded³⁴ US n77 band 5G base station signals as “seen” by “dumb” receivers, including radalts that do not know how to “read” the 5G encrypted and QAM modulated (QAMed) information, will look like uncorrelated, time-gated (up to 70 percent duty cycle), bandwidth-limited (up to 100 MHz wide) Gaussian noise at a total EIRP of not more than +77.5 dBm.

4.2 Spectrum Domain Characteristics of US n77 Band 5G in Finer Detail

4.2.1 Channel Physical Resource Blocks and Sub-Carrier Spacings

Within a 5G channel, the traffic is divided among, and carried by, smaller-bandwidth segments called physical resource blocks (PRBs) with allowed sub-carrier spacings of 15, 30, and 60 kHz ([25], Band n77 entry in Table 5.3.5-1). Figure 14 shows a digital capture of an operational channel, with time-varying traffic structure seen among the component PRBs.

4.2.2 Available Channel Bandwidths in the US n77 Band

The 3GPP standard for 5G NR base stations allows base station channel bandwidths of 5 MHz to 100 MHz with increments of 5 MHz (up to 30 MHz) and 10 MHz (from 30 MHz to 100 MHz) ([25], Band n77 entry in Table 5.3.5-1). However, the available 5G radio models in the US n77 band, made by three manufacturers, only offer bandwidths of 20 MHz, 40 MHz, 60 MHz, and 100 MHz.³⁵ Of these, 20 MHz is only used for relatively slow data-rate QPSK modulation. Channel bandwidths of 60 MHz and 100 MHz have been observed by the authors to be the most often implemented (“most popular”) bandwidths used by the US-deployed 5G n77 band base stations.

³³ According to private communications with a major 5G equipment manufacturer.

³⁴ 5G base stations with no UEs to talk to will beacon brief, low duty cycle bursts announcing themselves to any new UEs that might enter their coverage area.

³⁵ Not every US 5G base station transmitter model offers all of these bandwidths. The exact channel bandwidths currently available for each US 5G n77 band transmitter model are provided in Table 9.

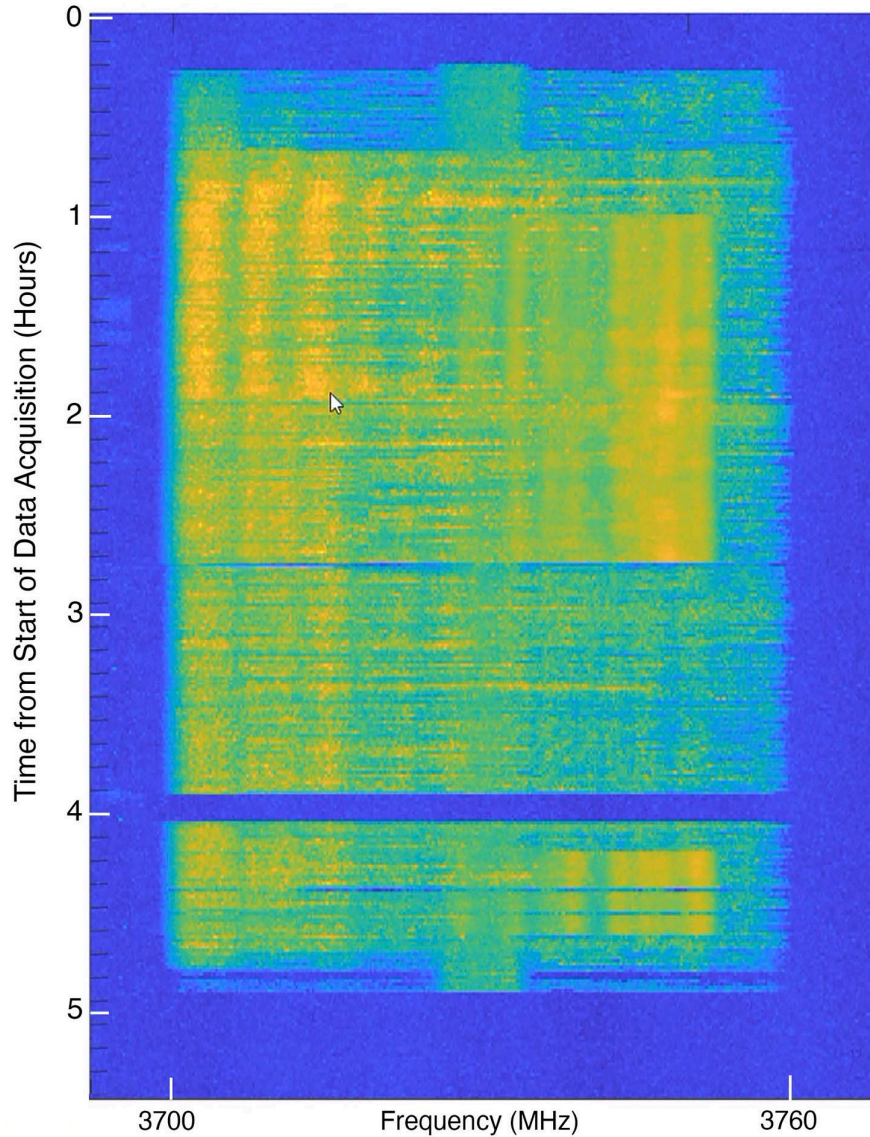


Figure 14. A 5G NR 60 MHz RF channel with time-varying PRB structure (yellow). Graphic is adapted from data provided courtesy of the NOAA-sponsored Radio Frequency Interference Monitoring System Project at NTIA/ITS.

4.2.3 Maximum Power Spectrum Density and Maximum Total EIRP in 5G Base Station Transmitter Channels

As shown in Table 4, the US n77 band 5G base station transmitters that were tested typically generate a maximum total EIRP of $+77.5 \text{ dBm} = 56.2 \text{ kW}$. This is a *physico-technical limit* based on *maximal performance* of the transmitter power amplifiers (PA) and MIMO beamforming.

The *regulatory limit* on these base stations' output power is not, however, on total EIRP. Rather, the regulatory limit is (from [1] and [26]) $+62.15 \text{ dBm/MHz}$ for higher density areas and

+65.16 dBm/MHz for lower-density rural areas.³⁶ In principle, for a high-density area 100 MHz channel, this could lead to as much as $(10 \cdot \log(100)) + 62.15 = +82.15$ dBm of total EIRP, and a maximum total EIRP of +85.16 dBm for rural-deployed base stations.

Currently an upper *physico-technical power limit* is, as noted above, determined by physical limitations on the 5G MIMO array PAs' available output power and maximal MIMO antenna gains. Since the existing base station transmitters can only generate 200 watts (+53 dBm) from their PAs, and since their directed antenna gains do not exceed +24.5 dBi (because the beams can only be formed down to a physically limited narrowness from the MIMO arrays), the physico-technical limit on their total EIRP is about (+53 dBm maximum PA power) + (+24.5 dBi maximum antenna gain) = +77.5 dBm = 56.2 kW, as noted in Table 4.

The fact that the 5G regulatory limit is a *power density* (per megahertz) rather than a limit on *total EIRP* can cause confusion as to what is meant by 5G *maximum power*. In the regulatory limit, the power per megahertz of +62 dBm/MHz (for urban deployments) *can only be achieved by currently-available PAs in a radiated channel bandwidth of 35.5 MHz or less*. In wider channel bandwidths such as 100 MHz, the regulations still allow up to +62 dBm/MHz, but the total EIRP would then have to reach $(100/35.5) = 2.8$ times more power than the current PAs can generate, or 560 watts. For future rural base stations with a +65 dBm/MHz limit, the increased PA power output requirement would be 5.6 times more power than currently available PAs can generate, or 1120 watts. This of course begs the question of whether future PAs will possibly be capable of generating up to 560 watts or 1120 watts, respectively, in the future instead of the current maximum of 200 watts, while thermally dissipating concomitantly larger amounts of waste heat. We do not know whether such large EIRPs in 100 MHz channel bandwidths may eventually come to pass—we can only offer that, if future generations of PAs are able to generate output power up to the regulatory limit in a full (maximum allowed) channel bandwidth of 100 MHz, that factor might need to be addressed at such a future point. Right now, we cannot obtain such power out of any existing 5G base station radios in the n77 band.

For the JI-FRAI JT&E and radiation measurements, the consensus of the group's membership was that tests and measurements should be performed in the maximum possible channel bandwidths. Various JI-FRAI members argued that using widest-available bandwidth of 100 MHz was thought to provide maximum stress on: 5G radiation spectra; channel data throughput and loading; and MIMO array performance. A 100 MHz channel bandwidth was also thought to represent a most-likely, or at least very-likely operational case for actual carrier deployment scenarios compared to a channel bandwidth of 40 MHz (which would be the nearest available bandwidth to the computed maximum power-density bandwidth of 35.5 MHz).

This being the case, the JI-FRAI tests and measurements operated the 5G base stations at *all available, maximum total, EIRP in a 100 MHz channel bandwidth* for Radios 1 through 3. (For Radio 4, the channel bandwidth was 60 MHz because the manufacturer has locked that model to

³⁶ US base stations have not yet been developed for the rural-area +65 dBm/MHz EIRP limit [FCC, private communication with R. Pavlak, 21 June 2022].

that single channel bandwidth.) The resulting *power per megahertz* for tests and measurements was therefore, however, automatically constrained to be 4.5 dB less than the regulatory limit.

We emphasize that, no matter which channel bandwidth these base stations transmitters radiate in, *the total radiated power is always 200 watts from the PAs, multiplied by the antenna gain of +24.5 dBi*. No matter the selected channel bandwidth, the maximum EIRP is always +77.5 dBm for all currently available US n77 band base station transmitters. That quantity is irrevocably fixed until or unless higher-power PAs are developed and fielded (while holding maximum antenna gain constant, obviously). *J1-FRAI always tested and measured at maximum 5G EIRP*.

This spectrum power is distributed (nominally uniformly but sometimes a bit non-uniformly, as shown in Figure 14) across the 5G channel bandwidth. The authors have directly observed and confirmed, by measuring the power per megahertz of 5G radiated emissions, that the power spectrum density in the channels is inversely linearly proportional to the channel width. Total 5G base station EIRP is thus a *conserved* quantity; that conservation forces power spectrum density to vary in direct inverse proportion to channel width, even as total output power remains constant (i.e., conserved). Table 5 shows the power per megahertz as a function of channel bandwidth.

For the FCC limit of +62.15 dBm/MHz, we see in Table 5 that, for a total nominal EIRP of +77.5 dBm, this limit has the effect of making the channel bandwidths be 40 MHz or wider.

Table 5. Power spectrum density as a function of channel bandwidth for tested US n77 band base station transmitters for +77.5 dBm total EIRP.

Channel Bandwidth (MHz)	Total Channel EIRP (dBm)	Power per Megahertz Computation (dB)	Spectrum Power Distribution (dBm/MHz)
100	+77.5	$10 \cdot \log(1/100) = -20$	+57.5
60	+77.5	$10 \cdot \log(1/60) = -17.8$	+59.7
40	+77.5	$10 \cdot \log(1/40) = -16$	+61.5

The only way for 5G base stations to use channel bandwidths narrower than 40 MHz would be to reduce the total EIRP by cutting either the effective 5G PA output power output or the MIMO array antenna beam gain, or both. As far as we know, the PA output power is fixed and cannot be reduced via 5G hardware or software control systems.

4.2.4 Selection of Measurement Bandwidths for 5G RF Signals

Measurements of 5G RF power will not normally be performed in the full bandwidth of the channel (which can range from tens of megahertz wide to as much as 100 MHz wide for 3GPP compliant 5G in the US n77 band). The reason is that the channel power is distributed (nearly uniformly) across the occupied PRBs of the 5G channel width as Gaussian noise. For this distribution, measurement gear only needs to measure across a fraction of the channel bandwidth. Then the full power in the channel (if that is needed) is computed by multiplying the measured power by the ratio of the channel bandwidth to the measurement bandwidth.

For example, if a 5G channel is 100 MHz wide and is measured in a bandwidth of 1 MHz, then we know that the ratio of the channel width to the measurement width is 100. Therefore (for a uniform power distribution across the channel) the measured power is multiplied by 100 to obtain the full channel power. In decibels, this difference is $10 \cdot \log$ of the ratio: $10 \cdot \log(100/1) = 10 \cdot \log(100) = +20$ dB, in this example.

Another reason to use a relatively small measurement bandwidth of (specifically) 1 MHz is that many 5G specifications are given as power per megahertz (e.g., +62 dBm/MHz maximum allowed EIRP), as discussed above. Although small quibbles may exist about the exact definition of a 1 MHz measurement bandwidth (Gaussian filter shape or raised-cosine filter shape? Percent roll-off rates at filter edges? Etc.), a measurement made directly in the same bandwidth as the specification obviates later, or further, conversions to the specification's bandwidth. If the specification is per-megahertz power, then a direct measurement in a (nominal, for the selected measurement gear) bandwidth of 1 MHz will ordinarily suffice to directly check against that specification.

Moreover, for the particular study at hand, radalt manufacturers, testing labs and theoreticians ordinarily (but not always) specify radalt RF interference power in the receivers on the basis of interfering 5G power-per-megahertz. We therefore suggest doing most 5G power measurements in 1 MHz and then adding (in decibels) $10 \cdot \log$ of the ratio of the channel bandwidth to the measurement bandwidth if the full channel power is needed for whatever reason.

4.3 Time Domain Characteristics and Peak versus Average Power of 5G in Finer Detail

4.3.1 Time Base and Periodicity of 5G TDD

Figure 15 shows a time-domain capture of a 5G base station's TDD behavior. The base station was running maximal traffic loading and was linking to 11 UEs when this capture was performed.³⁷

³⁷ The measurement system's ½-meter diameter dish antenna was located close to two of those UEs, placed 3 meters vertically below the dish antenna. The UEs' proximity helped to keep a 5G MIMO beam aimed at the measurement system, but the UEs' location well outside of the dish's main beam kept their emissions out of the measurement of the base station's signal.

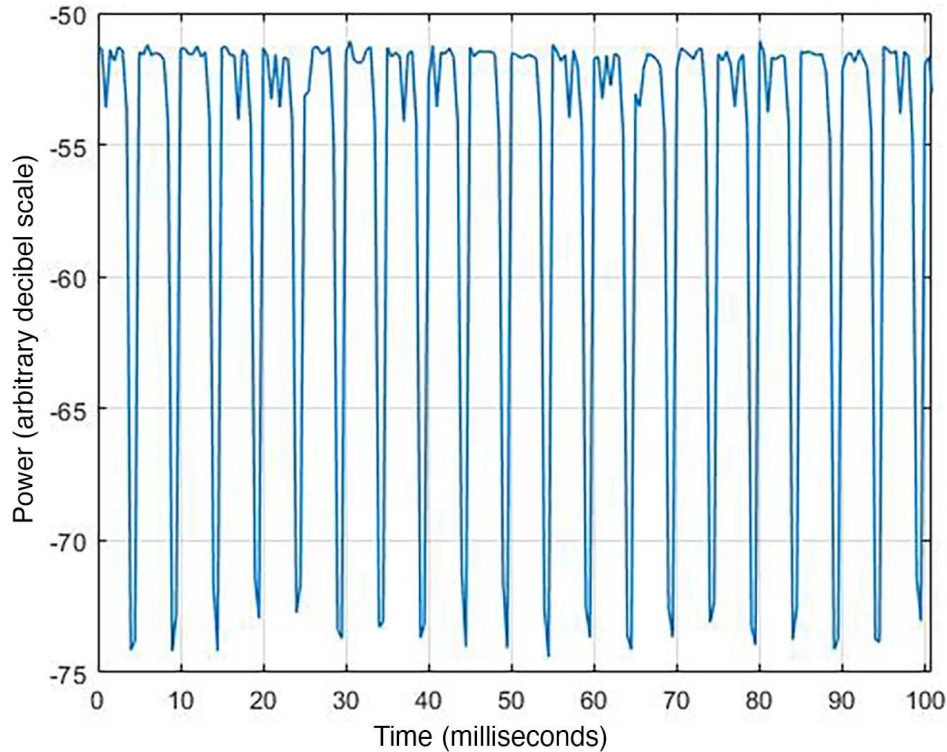


Figure 15. 5G time domain capture (at 3928 MHz) for a 3880–3980 MHz channel showing 70 per cent TDD duty cycle at 3.5 milliseconds ON and 1.5 milliseconds OFF, repeating.

In Figure 15, peak detected³⁸ time-domain data have been taken on a single frequency in the middle of a 100 MHz 5G channel (3928 MHz in a 3880–3980 MHz channel) in a 1 MHz measurement bandwidth over a duration of 100 ms. The base station completes a total of 20 TDD cycles in exactly 100 ms, for a TDD periodicity of 5 ms. Within each TDD period, 3.5 ms are ON (occupied by the base station’s DL transmissions) and 1.5 ms are OFF (occupied by the base-station’s listen-only mode for UE UL transmissions). The authors have found this to be a commonly used TDD cycle for 5G base stations in the US n77 band.^{39, 40}

³⁸ Tradeoffs between peak detection and average detection for 5G signals are discussed below.

³⁹ This is consistent with the “7:1.2” TDD pattern that carriers (private communications) tell us is deployed on C-band 5G base stations in the United States. It has been observed that not all models of base station maintain this exact periodicity under all circumstances, but this is a nominal time base periodicity when 5G channels are heavily loaded.

⁴⁰ The authors have observed that, when a base station has no UEs to communicate with, it will run low duty cycle beaconing. This is believed to be the 5G signal synchronization block (SSB). UEs use received SSB power level to determine which local 5G base station to communicate with. The SSB, having a low duty cycle, does not further concern us for the work described in this report.

4.3.2 Maximum Base Station Duty Cycle versus Channel Loading by Numbers of UEs

As noted above, the n77 band, both internationally (3300–4200 MHz) and in the US (3700–3980 MHz) is so narrow that base stations and UEs must share channels on a time-sharing, TDD basis. This means that, no matter how much traffic a channel needs to carry, there is a minimum percentage of time that the base stations must go into listen mode for UE transmitters to communicate to the base station receivers. Although under some circumstances this is supposedly as low as 20 percent (for a complementary 80 percent base station duty cycle), the authors have mainly encountered 30 percent for the minimum UE duty cycle, with a complementary (maximum or near-maximum) 70 percent for the base station duty cycle, as shown for example in Figure 15. *A duty cycle of about 70 to 75 per cent seems to represent a practical upper limit for 5G base station transmissions, based on empirically observed limits for the radio base stations in this project.*

The degrees of freedom for the base station’s transmissions within a given antenna beam (discussed separately below) are power, TDD duty cycle percentage, and modulation. Power is already ordinarily maximized at 200 watts (+53 dBm). Duty cycle does not usually exceed about 70 percent (perhaps 80 percent in some cases), as we have seen. So, as a channel’s data-loading requirements (in a given antenna beam) grow, the only remaining degree of freedom that can be adjusted is the modulation. This can be set, as we have seen, to as high as 256 QAM and as low as QPSK. Such adjustments are automatically controlled by the 5G system controllers.

The salient point here is that, once a channel has been loaded by enough UEs carrying enough data to make the base station go to its maximum allowed duty cycle at its full power, adding more UEs or trying to push more data through the channel does not further change the situation at RF. This is what we have observed at first hand when we have loaded the 5G channels during tests and measurements. The transmissions themselves always look like Gaussian noise. The data modulation may drop from 256 QAM to 64 QAM to 16 QAM and so on as the channel is additionally stressed in one way or another, but at the RF level, with the baseband 5G data already having been encrypted, “dumb” receivers such as radalts that cannot demodulate (“read”) the 5G data will see no difference as UEs are added and data transmission needs are pushed higher.

The ultimate limits on 5G base station TDD duty cycle and power output mean that it is not necessary to operate a base station with dozens or hundreds of UEs to make its emissions look “fully loaded.” As it turns out, about a dozen UEs are adequate to achieve this state.

4.3.3 Base Station Channel Loading Tools for 5G: Are the Generated Loads “Real”?

Passive intermodulation (PIM) is a general technical problem for wireless base stations, especially as transmitted power levels become as high as they are for 5G. To allow engineers to study PIM, manufacturers and service providers offer tools for fully populating and loading all of the PRBs in a given 5G channel. These are orthogonal channel noise simulation (OCNS) and air interface load generation (AILG). In ordinary use by a channel that is already carrying traffic, these tools are used to artificially add activity to otherwise-unoccupied PRBs within the channel.

In the testing described in this report, where 5G channels were in fact not carrying live traffic, OCNS and AILG were used to fill not just a few sporadically unoccupied PRBs, but rather to occupy *all* PRBs with RF power, all across a given channel.

Another tool needed to achieve full 5G channel loading and utilization is IP Performance (Iperf). Iperf is an open-source, cross-platform (Linux, Windows©) utility that provides standardized data-stream measurements for communication networks. Working between clients and servers, Iperf creates known baseband data stream rates and then measures resulting network data throughputs and rates. Iperf particularly inserts its own dummy data into otherwise low-rate (or, for our 5G testing, zero-rate) baseband data streams, in order to push baseband channel loading to the maximum that is possible.

Although we use the words “artificial” and “dummy” here for the achievement of full PRB occupancy and maximum-possible baseband data rates, respectively, there is nothing artificial or unreal about the occupancy of PRBs by the OCNS/AILG tools and the maximum baseband channel data-push generated by Iperf. The RF channel occupancy that they produce is entirely real. Given that 5G baseband traffic inputs are always encrypted, by 3GPP design specifications, before they reach the RF transmission stage; and that *any* type of baseband input that produces QAMed activity in a PRB at RF is entirely indistinguishable from any other type of input; and that PRB occupancy with 5G statistics is the only goal of the testing described here; the end result of using Iperf and OCNS/AILG is always the same: entirely realistic and genuine 5G Gaussian noise exists in all PRBs across a channel. If a “real” traffic load generated from enormous numbers of actual physical users were to be carried by a 5G base station, that traffic would be indistinguishable from the traffic and loads, and the resulting Gaussian noise across an entire 5G channel, as generated by Iperf and OCNS/AILG.

4.4 Peak versus Average Statistics and Measurement for 5G Signals

As already described, 3GPP-compliant 5G RF signals look like Gaussian noise during every TDD ON cycle interval. This has implications for effective measurement of these RF signals.

4.4.1 RMS Averaging Applied to 5G RF Signals

A naïve approach for measuring 5G RF signals would be to use root mean square (RMS) averaging in a spectrum analyzer or signal analyzer. RMS average detector mode would be consistent with the definition of 5G power as being the time-averaged output of the transmitter.

The problem with using this mode is that RMS averaging in analyzer gear is not as straightforward as might be thought, especially with respect to how it interacts with 5G signals. RMS averaging is not a simple response function. Instead, RMS averaging requires the following steps to occur in measurement gear: first, a digitizer⁴¹ running at high speed (perhaps 96

⁴¹ This discussion pertains only to digital measurement machines. Older, analog measurement gear, ordinarily spectrum analyzers, have never had averaging detection as no analog method for direct averaging detection was ever

megasamples per second (96 MSa/sec)) has to sample the 5G waveform in some bandwidth in the time domain. Those samples will occur in some unknown, and unknowable, time-sliced way relative to the TDD intervals of ON and OFF; some will be collected when the TDD is ON and some will be collected when the TDD is OFF. This might still be acceptable for a sufficiently long analyzer sampling interval relative to the TDD cycle time. But for the (ordinarily) unknown behavior of the analyzer's sampling relative to the TDD cycling, and then with the added complexity of a swept-frequency sampling across a 5G channel bandwidth, the resulting sampling can be regarded as (in some cases) a colloquial mess.

The problem of RMS averaging continues after sampling. The RMS average necessarily requires that a large number of raw samples be converted into a time-series of linear power quantities that are summed together. How many samples need to be summed, and the time interval that they represent, is not ordinarily known to the operator of the measurement analyzer. How that time interval compares to the TDD cycle, much less the time-domain behavior of the 5G signal across all the PRBs in the occupied channel, is also an unknown. In any event, the sum of the powers in that the “unknown” number of power samples is then divided by the number of samples. The analyzer displays that numerical result of sampling, adding some number of power samples together, dividing by the number of samples, and then taking $10 \cdot \log$ of that number as the “RMS average power” of the signal.

In the best case, the RMS averaging output of the analyzer will reflect the average power of the TDD waveform over multiple TDD cycles. This result has been successfully obtained by the authors by putting an analyzer into a zero-hertz (time domain) mode so that the machine behaves like a sort of high-speed strip chart recorded in the time domain.

The RMS average of 5G signal has been found to often look discontinuous and spiky. The discontinuities and spikiness are not characteristic of the 5G signal; they are shortcomings of RMS averaging detection as applied to 5G signals.

4.4.2 Peak Detection Applied to 5G RF Signals

Peak detection eliminates the problems that occur with RMS averaging of 5G signals. And since peak detection gives a known offset to the average power of a 5G signal, a peak measurement can be used to easily obtain that 5G average power.

Peak detection begins (in digital analyzers) the same way as RMS averaging detection: a high-speed sampler running at something like 96 MSa/sec obtains a time series of power levels from the input waveform. But the action taken with these samples is simpler and more straightforward than for the RMS averaging mode. The analyzer simply displays the highest-power sample that has occurred within each output bin on its front-panel display.

devised. In analog spectrum analyzers, a rough, approximate average power measurement could only be obtained by using a baseband (video) bandwidth that was substantially narrower than the intermediate frequency (IF, or resolution) bandwidth.

For example, suppose that an analyzer is running in zero-hertz span on a frequency of 3928 MHz, as in Figure 15. If the time display shows 10,000 points (bins) in 100 milliseconds, then the time per bin is $(100 \text{ milliseconds}/10,000) = 10 \text{ microseconds/bin}$. A peak detector simply retains (latches to) the highest power level that has occurred in each 10 microsecond interval and displays that value. The complexities of sampling and averaging across a TDD waveform are eliminated; the peak detector result is unambiguous.

4.4.3 Average 5G Signal Power Derived from a Peak Detected Measurement

The offset between a peak detector measurement of Gaussian noise and the average of Gaussian noise is ordinarily 10 dB.⁴² This same offset will occur for a 5G signal during the TDD ON portion of its time-domain cycle.

The TDD cycle's duty cycle will itself introduce a slight correction to the total offset. At 70 percent, this additional offset will be $10 \cdot \log(0.70) = -1.55 \text{ dB}$. The total offset between peak and average across entire TDD duty intervals will therefore be $(10 \text{ dB} + 1.55 \text{ dB}) = 11.55 \text{ dB}$. Figure 16 shows exactly this offset for a carefully measured 5G signal.

We have observed, through measurement of many 5G base station signals, that the approach of measuring 5G power with a peak detector on a single frequency at a time (that is, in a zero hertz span analyzer mode) is the most reliable approach for the power measurement. The data traces are better behaved (or at least as well-behaved) with peak detection as with RMS average detection.

As will be explained in Section 6 on airborne measurement methodology, this approach is what we used for the three-dimensional airborne radiation patterns around 5G MIMO array transmitters. We measured with peak detection in a 1 MHz bandwidth on a single frequency in the time domain, and then converted that to average 5G power using the known offset.

⁴² In principle the size of instantaneous excursions of Gaussian noise power from the Gaussian's average can be unlimited. But peak detector circuitry or algorithms are usually built to register a 10 dB peak-to-average offset. This is easily checked for any signal analyzer by terminating its input and then simply running RMS average detection on one trace and peak detection on a second trace, on the analyzer's own internal thermal noise. The observed trace difference will be the machine's actual peak-to-average detection offset.

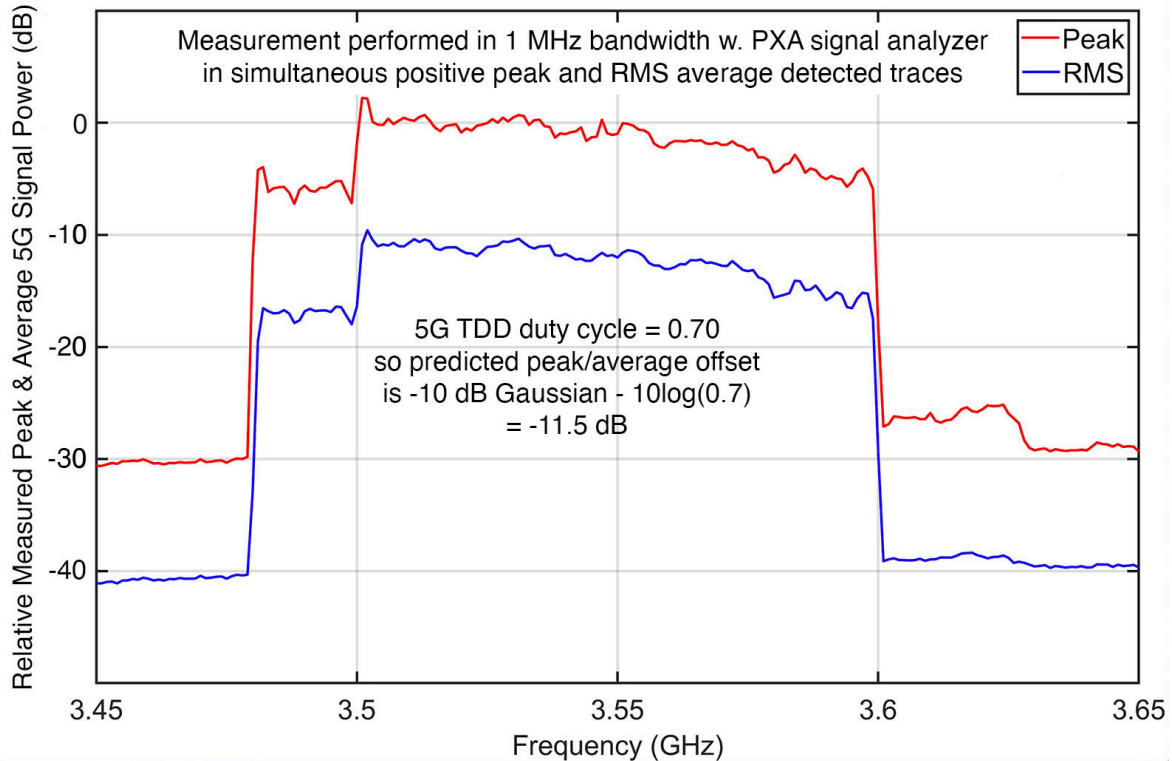


Figure 16. Measured peak and average detection offset for a 5G signal at 70 percent TDD duty cycle.

In Figure 16, the observed offset is about -11 dB between peak and average detection, consistent within the measurement error (about ± 0.5 dB) with the computed -11.5 dB offset. Note that this offset is overall, including the -1.5 dB effect of the TDD duty cycle. The 3GPP standard does not use that definition for 5G average signal power. Instead, the 3GPP standard specifies 5G average power during the TDD = ON portion of the duty cycle ([25], Section 9.2.1, p. 139). This definition would give only -10 dB offset between 5G peak average.

For the work presented in this report, we have followed the 3GPP-standards definition and used a *-10 dB offset between our measured peak power and our computed RMS average power*. This makes our computed 5G RMS average power levels conservatively *high*, by 1.5 dB, compared to using the -11.5 dB offset that would include the effect of the overall TDD duty cycle. It also eliminates any quibbling about actual overall TDD duty cycle percentages for any given 5G transmitter mode.

4.5 Antenna Radiation Patterns for 5G MIMO Arrays

As pertains to the potential for radiated 5G signal power to interfere with radalt receivers, a topic of extreme importance is the actual pattern of radiation produced in space around the 5G MIMO arrays.

4.5.1 64T64R MIMO Array Designs, Briefly

One of the major differences between 5G and 4G base stations is the use, in 5G transmitters, of MIMO arrays that can form directed, individual antenna radiation beams. This selectable beam directionality is beneficial in allowing 5G base stations to maximize RF power with desired UEs while nulling (to an extent) against non-desired UEs. Figure 17 shows a diagram of the RF-level architecture of one of these MIMO arrays.

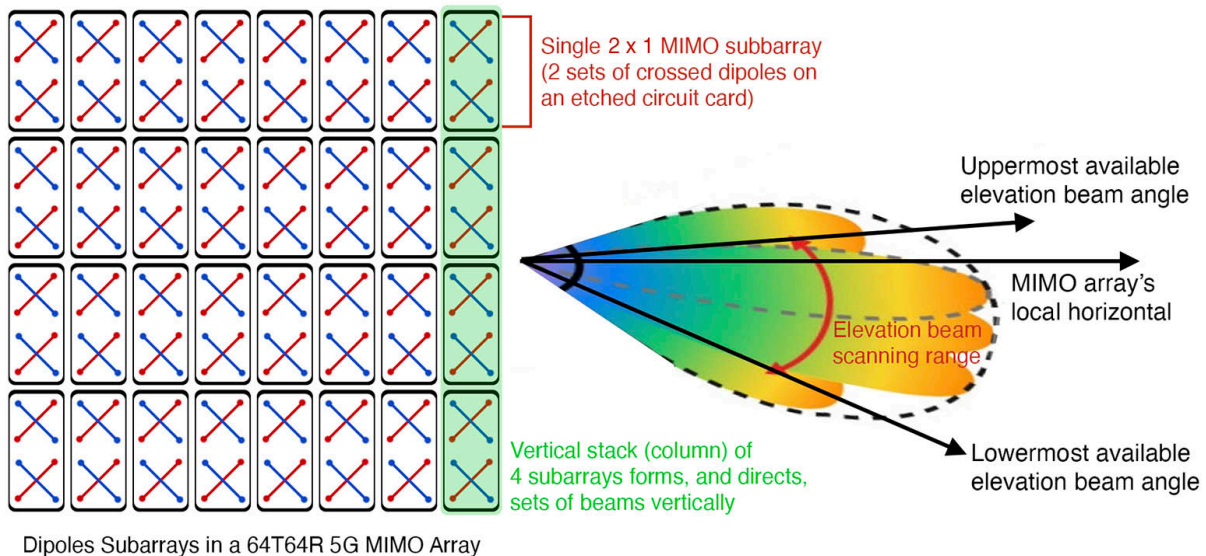


Figure 17. Diagram of 64T64R MIMO array architecture and beam-directing capability.

The 5G radios in the US n77 band use a MIMO transmitter design designated 64T64R, for 64 transmit and 64 receive sections. Each such MIMO box (see Figures 17 and 18 for examples) contains 64 pairs of crossed dipole antenna elements. The pairs are laid out in an 8×8 circuit-card planar array. Pairs of these crossed dipoles are grouped into subarrays.



Figure 18. A MIMO 64T64R transmitter-receiver box for a US n77 band 5G base station. It is an integrated, weather-sealed unit with connectors on the lower edge for power and data.

4.5.2 5G MIMO Beam Elevation Angle Range and Control for the US n77 Band

4.5.2.1 Beam Elevation Angle Range for US n77 Band 5G MIMO Arrays

For the purposes of this study, we are primarily concerned with the elevation angle dimension of MIMO beam control. We begin with the maximum range of elevation angles that are available to 5G MIMO arrays in the US n77 band.

Vertically arranged groups of MIMO subarrays, as shown for example in Figure 17, use phase control to form beams at various elevation angles relative to the array's broadside axis.⁴³ Table 6 lists the manufacturer's stated limits of electronic elevation beam scanning for the three models of 5G base station MIMO arrays deployed in the US n77 band. Table 6 lists the maximum range of elevation angles for the US-deployed 5G n77 band base station transmitter MIMO arrays.

⁴³ MIMO arrays can be mounted with varying, but limited, amounts of mechanical elevation tilt.

Table 6. Manufacturer-specified electronic elevation beam scanning limits for 5G MIMO arrays in the US n77 band, relative to the MIMO broadside axis.

Manufacturer⁴⁴	Lowermost Elevation Below MIMO Array Broadside	Uppermost Elevation Above MIMO Array Broadside
A	-19 degrees	+7 degrees
B	-3 degrees	+3 degrees
C	-10 degrees	+3 degrees

Although 5G elevation angles can go above the broadside axis for these base stations, as shown in Table 6, the 5G technical literature seems to focus mostly on how to tilt 5G beams downward rather than upward. In the 5G tutorial of [27], for example, the term “downtilt” occurs 118 times whereas the term “uptilt” never appears even once. Similarly, in [2] the term “downtilt” occurs nine times but the term “uptilt” never occurs.

In another reference, by 5G America ([28], pp. 49–51), there is substantial discussion of tilting or directing 5G MIMO beams downward for coverage in various environments including high-rise buildings. This source states (p. 50) that coverage inside high-rise buildings is more effectively accomplished with dedicated indoor wireless systems than with either external macro-cells on the high-rise rooftops or from external base stations at street level that would be up-tilted toward the buildings’ upper floors.

In a third reference, by RTCA ([2], Appendix B, “TWG-3 Information Exchange,” p. 144), the “wireless experts”⁴⁵ answer to a question from the “aviation experts”³⁵ in Technical Working Group 3 (TWG-3) about 5G elevation coverage angles includes a table listing “vertical scan (below horizon)” for the subject 5G base stations as ranging from “0 to -10” and “0 to -30” degrees. No value is provided there for any elevation angle above the local horizon.

In a fourth reference point also from RTCA ([2], Tables 6-3 and 6-4, pp. 20–21, Appendix B), material is reiterated by listing “vertical scan range” upper limits that never exceed zero degrees above the broadside axis.

This background information from multiple informed technical sources seems to converge on a shared technical perspective that deployed US n77 band 5G MIMO base station arrays will not ordinarily or commonly, if ever, produce elevation beams at angles above, or at least not substantially above, the MIMO arrays’ local horizontal plane.

⁴⁴ There are three manufacturers of US n77 band 5G MIMO radio base stations whose products are being procured and deployed by carriers in the US. These manufacturers are referred to in this report as A, B and C.

⁴⁵ As they are referred to in the document.

4.5.2.2 Beam Elevation Angle Control for US n77 Band 5G MIMO Arrays

Regarding control of the antenna beam elevation angles through time, as the external UE locations shift, we are informed⁴⁶ that beams are not computed on the fly. Instead, large catalogs or codebooks of 5G antenna beams are ordinarily pre-computed and stored in what amount to look-up tables in 5G antenna-beam control software systems. These pre-computed beams are loaded and formed one after another in the US n77 band 5G 64T64R MIMO arrays as UEs move through each base station's coverage.

The UEs are therefore not tracked, *per se*, by the base station MIMO beams. Rather, optimal beam selections are taken from the codebooks for time-evolving DL/UL links to desired UEs, and for nulling to some extent against non-desired UEs. These individual selections are made on a discretely-stepped time-domain basis. The pre-computed beams are repeatedly located in the codebooks and formed one after another to maintain this desired UE coverage and nulling as the UE environment evolves in time. Beams that might theoretically be formable, but that have not actually been pre-computed and loaded into the codebooks are not (cannot be) formed by the MIMO arrays.

4.5.3 JI-FRAI Consideration of US n77 Band UE Operation Onboard Aircraft in Flight

Early in the development of its work program, JI-FRAI considered the possibility that terrestrial US n77 band 5G base station beams could be dynamically directed toward, and maintain DL/UL connections with, UEs inside airborne aircraft. This possibility had earlier been considered and discussed in [2]. JI-FRAI considered the material in this reference in its own early considerations of an airborne-UE/radalt testing mode for its work program.

Appendix B of [2] is a series of questions and answers between two groups in TWG-3 who are called wireless experts and aviation experts. Two of the TWG-3 Questions (5 and 8) raise the issue of operation of UEs in aircraft. In these Q&As, wireless experts state ([2], p. 145) that FCC rules (47 CFR Part 22.925⁴⁷) prohibit the use or operation of 5G UEs inside airborne aircraft in the US n77 band. They cite two reasons for the prohibition in their answer to Question 5: First, that the US 5G n77 band UEs will have cellular capability for multiple bands, including all currently prohibited FCC cellular bands; and second, that the Table of Allocations for the US 5G n77 band explicitly restricts the allocation to "mobile except aeronautical mobile" [11].

The wireless experts further state in their answer to Question 8 ([2], p. 149) that even if 5G UEs are turned on or left on when inside aircraft in flight, in violation of FCC rules, UEs in this band will in any event not successfully maintain sustainable DL/UL links in-flight inside aircraft for a number of technical reasons. Their stated reasons include: that 5G UEs will (cannot) not initiate transmissions "on their own" without having first identified a sustainable 5G base station signal;

⁴⁶ Various private communications with 5G carriers and manufacturers.

⁴⁷ Which is quoted in by one source as saying, in part, "The use of cellular telephones while this aircraft is airborne is prohibited by FCC rules, and the violation of this rule could result in suspension of service and/or a fine. The use of cellular telephones while this aircraft is on the ground is subject to FAA regulations."

that the UEs require a dominantly strong individual base station signal, which will not be found when dozens or hundreds of base stations within range of an aircraft are all competing at roughly the same signal strength at the UE; that propagation factors will be poor or unsustainable; and that aircraft fuselages will tend to shield against sustainable UL/DL connections.

The authors of [2] do address the possibility elsewhere in their report (Section 6.1.5, pg. 15; Section 6.3.3.3, pg. 29; Section 10.1.3, pg. 74; Section 10.5, pg. 85; 11.1.3, pg. 87; note on p. 164; note on pg. 177) that 5G UEs might somehow nevertheless operate inside aircraft cabins, in-flight, under one circumstance or another. The JI-FRAI QRT work program did not address the corner-case scenario of rogue UEs operating inside aircraft cabins in-flight. That would be a specialized sub-topic outside JI-FRAI's remit; it is however addressed briefly in Section 4.5.4.2.

4.5.4 Base Station Beam Elevations and Beam Control for the JI-FRAI QRT Work Program

4.5.4.1 MIMO Base Station Downtilt Angles and Controls for UEs Near the Ground

For the JI-FRAI QRT work program, a collective decision was made early⁴⁸ that by far the most realistic and likely scenario for 5G beam elevation angles in the US 5G n77 band would be for the MIMO base station beams to be downtilted between 1 and 2 degrees below the arrays' broadside axes, with the MIMO arrays' mechanical tilt angles being set to zero degrees.

The base stations' associated UEs would therefore need to be placed laterally from the MIMO arrays, at heights of a few feet above the ground, at distances that would give such downtilt angles. For example, for UEs that might be 1 m (~3 ft) above the ground communicating with MIMO arrays at 10 m (~30 ft) above the ground, a lateral separation distance of 400 m (~1300 ft) would give a downtilt angle of -1.2 degrees.

The UEs would remain stationary during testing. Keeping them stationary would keep the MIMO base station beam directions in space, and hence their associated overall radiation patterns, constant in time. This constancy would in turn provide for constant and consistent field strength levels in space that could be measured once at each testing location and then be used in subsequent analysis of testing results. The 5G base stations' automatic controls for establishing beam directions for the DL/UL communications with the UEs, and for maintaining those beam directions through time, would be used.

This scenario of a slight down-tilt for the 5G MIMO base station antenna beam elevation angles was used for JI-FRAI JT&E. It was likewise used for the work described in this report that was performed at the Table Mountain Radio Quiet Zone north of Boulder.

⁴⁸ In numerous live-discussion meetings of the JI-FRAI sub-working groups.

4.5.4.2 Operating UEs Onboard Aircraft in Flight

The possibility and desirability of operating UEs onboard aircraft in flight was initially considered for inclusion in the JI-FRAI QRT work program. Based on the factors described above in Section 4.5.3, JI-FRAI members' consensus was that the occurrence of time-sustained communications between 5G base stations and airborne UEs represented an engineering corner case that was unlikely, albeit not necessarily physically impossible. The JI-FRAI QRT work program, which was not open-ended and had to be completed within defined limits of time and funding, needed to focus on 5G/radalt coexistence engineering cases that were operationally likely and realistic.

Moreover, the real-world engineering challenges and difficulties of establishing and maintaining sustainable, measurable, and calibrated UL/DL communications between terrestrial base stations and airborne, in-flight UEs with 5G software and hardware that were categorically not designed to perform that way would have been substantial. It was concluded that any such tasking would probably go beyond the scheduling and funding resources of the JI-FRAI QRT work program.

Attempting such an effort would have entailed setting up an entirely separate engineering sub-program just to design, build, and verify the necessary engineering testbed for in-flight UE testing, with a concomitant diversion of JI-FRAI resources from the main target focus of the overall work program. In consideration of all these factors, the JI-FRAI QRT work program maintained focus on the core goal of understanding the interactions of 5G transmissions with radalt receivers for terrestrial-only communication links, at base station downtilt angles of 1 to 2 degrees below local horizontal. In the event that future commercial applications put UEs on board aircraft, this topic might need to be revisited.

4.6 Examples of Computed 5G MIMO Antenna Patterns for 3 GHz Spectrum

The phased-array nature of MIMO arrays, with precisely geometrically arranged and defined sets of phased dipole pairs, lends itself to theoretical numerical analysis and simulation of these antennas' radiation patterns. Figures 19 through 24 show some examples of these predicted radiation patterns for MIMO antennas in the 3300–3900 MHz (3 GHz) portion of the spectrum.⁴⁹

Taken in order, the first pattern (Figures 19 and 20) is for a narrow azimuthal beam. Its width is about $\pm 5^\circ$ at its half-power (3 dB) azimuthal points. It might be used for an established link with a UE, and would be supposed to tend to discriminate against non-desired UE links.

The second pattern (Figures 21 and 22) is for an intermediate azimuthal width. Its width is about $\pm 8^\circ$ at its 3-dB azimuthal points. Like the first pattern, it might be used for an established link with a UE.

⁴⁹ We thank Dr. Steven Best of MITRE for the patterns shown in Figures 19 and 20. The other patterns have been graphed from some manufacturers' 5G MIMO array antenna specification descriptions.

The last pattern (Figures 23 and 24) is for a beam with wide azimuth and low discrimination against non-desired UEs. Its width is about $\pm 20^\circ$ at its 3 dB azimuthal points. It might be used for signals that allow new UEs in its coverage zone to begin communicating with the base station.

In the elevation dimension, all three examples show significantly lower radiation power above their local horizontals than in their downtilted main beams. There is a tendency to develop a relatively high sidelobe (between -10 dB to -20 dB down, relative to the main beam's gain) at elevation angles between 10° to 20° above their local horizontals. All three examples show deep nulls in their predicted patterns at elevation angles between 60° to 90° above their local horizontals (i.e., within 30° of their zeniths). The radiation pattern measurements at Table Mountain, as described in Section 8 this report, can be compared to these examples.

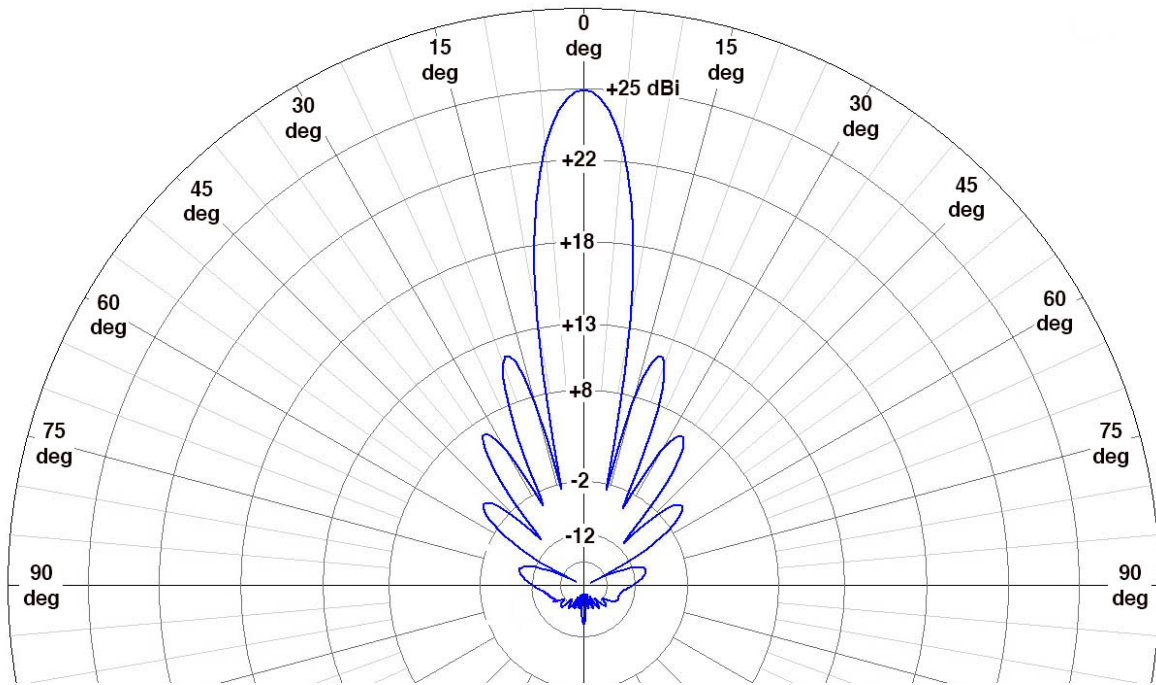


Figure 19. Azimuthal computed pattern for a 3 GHz band MIMO array antenna. Courtesy and permission of MITRE.

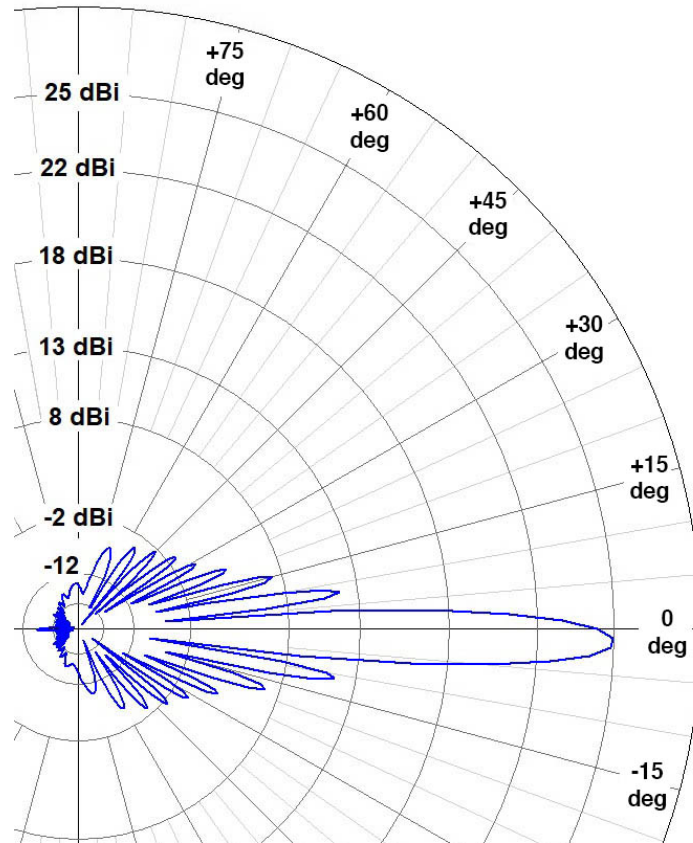


Figure 20. Elevation computed pattern for a 3 GHz band MIMO array antenna. Courtesy and permission of MITRE.

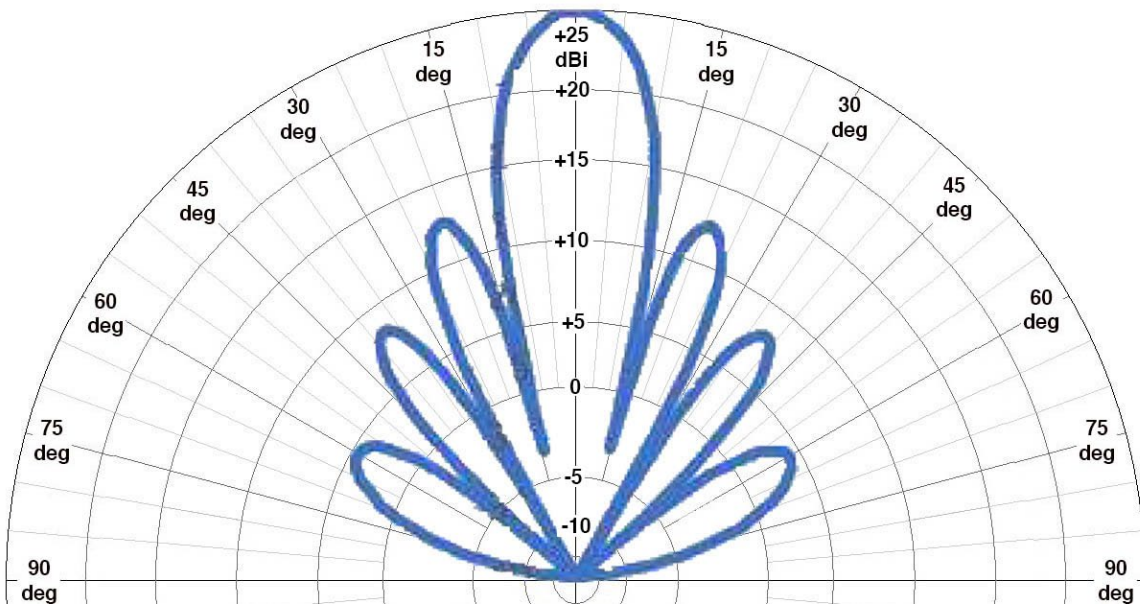


Figure 21. Azimuthal computed pattern for a 3 GHz band MIMO array antenna, from a manufacturer's specification.

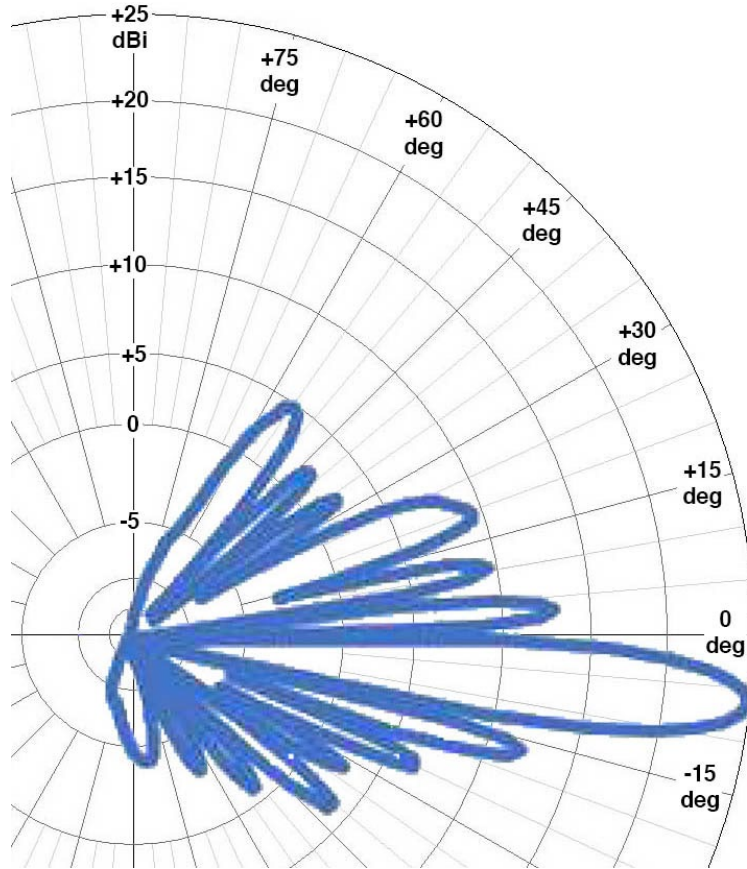


Figure 22. Elevation computed pattern for a 3 GHz band MIMO array antenna, from a manufacturer's specification.

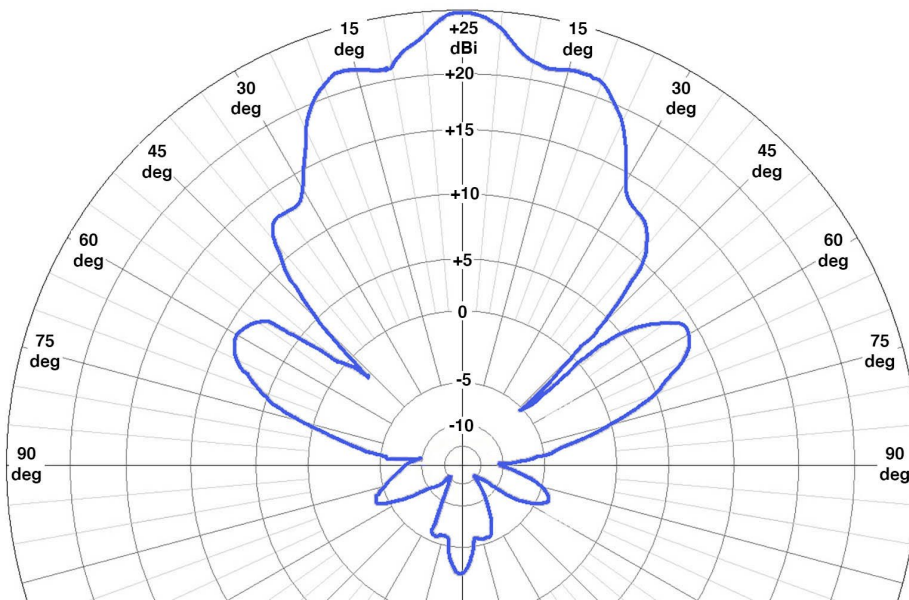


Figure 23. Azimuthal computed pattern for a 3 GHz band MIMO array antenna, from a manufacturer's specification.

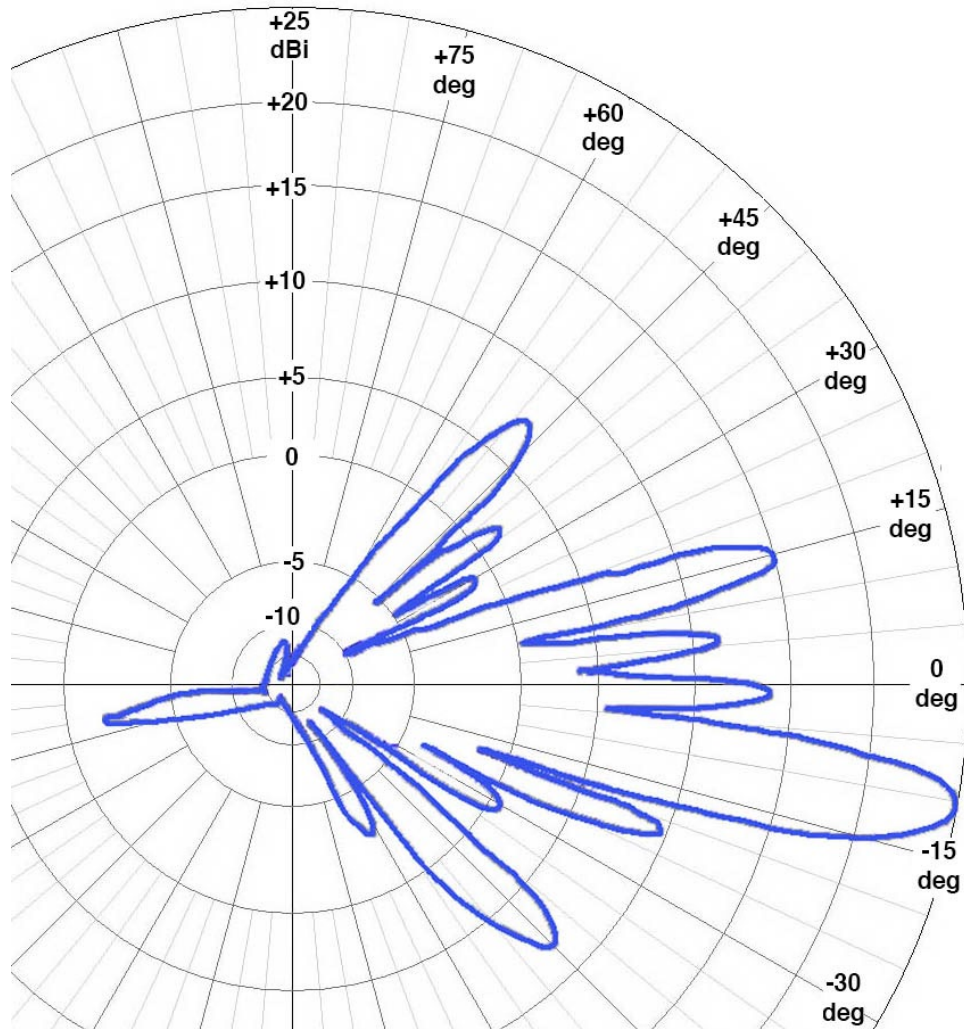


Figure 24. Elevation computed pattern for a 3 GHz band MIMO array antenna, from a manufacturer's specification.

5. POTENTIAL INTERFERENCE MECHANISMS FOR COEXISTING 5G TRANSMITTERS AND RADALT RECEIVERS

There are two possible RF interference mechanisms for transmitted 5G signals to radalt receivers. These are described here as concisely as possible, along with their respective implications for any mitigation options.

5.1 Co-Channel (to Radalt Receivers) RF Interference from 5G Unwanted Emissions

All transmitters produce non-zero spectrum emission power in frequencies other than their licensed, intentionally radiated frequencies. The radiation that falls just beyond the intentionally frequency or bandwidth of transmitter is called the out-of-band emission (OOBE). Other power that is radiated in even more extended parts of the spectrum is termed spurious. Together, these unintentional radiations are called “unwanted.”

All US n77 band 5G transmitters will produce some level of unwanted emissions within the 4200–4400 MHz band of radalt receivers. This condition is shown schematically in Figure 25. The question is, how high will those emissions’ unwanted power be in that band, versus what is the threshold at which such emissions will produce harmful interference to radalt receivers?

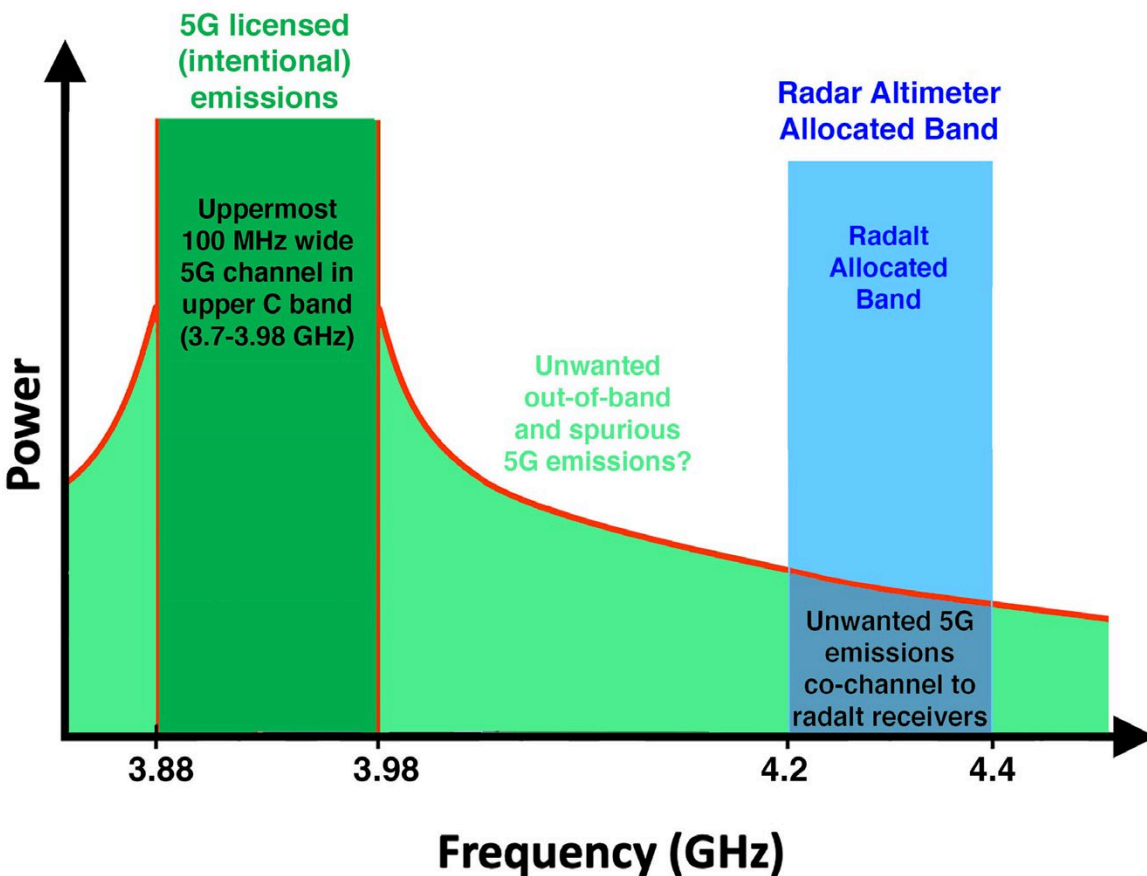


Figure 25. Schematic representation of 5G unwanted emissions within the radalt receivers’ band.

5.2 Out-of-Band (to Radalt Receivers) RF Interference from 5G Intentional Emissions

Although the scenario described above may be the most obvious, there is a second coupling mechanism whereby radalt receivers may experience harmful interference. In this interference mechanism, the radalt receivers “see” RF interference from the licensed, intentional RF emissions of 5G transmitters. This is diagrammed schematically in Figure 26.

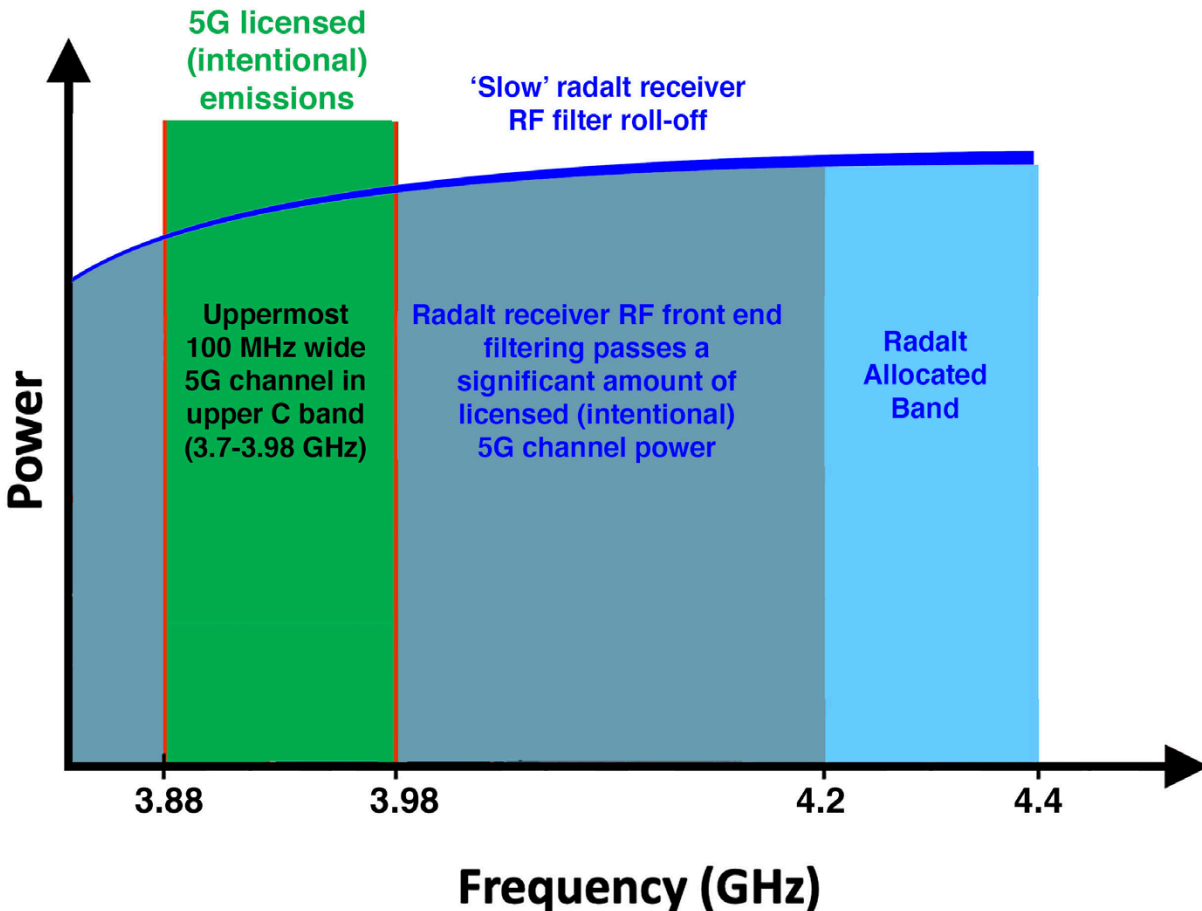


Figure 26. Schematic representation of 5G desired (intentional) emissions producing harmful interference to radalt receivers due to insufficient radalt receiver RF filtering.

In this interference mechanism, the radalt receivers’ RF front ends have such a wide frequency-response range that they “see” intentional 5G transmitter radiation power within their circuitry. This power is sufficiently high that it causes interference effects.

Such effects might be due to intentional-frequency transmitter power being so high that the low noise amplifiers (LNA) in the radalt receivers (see Figures 9 through 11) could experience overload. This receiver-LNA overload condition is described in [18] for a historical EMC problem between coexisting high-power radar transmitters running near 3 GHz and television receive only (TVRO) satellite downlink receivers operating in the 3700–4200 MHz band.

Interference effects might occur at power falling below the LNA overload threshold but nevertheless high enough to corrupt either acquisition or tracking, or to exceed receiver loop-loss limitations (see Sections 3.9 and 3.10, above) of radalt receivers.

5.3 Avoidance of Both Potential Interference Mechanisms

The key to avoiding either (both) of these interference mechanisms is for 5G unwanted emission power levels to be sufficiently low within the radalt band; and for radalt receivers to not “see” 5G intentionally-radiated power in 5G licensed channels. This condition is shown schematically in Figure 27.

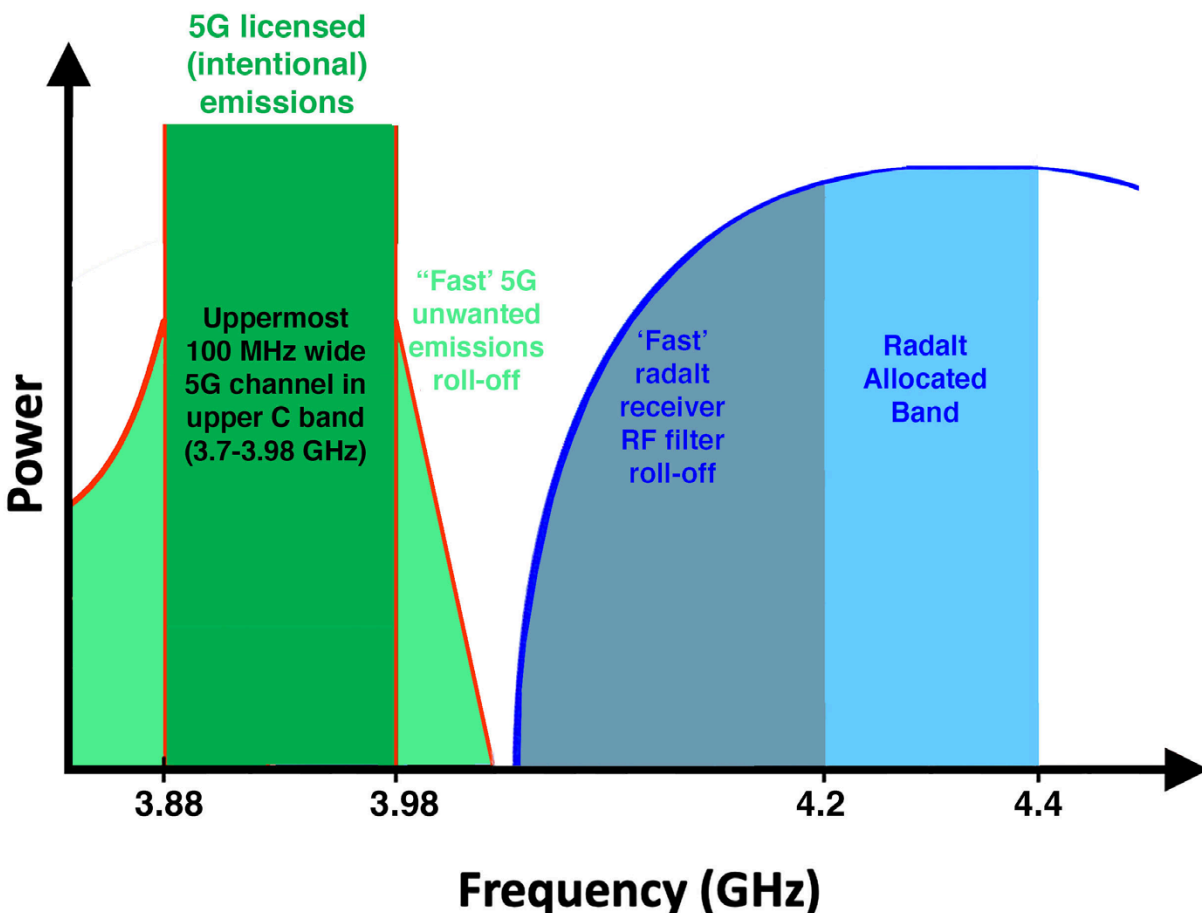


Figure 27. Ideal spectrum filtering and roll-off for avoiding *both* potential interference mechanisms between adjacent-band 5G transmitters and radalt receivers.

Achieving mutual adjacent-band spectrum electromagnetic compatibility can require careful and effective RF filtering of both 5G transmitter outputs and radalt receiver RF front end inputs. The 5G transmitter filtering will ideally be placed *after* the PA outputs, between the PA and the antenna radiating elements. The radalt receiver filtering will ideally be placed *before* the LNA inputs, between the receiving antennas and the receiver LNAs.

Although not the subject of this report, we note that such filtering is also crucially important in RF bench testing of 5G interference to radalt receivers. This is because, without careful filtering of transmitted interference signals and victim receiver inputs, it is impossible to know which interference mechanism is occurring.

5.4 Dependence of Harmful Interference Mitigation on the Interference Mechanism

Each potential interference mechanism has its own, independent mitigation option. If interference is due to 5G unwanted emissions within the 4200–4400 MHz band, then the 5G transmitters need to be more effectively filtered across that frequency range.

If, conversely, interference is caused by radalt receivers coupling power from 5G intentional, desired emissions, then the radalt-based solution is to implement better, more effective RF filtering in radalt receiver RF front ends. (This is as opposed to a 5G transmitter-based solution of turning off 5G transmitters in some areas altogether or else reducing their base stations' effective radiated power levels.) Radalt receiver de-coupling from 5G intentional emissions might conceivably be done by retrofitting existing radalt receivers with improved RF filters. Or it might be accomplished by replacing some radalt models with newer models incorporating more effective input filtering in their receiver front ends.

Again, effective mitigation of RF interference, if any is present, depends critically on understanding exactly which mechanism is occurring, or even whether both mechanisms are occurring.

5.5 Note on OOB and Spurious Mask Limits for Unwanted Emissions from Transmitters

We note that it is a common practice to make EMC computations and then predict the possibility of interference from transmitters (all and any transmitters, not just 5G) to subject receivers (not just radalts) by basing the computations on statutory emission mask limits on OOB and spurious-emission power levels. Such mask limits might for example be published as FCC limits in the CFR; or in International Telecommunication Union Radiocommunication Section (ITU-R) Radio Regulations or Recommendations; or might be other published limits such as are found in the Radar Spectrum Emission Criteria (RSEC) described in Chapter 5 of the NTIA/OSM Red Book [11].

While such mask-based EMC computations are not wrong *per se*, and may prove to be useful for many purposes, we have found that they may have limited predictive power for real-world EMC situations. The reason is that *actual* unwanted spectrum emission levels from many transmitters can routinely fall well below (-10 or -20 dB below) those transmitters' regulatory spectrum mask limits. Examples of this phenomenon are found in [12] and [13], where measured OOB and spurious emissions of LTE-type transmitters are seen to be substantially lower than the applicable emission masks for those units.

With this factor in mind, in this study we have measured radiated 5G base station transmitter emissions with 90 dB of dynamic range, across the frequency range of 3500–4400 MHz, at the Table Mountain Radio Quiet Zone facility. The results are shown in Section 9 of this report.

6. BASE STATION AND UE SETUP FOR MEASURING 5G EMISSIONS

In this section, we describe our methodologies and approaches for (a) measuring radiated 5G base station transmitter emission spectra; (b) measuring three-dimensional (3D) radiation patterns in space around those 5G MIMO arrays with helicopter-mounted equipment; and (c) using ground-based monitoring to verify the 5G base station transmitters' performance and operational modes during the airborne data collections.

6.1 Table Mountain Measurement Location Description

The measurements described here were all performed outdoors at the Table Mountain Radio Quiet Zone⁵⁰ (Table Mountain) facility that is owned and operated by the US Department of Commerce. Table Mountain is located southwest of Longmont, Colorado, about halfway between Boulder and Lyons. Figure 28 shows an overview of the site.

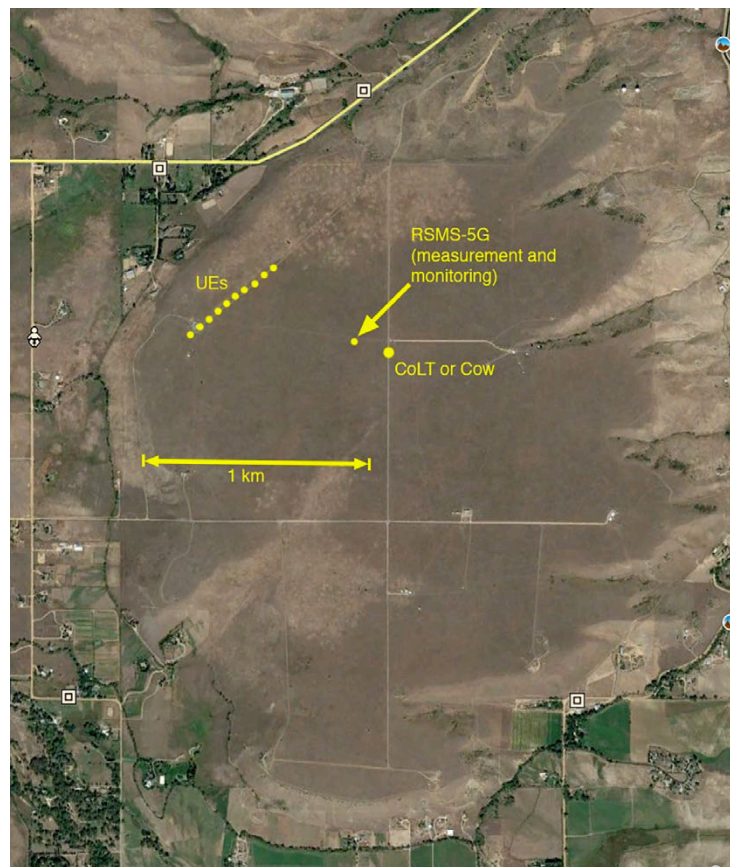


Figure 28. Overview of Table Mountain with the northeastern area where upper C-band 5G MIMO transmitter emissions were measured. Imagery data ©2021 Google.

⁵⁰ See 47 CFR Ch. 1, § 1.924: Quiet Zones; and Section 8.3.19 in the NTIA/OSM Red Book.

The site is an un-watered, semi-arid flat mesa at about 1680 m (5,500 ft) above sea level. It extends ~3.5 km (2.2 mi) north-to-south and ~2.5 km (1.5 mi) east-to-west. It slopes downward from northwest to southeast at an average grade of about $-1/69 \approx -0.83^\circ \approx -1.45$ percent.

Table Mountain is alluvial, deposited from a source area in the foothills to the northwest. Truncated from its source by an intervening drainage, it is a topographically isolated island of locally high terrain. The ground is well-drained with no surface water. The soil is a well-compacted, coarsely conglomeratic, mostly unsorted Pliocene-Pleistocene alluvium of dirt, cobbles, and small metamorphic boulders. The flat, moderately rough ground can mostly be driven with all-terrain vehicles of medium ground clearance. The semi-arid climate sustains a moderately dense vegetative cover of native and introduced grasses, weeds, and yuccas. There are no trees. Buildings and other human-made structures, especially things made of metal, are few across the mesa. Looking across the mesa a visitor sees only flat ground with low grasses and essentially no buildings or other artificial infrastructure.

6.2 Base Station 5G Radios Operated at Table Mountain for the JI-FRAI Program

A total of four 5G MIMO-array base station transmitter models (called Base Station Radios 1 through 4) from three manufacturers (called A, B, and C) were set up and measured for emissions at Table Mountain for the JI-FRAI project. Their manufacturers and bands are shown in Table 7. Note that cellular base stations on trailers, with associated extensible masts and power generators, are called cells on wheels (CoWs). If the same base stations, masts and power generators are mounted in truck chassis they are called cells on light trucks (CoLTs).

Table 7. 5G MIMO base station radios deployed at Table Mountain for the JI-FRAI program.

5G MIMO Base Station	5G Radio Manufacturer	Operational Band	Number of Base Station Towers Deployed at Table Mountain	MIMO Arrays/Tower (# of arrays x azimuth coverage)
1	A	3300–3600 MHz (lower C-band)	2 CoWs	3 (3 × 120°)
2	B	3700–3980 MHz (upper C-band)	1 CoLT	1 (1 × 120°)
3	A	3700–3980 MHz (upper C-band)	1 CoW	1 (1 × 120°)
4	C	3700–3980 MHz ⁵¹ (upper C-band)	1 CoLT	1 (1 × 120°)

6.2.1 5G MIMO Base Station Radio 1, Lower C-band

Of these, Radio 1 from Manufacturer A was a lower C-band (3300–3600 MHz) 5G MIMO base station radio. Although it was not a candidate model for potential interference to radalt receivers, its antenna radiation patterns were measured as part of the JI-FRAI risk reduction effort undertaken prior to JT&E at Hill AFB, because other than its slightly lower frequency range (3300–3600 MHz versus 3700–3980 MHz, a frequency difference of only 11 percent), it shares

⁵¹ This radio’s manufacturer currently locks its emission frequencies to 3700–3800 MHz in the US.

the same 5G 64R64T MIMO architecture, TDD signaling structure, and emission modulations as its upper C-band siblings. It was deployed in a pair of CoWs arranged north-to-south on the western side of Table Mountain, as described in more detail in Section 6.4 below.

6.2.2 Base Station and UE Geometry for Radios 2 through 4, Upper C-band

The three remaining 5G MIMO base stations, Radios 2 through 4 from Manufacturers A, B and C, were upper C-band (US n77 5G band, 3700–3980 MHz) designs. *They are believed to be the only upper C-band 5G base station models that are, and will in the foreseeable future be, deployed in this band for this service in the US.* The radios were set up at Table Mountain with the geometry shown in Figures 28 (large-area view) and 29 (closer, more detailed view).

6.3 Table Mountain Geometry and Configuration of 5G Radio Models 2–4

Figure 29 shows the measurement geometry of the previous figure in more detail.

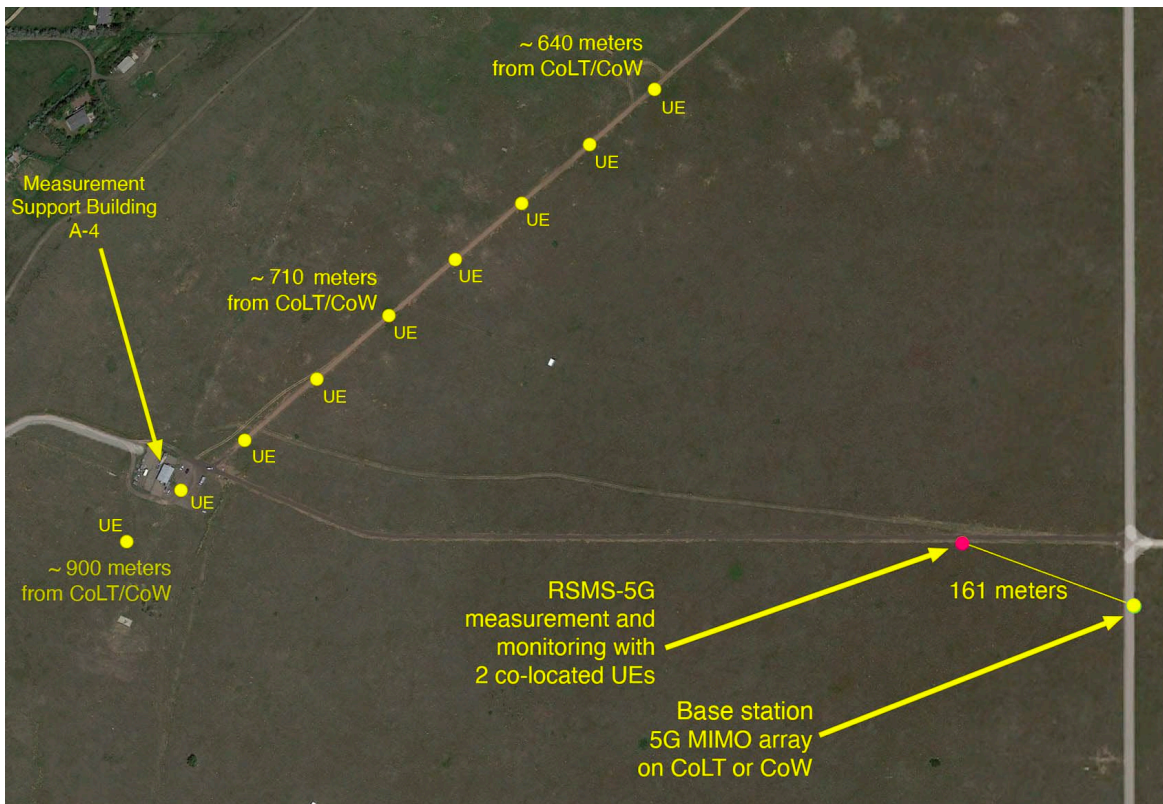


Figure 29. Detailed overview geometry of locations of 5G base stations; 5G UEs; and spectrum measurement and signal monitoring (RSMS-5G) at Table Mountain for the JI-FRAI project. Imagery data ©2021 Google.

Manufacturer A shipped a pair of their lower C-band Radio Model 1s to Table Mountain and set them up in a pair of CoWs as described in Section 6.4.

For base station Radios 2–4, US carriers who had themselves purchased these radio models brought them to Table Mountain for the JI-FRAI QRT work. One carrier brought two separate radio models (2 and 4) to Table Mountain and another carrier brought the third radio model (Radio model 3) to Table Mountain. Only *one carrier and one radio model* were ever present for testing at Table Mountain at any one time.

The setup and geometry of base station Radios 2–4 (all in upper C-band) were as follows. Each 5G base station was brought to Table Mountain by a US carrier. The mounting was always in a CoLT or a CoW. The base station and its auxiliary 5G-support (“core”) communication links were set up at the location shown in Figures 28 and 29, on the side of a smooth gravel north-south road. Powered by an on-board diesel generator, the 5G MIMO arrays would be raised on a (nominally) 10 m high mast. Auxiliary communication links (which included, variously, 14 GHz Ku band geosynchronous satellite; 700 MHz LTE; and 2.2 GHz MIMO) were connected to remote 5G network support. The base station was activated. Figure 30 shows one such CoLT during deployment.



Figure 30. An upper C-band (3700–3980 MHz) CoLT deployed at Table Mtn. The US 5G n77 band MIMO array is at right. Support links are a Ku-band (14 GHz) satellite dish and a UHF (700 MHz) LTE panel (upper left).

Meanwhile, a set of associated UEs was deployed as shown in Figures 28 and 29. The UEs were arranged on a line at a nearly right angle to the 5G MIMO array. The carriers brought their own UEs to each test. Ordinarily 9–11 UEs were deployed on this line at distances that ranged from about 640 m (2100 ft) to 900 m (3000 ft), with a median distance of about 700 m (2300 ft). Their mounting height was about 1 m (3 ft) above the ground on improvised supports such as plastic tabletops. They were provided with weather covers and external power supplies. One of these deployed UEs is shown in Figure 31.

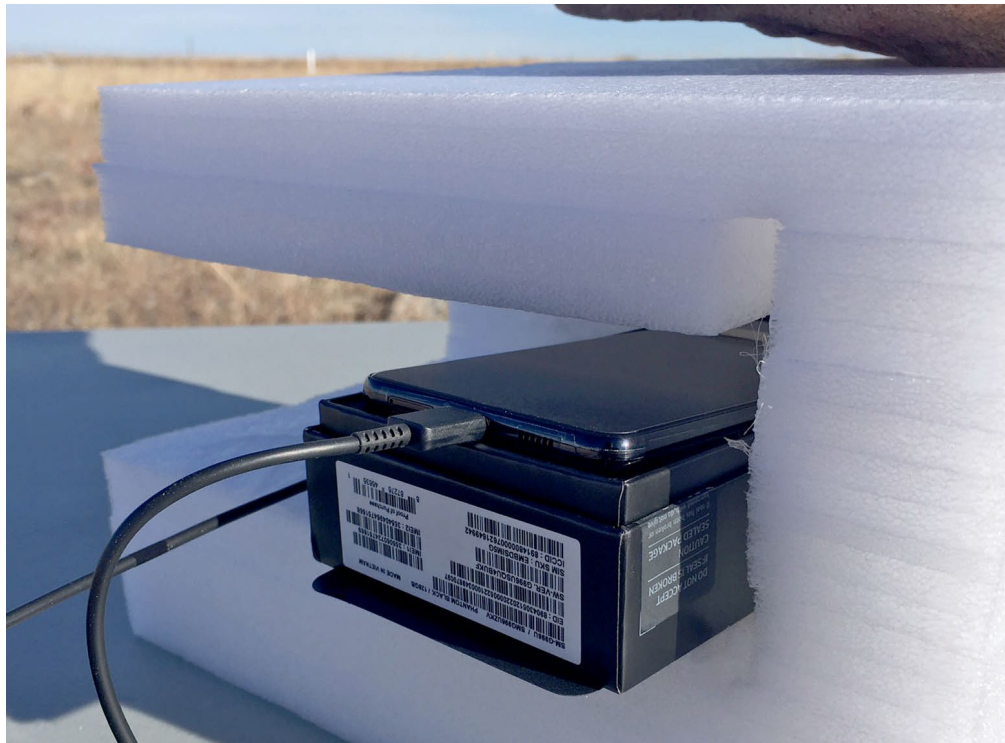


Figure 31. Example of a 5G-capable UE with an external power supply deployed on a plastic table top while supporting 5G base station measurements at Table Mountain.

One or two more UEs were set up at the RSMS V5. These were placed on the truck’s rear platform, 1 m (3 ft) high, and below the parabolic antenna (itself 4 m (13 ft) to 5.8 m (19 ft) high). Their location placed them in a dish null.

6.3.1 Downtilt Angles from Base Stations to UEs for 5G MIMO Radios 2–4

The downtilt angle from the base station MIMO arrays at 10 m height AGL to the distant line of UEs at a (median) distance of 700 m would nominally be about $\tan^{-1}(10/700) = -0.8^\circ$. Noting however that the overall average downward slant of the terrain at Table Mountain is -0.83° from NW to SE (see 6.1 above), and that the direction of the base station beams to the UEs was exactly opposite this gradient (SE to NW), the overall downward tilt from the base station MIMO arrays to the distant UEs was very near to zero degrees. Figures 32 and 33 further elucidate the Table Mountain base station, RSMS V5, and UE geometry for Radios 2–4.

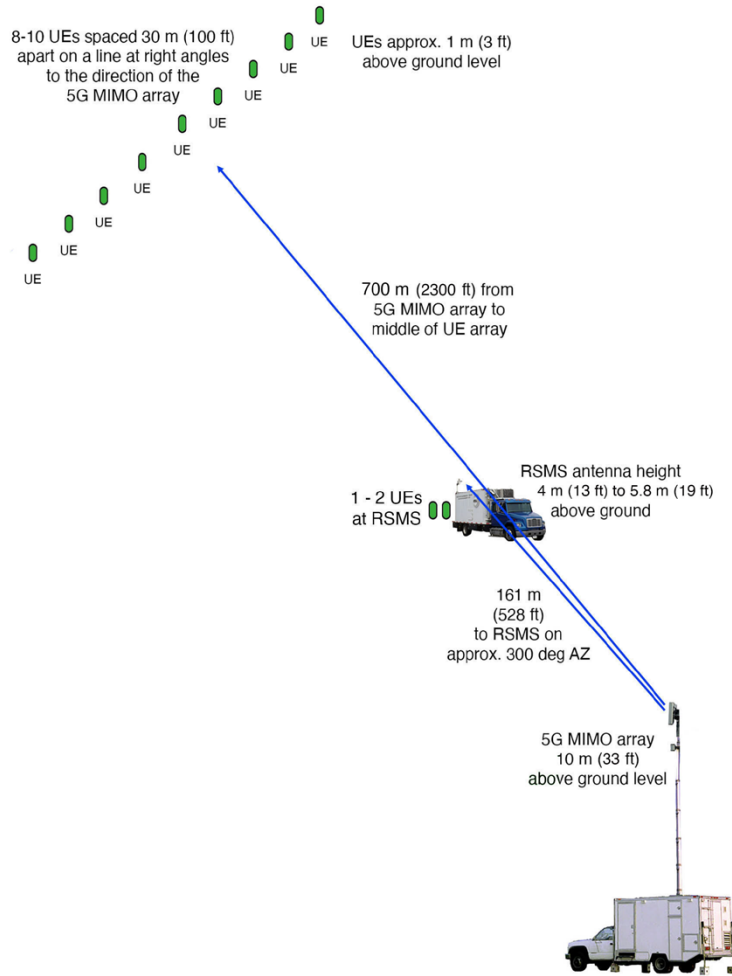


Figure 32. Overhead view of Table Mountain measurement geometry for 5G base station Radios 2-4.

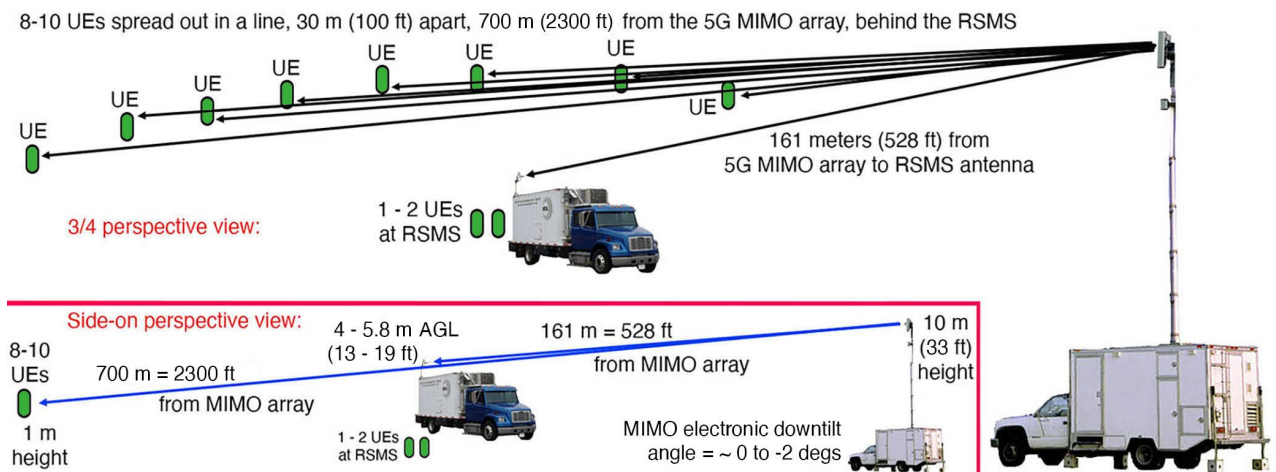


Figure 33. Side view and 3/4 view of the Table Mountain setup geometry for 5G base station Radios 2-4.

Similarly, the nominal downtilt from the MIMO arrays to the UEs on the back platform (1 m AGL) of the RSMS at 161 m from the arrays would nominally be $\tan^{-1}((10 - 1)/161) = 3.2^\circ$. But taking the 1/69 gradient (Section 6.1) into account, the MIMO array height would be dropped by another $161/69 = 2.3$ m, for an overall actual downtilt of $\tan^{-1}(10 - 1 - 2.3)/161 = \tan^{-1}(6.7/161) = 2.3^\circ$. This was roughly verified (to within an error of $\pm 0.5^\circ$) by one of the authors (F. Sanders) with an optical clinometer.

Thus, during the 5G measurements at Table Mountain, the bulk of the communications were being run between the base station MIMO arrays and the distant UEs at an elevation beam angle of very nearly zero degrees. A minority subset of MIMO beam communications was running to and from the RSMS V5 location at a MIMO elevation beam angle of about -2.3° below the MIMO array's broadside axis.

These elevation beam angles take into account the following factors: The *mechanical* tilt of the MIMO arrays was set to zero; the physical elevation angles to the various UEs were well within the capabilities of all of the 5G base stations that were measured (see Table 6); and within those outer-limit constraints, the MIMO arrays do automatically seek the optimal beam azimuths and elevation angles necessary to sustain the best-possible DL/UL quality.

6.3.2 Base Station to UE Communication (DL/UL) Quality During Table Mountain Measurements

As described above (Section 4.3.3), the carriers used 5G software tools such as Iperf and AILG to load their data networks at baseband and their channel PRBs at RF. They always maintained the maximum available EIRP output from their base stations. (We discuss base station EIRPs further, below.) Bandwidths were set manually. They were 100 MHz for Radios 2 and 3, and 60 MHz for Radio 4 (which was the maximum bandwidth that base station could transmit).

The base station to UE communication (DL/UL) quality was verified during measurements by manually spot-checking the UEs at various locations, including at the RSMS. Diagnostics in the UEs verified that the links were ordinarily sustained at the maximum possible modulation level of 256 QAM while measurements were in progress. Occasional, brief reductions to 64 QAM were observed. Lower levels of modulation were not observed.

6.4 Table Mountain Geometry and Configuration of 5G Radio Model 1

As noted above, base station Radio 1 represented a special case for both setup and operations. This system consists of a pair of CoWs that were built at Table Mountain for a larger project, of which JI-FRAI represents a subset for ITS. The 5G manufacturer (Manufacturer A, Table 7), rather than a carrier, brought the radios to the site and built them on a pair of trailers. One of these CoWs is shown in Figure 34. The masts on these CoWs are 12 m (40 ft) high.⁵² Each CoW

⁵² With a capability to extend to 18 m (60 ft) height if guy lines and ground anchors are deployed.

mast has three lower C-band (3300–3600 MHz) MIMO panel arrays installed at the top, for 360° azimuthal coverage. Figure 35 shows the CoW locations at Table Mountain.



Figure 34. One of the pair of Radio 1 CoWs at Table Mountain, with a set of three lower C-band (3300–3600 MHz) MIMO panels at the “normal” 12 m (40 ft) height.

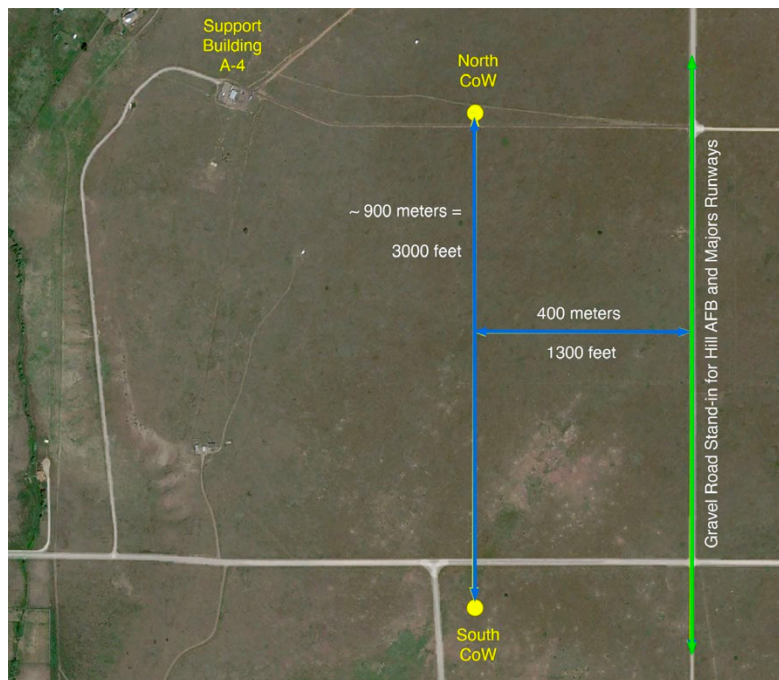


Figure 35. Lower C-band CoW locations at Table Mountain. This siting replicates the dual-CoLT siting at Hill AFB and Majors Field, with the Table Mountain N-S gravel road being in the same relative position as the runways at the airfields. Imagery data ©2021 Google.

6.4.1 Radio 1 5G Base Station Setup and Operation at Table Mountain

The pair of Radio 1 CoWs were built at Table Mountain in January 2022, well before any other 5G base stations (Radios 2 through 4) were available. Although the transmitter band for these radios is slightly lower (3300–3600 MHz) than the upper C-band (3700–3980 MHz), their MIMO panels are the same design and architecture (64T64R) with the same channel widths, antenna gain, and transmitter power as in upper C-band. Their 5G transmitted waveform is also identical to upper C-band, being equivalent to channel-limited Gaussian noise that operates on a 70 percent TDD duty cycle. These radios are the same as upper C-band units, but are just slightly down-shifted by about 11 percent in radio frequency.

Given that initial risk-reduction measurements needed to be performed at Table Mountain to verify airborne field strength measurement techniques prior to JT&E at Hill AFB, and that these CoWs produced the same signals at the same RF power levels with the same modulations, radiation patterns, and bandwidths as upper C-band base stations, we and JI-FRAI undertook airborne measurements with these units first, in January, while we were still awaiting availability of *any* upper C-band 5G base stations in the US.

Working with Manufacturer A, we had the two Radio 1 CoW trailers built 900 m (3000 ft) apart, the same inter-unit spacing as would be used at Hill AFB and Majors Field. We put them on a north-south line that was parallel to a north-south gravel road at Table Mountain (see Figure 35). This was the same layout relative to the road as was planned for the dual-CoLT 5G base station locations relative to the two airfield's runways (see Figure 36).

Regarding transmitted signals, no UEs could be used with the Radio 1 CoWs because no 5G core was available for them in the US. Without any UEs, the two CoWs were operated in a stand-alone maintenance mode. In this mode, they transmitted a 70 percent duty cycle TDD signal, looking like channel-limited Gaussian noise with no actual DL/UL connection to anything. Their EIRP was set to the maximum available (+77.5 dBm), and their bandwidth was set at 100 MHz.

Their antenna patterns were static. They were similar to Figures 23 and 24, wide in azimuth and narrow in elevation angle with as much as -3° of electronic downtilt available. Their signals were monitored from a fixed installation (Building I-10C) at Table Mountain (just east of the lower right corner of Figure 35) in lieu of the RSMS-5G.⁵³

6.5 March 2022 Hill AFB Setup and Measurements

The base station and UE setup of Figure 35 was a replication of what would be set up in the following week (of March 2, 2022) at Hill AFB in Utah. At Hill AFB, a pair of CoLTs using Radio Model 2 were deployed with associated UEs as shown in Figure 36. The JT&E that was performed there, with the two CoLTs communicating with the UEs at full power, will be described in a separate JI-FRAI report. For our work, the three dimensional radiation patterns

⁵³ Wideband, wide dynamic range measurements of these CoWs' emission spectra are provided in Appendix C of this report.

generated by the two Hill AFB CoLTs were measured, airborne, using the same UH-60, measurement system, and pilots as had been done earlier at Table Mountain.

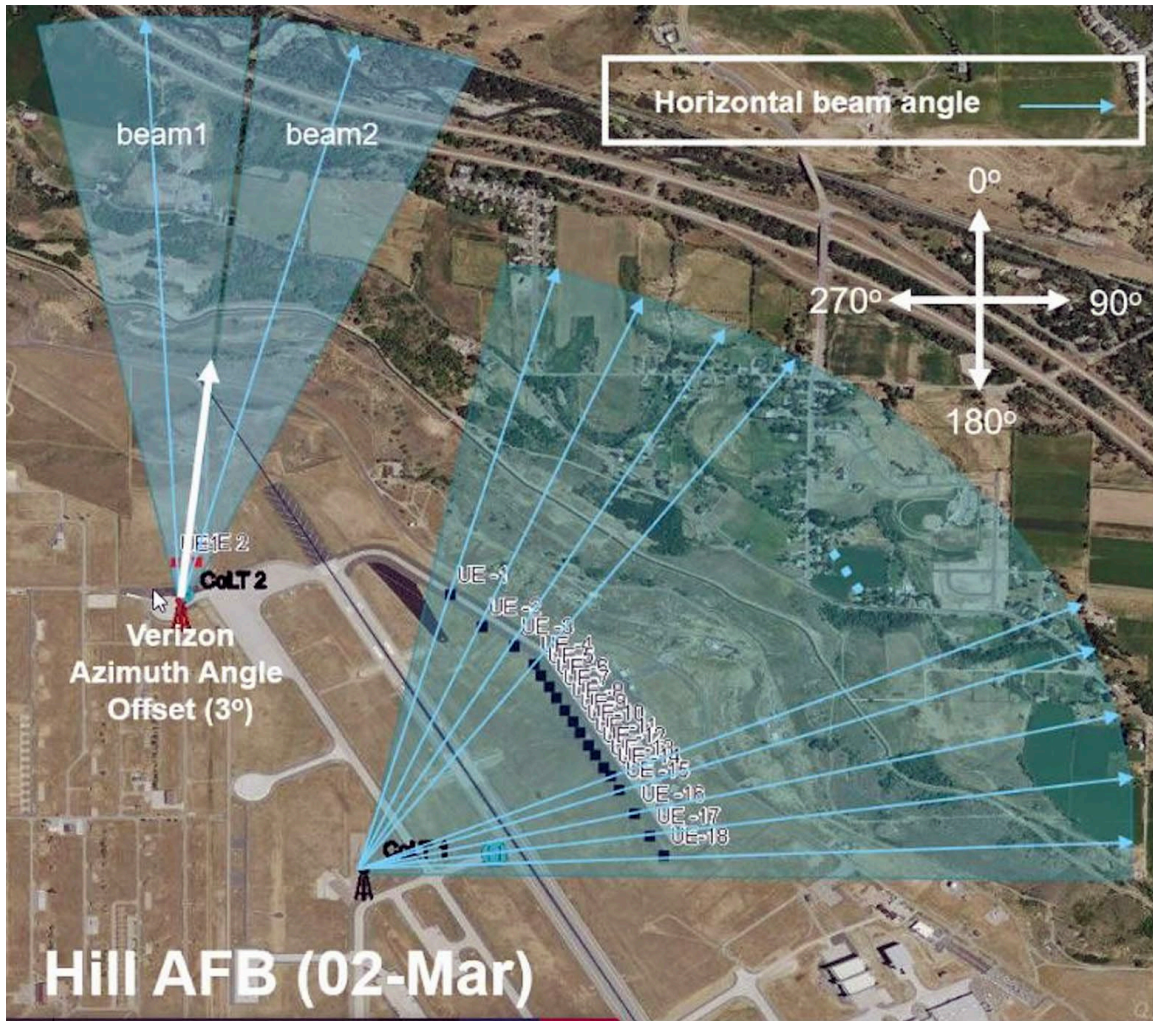


Figure 36. Layout of two CoLTs and UEs at Hill AFB, earlier replicated at Table Mountain. Imagery data ©Google

6.6 Schedule and Completed Measurements at Table Mountain and Hill AFB for 5G Base Station Radios 1 Through 4

Table 8 shows the measurements performed for JI-FRAI at Table Mountain on the 5G base station transmitters, Radios 1 through 4. The measurements dates are included. A normal setup and operations routine was to bring the transmitters on-site and get them running with their auxiliary links on the first day. The second day was devoted to verifying proper transmitter operation including verification of beam-tilts. Wideband, wide dynamic range spectrum measurements were performed on the second day as well. Airborne measurements were performed on the third day, with the RSMS V5 used as a monitor to verify transmitter operation on the selected channel, EIRP output, and TDD modulation while the data collection helicopter

flew overhead. The fourth day was a bad-weather backup date, which we did need for the measurements on the two lower C-band CoWs in January.

Table 8. Schedule and completed measurements for 5G base stations at Table Mountain and Hill AFB for JI-FRAI.

5G MIMO Base Station Radio Model	5G Radio Manufacturer	Location	Dates Measured	Wideband, Wide Dynamic Range Emission Spectrum	3-D Airborne Radiation Patterns
1 (lower C-band)	A	Table Mtn	18–21 January 2022	No (because not upper C-band)	Yes
2 (upper C-band)	B	Table Mtn	8–10 February 2022	Yes	Yes
3 (upper C-band)	A	Table Mtn	9–11 May 2022	Yes	Yes
4 (upper C-band)	C	Table Mtn	7-9 June 2022	Yes	Yes
2 (× 2) (upper C-band)	B	Hill AFB	26 February–4 March 2022	No (because already measured at Table Mtn)	Yes

6.7 Summary Table of 5G Base Station Radio Model Characteristics

Table 9 summarizes the specified (not measured) technical characteristics of 5G base station Radio Models 1 through 4.

Table 9. Specified technical characteristics of 5G base station transmitters 1 through 4.

Characteristic	5G Base Station Transmitter Radio 1	5G Base Station Transmitter Radio 2	5G Base Station Transmitter Radio 3	5G Base Station Transmitter Radio 4
Manufacturer	A	B	A	C
Compliance Standard	3GPP NR	3GPP NR	3GPP NR	3GPP NR
Frequency Range	Band n78 3300–3600 MHz	Band n77 3700–3980 MHz	Band n77 3700–3980 MHz	Band n77 3700–3980 MHz (but currently locked by the manufacturer to only operate 3700-3800 in the US)
Radio Head Ports	64	64	64	64
Max Power per Port	3.125 W	Up to 5 W	3.125 W	3.125 W
Nominal Total Max Output Power	200 W +53 dBm	320 W +55 dBm	200 W +53 dBm	200 W +53 dBm
Available Channel Bandwidths	20 MHz 40 MHz 100 MHz	20 MHz 40 MHz 60 MHz 100 MHz	20 MHz 40 MHz 100 MHz	60 MHz

Characteristic	5G Base Station Transmitter Radio 1	5G Base Station Transmitter Radio 2	5G Base Station Transmitter Radio 3	5G Base Station Transmitter Radio 4
Modulations	QPSK, 16 QAM, 64 QAM, 256 QAM	QPSK, 16 QAM, 64 QAM, 256 QAM	QPSK, 16 QAM, 64 QAM, 256 QAM	QPSK, 16 QAM, 64 QAM, 256 QAM
Modulation Codes (per NTIA OSM Red Book)	18M5G7D (QPSK) 18M5W7D (16, 64, 256 QAM with OFDM) 38M5G7D (QPSK) 38M5W7D (16, 64, 256 QAM with OFDM) 98M5G7D (QPSK) 98M5W7D (16, 64, 256 QAM with OFDM)	18M5G7D (QPSK) 18M5W7D (16, 64, 256 QAM with OFDM) 38M5G7D (QPSK) 38M5W7D (16, 64, 256 QAM with OFDM) 58M5G7D (QPSK) 58M5W7D (16, 64, 256 QAM with OFDM) 98M5G7D (QPSK) 98M5W7D (16, 64, 256 QAM with OFDM)	18M5G7D (QPSK) 18M5W7D (16, 64, 256 QAM with OFDM) 38M5G7D (QPSK) 38M5W7D (16, 64, 256 QAM with OFDM) 98M5G7D (QPSK) 98M5W7D (16, 64, 256 QAM with OFDM)	58M2G7D (QPSK) 58M4W7D (16, 64, 256 QAM with OFDM)
Channel Duplexing (Frame Type) (DL/UL)	TDD 70% DL (base station) 30% UL (UEs) Observed timing is 35 ms base station (DL) transmit, 15 ms UE (UL) transmit	TDD 70% DL (base station) 30% UL (UEs) Observed timing is 3.5 ms base station (DL) transmit, 1.5 ms UE (UL) transmit	TDD Nominal 75% DL (base station) (but only 70% observed) 30% UL (UEs) Observed timing is 3.5 ms base station (DL) transmit, 1.5 ms UE (UL) transmit	TDD 74% DL (base station) 26% UL (UEs) Observed timing is 3.7 ms base station (DL) transmit, 1.3 ms UE (UL) transmit
MIMO Antenna Design	64T64R MIMO	64T64R MIMO	64T64R MIMO	64T64R MIMO
Antenna Elements	128 (8 × 8 × 2 pol) crossed dipole subarrays	128 (8 × 4 × 2 pol) crossed dipoles	128 (8 × 8 × 2 pol) crossed dipoles	128 (8 × 8 × 2 pol) crossed dipoles
Spatial MIMO Streams	Up to 4	Up to 4	Up to 4	Up to 4
Nominal Antenna Gain (dBi)	+21.5 dBi (typical) +24.5 dBi (max)	+24.5 (typical) +26.65 dBi (max)	+24.5 dBi	+25.5 dBi
Maximum EIRP (average detected)	56.2 kW +77.5 dBm	56.2 kW +77.5 dBm	56.2 kW +77.5 dBm	70.8 kW +78.5 dBm
Azimuthal Beam Scanning Limits (per MIMO panel)	±60° (120° total)	±60° (120° total)	±60° (120° total)	±60° (120° total)
Azimuthal Half Power Beam Widths	10° for a nominal “spot beam”	11°	10°	10°
Elevation Beam Scanning Limits	±3°	+7° (above horizontal) to -19° (below horizontal)	±3°	+3° (above horizontal) to -10° (below horizontal)

Characteristic	5G Base Station Transmitter Radio 1	5G Base Station Transmitter Radio 2	5G Base Station Transmitter Radio 3	5G Base Station Transmitter Radio 4
Elevation Half Power Beam Widths	12°	6°	12°	11°
Antenna Polarization	±45° (cross-polarized)	±45° (cross-polarized)	±45° (cross-polarized)	±45° (cross-polarized)

7. MEASURING 5G MIMO BASE STATION EMISSION SPECTRA

7.1 Approach for Measuring 5G MIMO Base Station Emission Spectra

Most spectrum measurement systems attain a maximum dynamic range of about 60 dB. This includes conventional spectrum analyzers and signal analyzers. Such dynamic range is inadequate for measuring 5G MIMO emission spectra in this project, where we needed a least 90 dB of dynamic range to observe possible unwanted emissions in the radalt band between 4200 and 4400 MHz.

We instead implement a custom-designed and engineered (hardware and software) spectrum measurement system. Called the NTIA/ITS Radio Spectrum Measurement Science (RSMS) system,⁵⁴ and now in its fifth generation of design (RSMS-5G),⁵⁵ it is capable of up to 130 dB of dynamic range in its spectrum measurements. The system was originally designed to measure radar emissions. It has turned out that the radar-measurement design is pre-adapted to measuring emissions from MIMO base station antenna arrays.

7.1.1 RSMS-5G Hardware

The schematic core of the RSMS-5G is shown in Figure 37. The measurement antennas are selectable; for 5G base station emission measurements a 0.5 m diameter parabolic dish reflector with a 1–18 GHz log periodic feed was selected. This antenna is shown along with a 5G MIMO array mounted on a cell on light truck (CoLT) during a JI-FRAI measurement at Table Mountain.

⁵⁴ Its first generation was developed in a special joint technical effort between NTIA/ITS and the Hewlett Packard Company in Santa Rosa California in the mid-1970s. It was the world's first computer-controlled spectrum analysis system, the precursor of the later HP-8566 and HP-8568 spectrum analyzers.

⁵⁵ "5G" in the term RSMS-5G refers to the generation of RSMS software, not the generation of cellular technology.

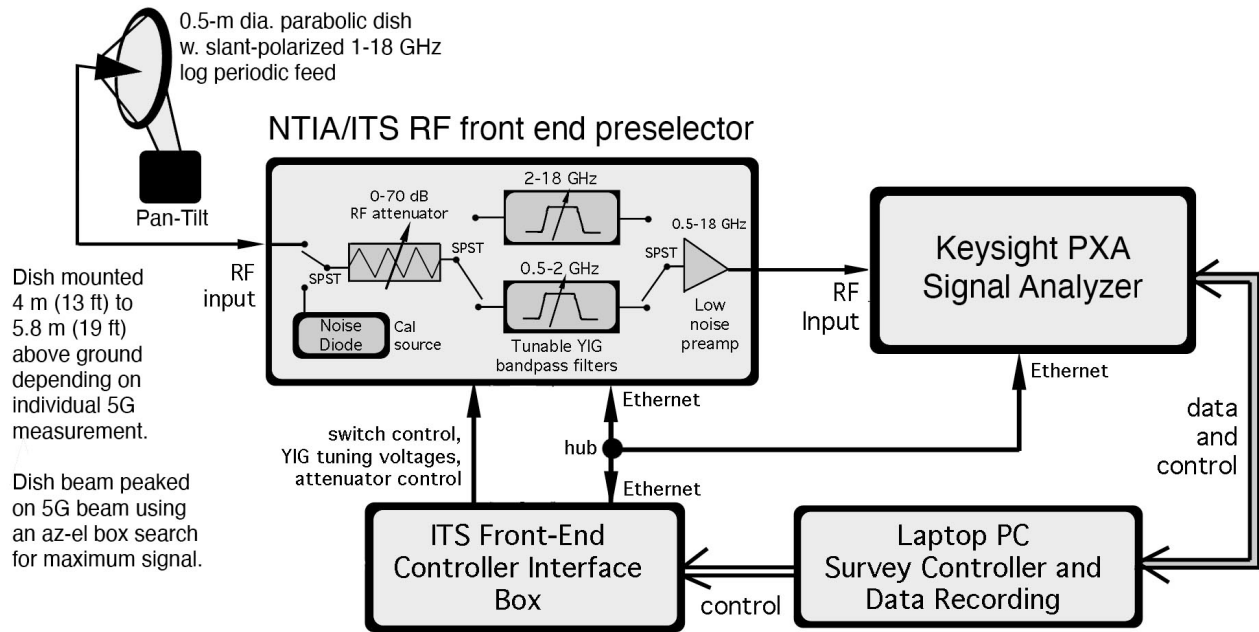


Figure 37. Schematic of the critical hardware core of the NTIA/ITS RSMS-5G.

The configuration of Figure 38 for the relative positioning of the MIMO arrays being measured for spectrum and being monitored during airborne measurements, relative to the RSMS-5G measurement antenna, was used for all three of the US n77 5G band radios at Table Mountain.



Figure 38. RSMS-5G measurement antenna (front & back) with a target 5G MIMO CoLT in the background, at 161 m distance. RSMS antenna heights were between 4 m (13 ft) and 5.8 m (19 ft) AGL, depending on circumstances. MIMO arrays were at ~10 m (33 ft) AGL. (A UE is on the rear platform at the base of the mast.)

Following the antenna is the RSMS RF front-end box. This unit, custom designed and built by ITS, works as follows.

7.1.1.1 Pre-Measurement Gain and Noise Figure Calibration

Prior to performing any measurement, a noise diode in the front-end box is switched to the RF input in lieu of the measurement antenna. The diode is alternately turned on and off while the power flowing through the measurement system is measured across the frequency range that will be used for the planned measurement (e.g., across 3000 MHz to 4400 MHz for the JI-FRAI spectrum measurements). Using the measured decibel difference between power observed in the diode ON versus OFF condition, along with the known, pre-calibrated excess noise ratio (ENR) of the noise diode, the custom-written computer software computes the gain and noise figure of the measurement system as a function of frequency. The noise figure data are stored for future use. The gain data are used to later correct the indicated power level in the measurement system to the true power level that the antenna is putting into the front end of the measurement system. All of this is performed under automated control, the operator only inputting the desired frequency range for each calibration. The uncertainty in the calibration is about ± 0.5 dB.

7.1.1.2 Dynamic Power-Range Control

Although the dynamic range of the system's signal analyzer or spectrum analyzer is ordinarily 60 dB, we extend that dynamic range using a variable, stepped-level RF attenuator. This attenuator has levels of 0 dB to 70 dB of attenuation, available in 10 dB steps. Adding the 70 dB of the attenuator to the instantaneous 60 dB of the down-stream analyzer gives a maximum measurement dynamic range of 130 dB (non-instantaneous).

This extension of dynamic range depends on two additional factors: the use of a stepped-frequency instead of a conventional swept-frequency spectrum-coverage algorithm (described below); and having enough power available from a transmitter to illuminate its emission spectrum that far down.

In practice, our dynamic range may be limited by not necessarily being able to get sufficiently close to a transmitter's antenna, while still remaining in its main antenna beam and not being in its far field, to obtain the maximum-possible 130 dB.

For multi-gigawatt (sometimes 45 to 60 GW) EIRP radars, we routinely obtain 110–120 dB of dynamic range, and sometimes the maximum possible 130 dB. For the relatively low-powered (about 56 kW EIRP) 5G base station transmitters that we examined in this study, the maximum dynamic range that we obtained was a little more than 90 dB. (But see further discussion for why we therefore have a little more than 100 dB of effective dynamic range on these emitters' possible emission levels in the radalt band of 4200–4400 MHz.)

7.1.1.3 YIG RF Filter Pre-Selection

Following the RF attenuator, the signal passes through our RF front end filtering. Although the RSMS-5G front end contains a complex filtering arrangement, we have simplified it in Figure 37 to show only a pair of yttrium iron garnet (YIG) filter paths. The path used for these

measurements was the one labelled “2–18 GHz.” (This was actually a pair of parallel YIG filters, one 2–4 GHz and the other 4–8 GHz.) The YIGs provide about 70 dB of isolation outside their passbands, at the cost of a few decibels of insertion loss.

The YIGs’ tuned center frequencies are adjusted automatically as the measurement progresses, to keep the YIG center frequencies matched to the tuned frequencies of the associated signal analyzer. This matching of YIG bandpass center frequencies to signal analyzer frequencies depends, like the attenuator settings, on using a custom-written stepped-frequency measurement algorithm instead of a conventional swept-frequency algorithm. That algorithm is described further below.

7.1.1.4 RF Front End Low-Noise Preamplification

The next stage is a low noise amplifier (LNA) that combines a low noise figure of a few decibels with enough RF gain to overdrive the inherent noise (noise figure) of the following signal analyzer. Although the RSMS-5G front end has an automatically switched set of LNAs, the diagram in Figure 37 condenses all of these into a single stage labelled “LNA.” The point of the LNA is to maintain the lowest possible overall noise figure with just enough gain (not too much gain!) to overdrive the analyzer’s noise floor.

The LNA(s) is/are protected from overload in strong-signal environments by the bandpass filtering of the YIG bank. But just as for the use of the attenuator and the YIGs themselves, the LNAs can only benefit from this protection via our custom-designed stepped-frequency (as opposed to conventional swept-frequency) measurement algorithm.

7.1.2 RSMS-5G Measurement Software Including Stepped-Frequency Algorithm

The entire spectrum measurement system is operated via custom-written fifth-generation (V5) software (largely written by one of the authors, G. Sanders). The software allows automatically controlled noise diode calibrations; custom-programmed spectrum and time-domain measurements; real-time display of results; and storage of the results for later retrieval and analysis.

7.1.2.1 Stepped Algorithm Measurements

The key to the radar measurement capability, adapted by us to the problem of measuring 5G emission spectra, is the stepped-frequency algorithm. With this algorithm, a spectrum is measured a single frequency at a time.

At the outset of a spectrum measurement, the operator selects a set of measurement parameters: start frequency; stop frequency; detector; IF (resolution) bandwidth; video bandwidth; number of frequency steps that will be taken across the specified frequency range; and the time interval (“dwell”) that will be used for each step.

The measurement then runs under computer control. The measurement system tunes to the start frequency. A zero-span (time domain) sweep is performed on the frequency for the specified dwell period with the selected detector and IF bandwidth. The measurement system stores the

time domain sweep at that frequency. It also extracts the maximum-power point that occurred within that sweep, corrects it for the gain-calibration factor that was stored earlier from the noise diode calibration, and displays that point on an evolving spectrum graph for the operator.

Next, the measurement system tunes to the second frequency to be measured. This stepped-frequency interval is equal to the frequency range of the measurement divided by the number of data points that were originally specified. For example, if the specified frequency range was 3500 MHz to 4400 MHz and the number of data points had been specified as 901, then the frequencies of the spectrum data points would be 3500 MHz, 3501 MHz, 3502 MHz, and so on until the 901st data point would be measured at 4400 MHz.

7.1.2.2 Resolution Bandwidth and Frequency Step Size

Ordinarily, the number of frequency-measurement steps (data points) taken across a spectrum is driven by the resolution bandwidth. This is because there are no spectra without measurement bandwidths; *all spectra exist only in conjunction with their specified measurement (also known as resolution or convolution) bandwidths*. The resolution bandwidth is selected first, based on any of a number of possible criteria. Then the number of steps to take across the spectrum is usually driven by that bandwidth choice.

If a spectrum is to be measured in, for instance, 1 MHz, then the most logical and straightforward frequency step size is the same: 1 MHz.⁵⁶ That way, the convolution size just equals the step-size between the measured points.

Our emission spectra measured for 5G base station transmitters have in fact been measured in 1 MHz for three reasons: (a) because the regulatory transmitter power limit is per megahertz; (b) because interference effects on radalt receivers are often assessed on a per megahertz basis; and (c) because many EMC assessments for many systems are in general performed on a per megahertz basis, making our spectra potentially usable in other work at later dates.

7.1.2.3 Dwell Time per Step

The dwell time per step is important because it needs to be long enough to capture whatever time-domain behavior in the measured signal waveform might be important, while not being overly long to the point of needlessly extending the total time required to complete the spectrum measurement. The operative concept behind the dwell interval is to ensure that it is long enough to “see” the entire periodicity of the waveform to ensure that the waveform’s maximum possible power is captured at each frequency during each step. For radars with rotating or electronically scanned antenna beams that may take anywhere from a few seconds to a minute to return to the same frequency and antenna beam direction, the step interval is set from perhaps 3 seconds for a rotating short-range navigation radar or a sector-scanned airborne fire-control radar; to 5 seconds for a short-range air traffic control radar; to 12 seconds for a long-range air search and

⁵⁶ There are some cases, not considered here, where the step size needs to be larger than the resolution bandwidth.

surveillance radar; to 20 or 30 seconds for a long-range weather radar; to perhaps 60 seconds or more for a super long range, frequency-hopping phased-array space-search and tracking radar.

For the 5G base station transmitter spectrum measurements in the JI-FRAI project, with a TDD cycle of 5 milliseconds, the dwell per step was set to 100 milliseconds. This gave us 20 TDD 5G cycles that were observed and recorded at each measurement frequency step. (Figure 15 is an example of one of these captures.) This ensured that we saw the maximum possible power transmitted by the 5G base station transmitters at every measured frequency across the selected spectrum-measurement frequency range of 3500 to 4400 MHz in 901 steps of 1 MHz.

7.1.2.4 Dwelling and Stepping versus Sweeping or High-Speed Digitizing

In the dwell-and-step approach to measuring a spectrum, we operate our measurement system like an ambush predator. Rather than chasing the signal as it moves in the time, space, and frequency, we wait patiently for the transmitter being measured to *come to us* on each measured frequency in time and space. The dwell-and-step approach only needs to make the dwell interval long enough to accommodate any transmitter's combined behaviors of antenna beam-pointing, frequency hopping or sweeping, and waveform time-behavior (e.g., pulsing or time division duplexing) to ensure that, within each dwell interval, all those factors will eventually align and give us a maximum-power "hit" on the frequency being measured.

In addition to allowing us to control our dynamic range this way (see below), another advantage of our wait-for-lunch-to-come-to-us strategy is that we know unequivocally (and can prove with our recorded time-domain sweeps at each measured frequency) that a maximum-power hit has definitely occurred on each measured frequency. We unambiguously capture the spectrum in its entirety, at full available power on all frequencies.

This is in contrast to more conventional frequency-sweeping and high-speed digitizing approaches, where the intersection between the digitization of the input time-varying waveform and the antenna beam-pointing and frequency-hopping or sweeping behavior of the transmitter being measured may combine so as to cause difficulty in entirely understanding or characterizing the results. Moreover, in experimental side-by-side measurements using the two approaches we have documented that the dwell-and-step approach ends up finishing the spectrum faster than high-speed digitization, for radars and other complexly designed transmitters.

The dwell-and-step approach turned out to be well pre-adapted to measuring the 5G base station transmitter signals. We merely set the dwell to 100 milliseconds (about 20 TDD cycles) and treated the rest of the measurement as if we were looking at a radar signal.

7.1.2.5 YIG Filter Tracking

One key to successfully using the stepped algorithm is to keep the front-end YIG filter tracking the measured frequency. The YIG is about 20 MHz wide at 3 GHz to 4 GHz, with several decibels of insertion loss. It is tuned by an input voltage that is directly linearly proportional to its tuned frequency. Its frequency tracking is automatically controlled by an open control loop from the signal analyzer to the YIG's control-voltage line, as shown in Figure 37.

7.1.2.6 Dynamic Range Control with Front End RF Attenuator

Another key to success with the stepped algorithm is to use the front-end attenuator at a setting that maintains the radio-spectrum input power within the instantaneous dynamic range of the rest of the measurement system. This control is dynamic. Dynamic input-power range control is effected by a closed feedback loop between the maximum time-domain power that has been read at the end of each step interval (that is, within each dwell interval) by the measurement software, and the amount of RF attenuation that has been currently invoked in the front-end stepped RF attenuator.

The maximum measured power within each dwell-interval step is compared by the RSMS V5 software to the measurement system's known instantaneous dynamic range limits. When the measured power comes within a defined range of that limit, either high or low, the RF attenuator is re-set upward or downward, as the case demands, by 10 decibels. If the new attenuation level keeps the new signal level within the system's dynamic range boundary, the measurement proceeds with that new RF attenuation level. If the modified attenuation setting does not keep the input signal level within the necessary (defined) range, then the RF attenuation is further modified until the dynamic range criteria are met. RF attenuator settings for each collected data point are stored along with those points for later reference and, if necessary, analysis.

The total dynamic range that is available is about 60 dB of instantaneous range, plus the 70 dB available in the front-end attenuator, for a total of as much as 130 dB. Attaining that much dynamic range, however, requires that the front end of our measurement system must "see" power at 130 dB above the measurement system's noise floor. For a peak-detected noise floor of perhaps -90 dBm in a 1 MHz bandwidth with a nominal noise figure of 14 dB (8 dB for the front end LNA plus 6 dB of YIG insertion loss), we need $130 - 90 = +40$ dBm of input signal power per 1 MHz of bandwidth. While this is achievable for radars running at EIRPs on the order of +135 dBm (~32 GW, peak), we cannot get this much power into the measurement system front-end from 5G base stations running at only +77.5 dBm EIRP (~56 kW, average) at a distance of 161 m (530 ft), as was the case at Table Mountain.

We were able to achieve a total spectrum-measurement dynamic range of 90 dB for Radios 2 and 4 at Table Mountain. For Radio 3 we attained about 80 dB of dynamic range because that radio transmitter was only operable at about 10 dB less power than the other two radios (as discussed more below).

As will be likewise discussed at more length below, however, we saw during our measurements across 4200–4400 MHz, the radalt band, that no 5G signal occurred at a level that was enough to even raise the measurement system's noise by as much as 0.4 decibel. Because $(-15 \text{ dB} + 0 \text{ dB}) = +0.1 \text{ dB}$, and because we did not see even a 0.1 dB impact in that frequency range, we know from our spectrum measurements that the 5G signals were *at least* 15 dB further down than implied by directly reading our measurement system's noise floor. This means that the 5G signals in the 4200–4400 MHz band, at 161 m with a ½-meter diameter dish antenna with a matched-polarization feed, were at least $(-91 - 15) = -106$ dB down from the fundamental-frequency power for Radios 2 and 4 and at least $(-80 - 15) = -95$ dB down for Radio 3. The implications of this result are discussed further below.

7.1.3 Stored Emission Spectra and Supporting Associated Data

At the conclusion of every stepped emission spectrum measurement, the spectra are automatically stored in MATLAB© formatted (.mat) electronic data files. The final, stored data for each spectrum include: the spectrum measurement parameter settings including start and stop frequencies, the measurement bandwidth, the dwell interval and the detector selection; the time domain scan that was taken in each dwell interval at each measured frequency; the raw (uncorrected) maximum power that was obtained (sorted) from each dwell cycle; that same power level but calibration-corrected for each data point; the RF attenuation level that was invoked at each measured frequency; and any operator notes for the measurement, including the given name of the transmitter and so forth. We can, if needed, reconstruct the entire spectrum measurement from the data stored in each spectrum file.

7.2 Monitoring 5G Transmitter Emissions on the Ground During Airborne Measurements

In addition to performing wideband emission spectrum measurements, the RSMS V5 was employed for on-the-ground monitoring of 5G transmitter functionality during all airborne measurements at Table Mountain. Typically, the wideband emission spectra were measured the day before the airborne collections. The spectrum measurements allowed us to familiarize ourselves with the emission characteristics of each transmitter. They also allowed us to verify that each transmitter would in fact operate at constant power level on a fixed channel for hours at a time.

On the day of each airborne data collection, the RSMS V5 system was configured to monitor the base station emissions on a continuous basis from the single on-the-ground location shown in Figures 28, 29, and 38. The RSMS' high-gain dish was locked in position, trained on the 5G MIMO array as seen in Figure 38.

The monitoring mode allowed us to watch the 5G base station emissions without interruption as the measurement helicopter flew its sortie overhead. The RSMS monitoring verified that the base station's channel frequency, channel bandwidth, emission power level and TDD cycling were all maintained properly and as expected as the airborne collections progressed and were completed. These monitoring scans were recorded and can be made available to third parties on request.

Using a high-gain parabolic dish antenna for the on-the-ground spectrum measurements and monitoring not only increased the power coupled into the measurement-monitoring system receiver, it also reduced the contribution of earth-scattered multipath propagation components in the measurement-monitoring receiver. Such multipath components, reduced in amplitude relative to the direct-beam path via scattering, have their contributions further reduced by the dish antenna's discrimination against off-axis signal reception. Further, the intervening ground between the 5G base station MIMO array and the RSMS' receiving antenna was rough and uneven. This terrain characteristic would further reduce the contributions of off-axis rays by cutting the specularly of any reflections. An entire family of off-axis rays would scatter off the intervening ground, leading to a Gaussian-distributed smear rather than a two-ray tabletop physics situation. All these factors would tend to make multipath contributions minimal.

8. MEASURING 5G MIMO BASE AIRBORNE RADIATION PATTERNS

8.1 The JI-FRAI Need for Three-Dimensional Antenna Radiation Pattern Measurements Around 5G MIMO Arrays

As noted earlier, the JI-FRAI effort needed to measure 5G MIMO array radiation patterns for two reasons. The first was that we needed to demonstrate, prior to the beginning of JT&E at Hill AFB and Majors Field, that we had a practical, calibrated, and accurate method for measuring 5G field strength levels along the routes that aircraft would fly during the flight tests. This would allow later back-analysis of 5G incident field strength levels that might cause harmful interference to radalt receivers in the flight tests, were such effects to be observed. These preliminary, pre-JT&E airborne measurements were called risk reduction events (RREs) in the JI-FRAI QRT work program.

The second reason that three-dimensional 5G MIMO array patterns were needed was for use with radalt receiver interference-effects bench-testing results. When a power threshold would be identified in bench testing for harmful interference within the circuitry of a radalt receiver, that would raise the question, “So, at what distance and in what direction from a MIMO array would that power level occur in a radalt receiver?”

That interference power threshold must be somehow relatable back to a power level radiated from a 5G MIMO array, to determine at what physical distance from the array, and in what given direction from the array, that power would be coupled into a radalt receiver.

For example, suppose that a bench-tested radalt receiver showed a harmful interference-effects threshold inside its circuitry at a power density level of -35 dBm/MHz for a 5G signal input at 3980 MHz. Suppose further that a -6 dB margin were to be added to that for an operative interference limit of -41 dBm/MHz in the receiver circuit. If that radalt receiver antenna had a gain of, for instance, +5 dBi at that frequency (3980 MHz) in some specified direction (for example, lateral to the aircraft’s flight path), then what would be the limiting field strength in space where that interference power would couple into the receiver?

The limiting field strength, we can compute,⁵⁷ would be +103 dB μ V/m at the radalt antenna in that lateral direction. That would equate (we can further compute) to an EIRP from a 5G array of not more than +48 dBm/MHz at a distance of 300 m (~1000 ft) from the array in a direction lateral to the aircraft’s flight path.

The point of this exercise is not to define limits on radalt interference thresholds (because we are not doing that here; every number given here is hypothetical for the example) but rather to show that, in order to *close the loop between bench test results and real-world places in space* where those power levels might occur around 5G MIMO arrays, *we need to know the actual 5G antenna radiation patterns in three dimensions around those arrays.*

⁵⁷ Section 11 discusses how to perform these computations.

Although such information can be derived to some extent from modeling, simulation and analysis of MIMO arrays (see Figures 19 through 24), actual measurements need to be performed around real arrays to at least validate and verify such analytical data. For the JI-FRAI project, this meant that in addition to needing the RREs for support of eventual JT&E at Hill AFB and Majors Field, we also needed to obtain the actual radiation patterns of all of the MIMO arrays deployed with 5G Radios 1 through 4 in order to connect bench testing results to 5G three-dimensional MIMO array antenna radiation patterns.⁵⁸

8.2 Outdoor Airborne versus Indoor Chamber Antenna Pattern Measurements

Although it might well be possible to put 5G MIMO arrays in anechoic chambers for such measurements (and such an approach was considered early-on in the JI-FRAI planning), the complexity of assessing in-the-sky radiation patterns was ultimately considered to only be solvable in any practical sense by doing open-air measurements. Going open-air allowed everything to be done that 5G base stations required for their operations, and which mostly could *not* be done inside chambers.⁵⁹ This included being able to set up the auxiliary communication links that 5G base stations need for their operations and having groups of UEs arranged at angles, distances, and above-ground heights that would represent realistic 5G deployments.

The Table Mountain Radio Quiet Zone environment, with its large open space and scarcity of human-built surface infrastructure, is ideal for not just for spectrum measurements but also for antenna radiation pattern measurements. Indeed, we routinely bring radars to Table Mountain to measure their spectra and their antenna patterns on an outdoor range we have built. For the JI-FRAI project we adapted this quiet, open environment and our in-house radar capabilities to measuring spectra and in-the-sky radiation patterns for all the upper C-band 5G base station transmitter models being deployed in the US.

Unlike the situation for most transmitters, the JI-FRAI radalt/EMC interest in 5G base station radiation patterns is not on the ground, but rather “up in the sky where airplanes fly.” As noted in Section 4, 5G radiation beams are rarely directed above the local horizon, at least not by more than a few degrees.⁶⁰ Array beam codebooks avoid high elevation angles; there are better ways of covering UEs at such angles; and in any event the 64T64R MIMO arrays are only capable of forming beams on elevation angles below, at, or just above the local horizon.

⁵⁸ Noting again that Radio 1 is a lower C-band MIMO array with a radiation pattern that will look highly similar to upper C-band array patterns, and that Radios 2 through 4 are the full complement of upper C-band 5G radio models being deployed in the US.

⁵⁹ See 8.2.1, below, for a discussion of outdoor multipath reflections.

⁶⁰ From Table 9, the maximum specified elevation angles available are +3 to +7 degrees, depending on 5G base station radio model. Dr. Monisha Ghosh of Notre Dame University cites (private communication) a specific documented case of a 5G base station on a 10-floor building rooftop that has communicated at 400 Mbps with a UE sitting on a 37-floor rooftop across Chicago’s Regent’s Park at an elevation angle of +9 degrees. As we noted earlier, this is not a normal installation.

Nevertheless, all antenna systems produce *some* non-zero power at all possible angles throughout any surrounding sphere, including 5G MIMO arrays. The issue is *how much* power is emitted as a function of any hemispherical (θ , φ) angle.⁶¹ Modeling provides guidance (Figures 19–24), but ultimately such solutions need to be verified and validated via actual measurements.

8.2.1 Multipath Considerations for Airborne Measurements

Both a direct ray and some group or family of ground-scattered rays would be expected to be received from the 5G base station MIMO array transmitter antennas at each point along the airborne flight path. Multipath components will be reduced in power relative to the direct-beam path via ground scattering. The question is, by how much is the amplitude of ground-scattered power reduced relative to the direct-ray power being coupled into our receiver from the MIMO array? Is scattered power enough to significantly change measurement results?

Scattered-ray power will be reduced due to at least three factors: i) only a fraction of ground-incident power is scattered, with the remainder being absorbed; ii) the scattered power will be re-radiated from the ground in some hemispherical or semi-hemispherical pattern, rather than being strongly reflected as if from a mirrored surface; and iii) on a related note, the intervening ground between the 5G base station MIMO array and the airborne receiving antenna is rough and uneven. It should be emphasized that the Table Mountain terrain characteristics would reduce the contributions of off-axis rays by producing a Gaussian-distributed, smeared-out *family* of reflected rays, rather than a two-ray (direct ray with a single secondary ray) tabletop physics situation.

All the above factors would tend to significantly reduce the power of scattered rays relative to the direct-propagated ray. We note that, in 43 years of measurement experience, we have seen two-ray diffraction and a concomitantly strong multi-ray interference effect exactly once during an outdoor measurement. That one event was when we were configured to measure the radiated emission spectrum of an X-band (9 GHz) radar with a salt water embayment between the radar and the measurement system's antenna. The salt water was glassy-smooth and the incidence and reflection angles between the two system's antennas (radar transmitter antenna and measurement receiver antenna) and the surface of the water were very shallow, on the order of only a couple of angular degrees.

The emission spectrum measurement, stepped in frequency a megahertz at a time as described above, progressed across several gigahertz of bandwidth from 7 GHz to 12 GHz. Across a subset of spectrum measurement frequencies spanning just a few megahertz, in the radar's spurious emission spectrum near 10 GHz, the received power was reduced by 20 decibels or more, as if a notch filter had been inserted into the spectrum. This unexpected "notch" was re-measured and found to repeat. But when winds later rose and the water surface became rippled, the notch-out disappeared. This was interpreted as a case of genuine two-ray diffraction-and-interference that had formed as if in a tabletop physics experiment, and that had subsequently been disrupted by

⁶¹ We need ordered triples of (EIRP, θ , φ) throughout the hemisphere around and above each 5G MIMO array. Mathematically this set of ordered triples of directions (θ , φ) with a scalar (EIRP) is a vector array.

the rippling of the intervening surface. It required a special set of circumstances to produce the effect in the real world; such circumstances seem to rarely occur outside laboratories.

While no outdoor measurement can completely eliminate all contributions from scattered off-axis rays, we are confident, based on the physical situation at Table Mountain and contrasting it with the situation where we have seen *bona fide* two-ray interference, that off-axis scattering made no significant contribution to the results of the measured airborne data collections.

8.3 Airborne 5G MIMO Antenna Pattern Measurement Methodology

8.3.1 Airborne Flight Slices Taken Through 5G MIMO Hemispheres

The airborne data were collected by a platform⁶² that flew linear slices through the hemisphere. The four types of slices are shown in Figure 39.

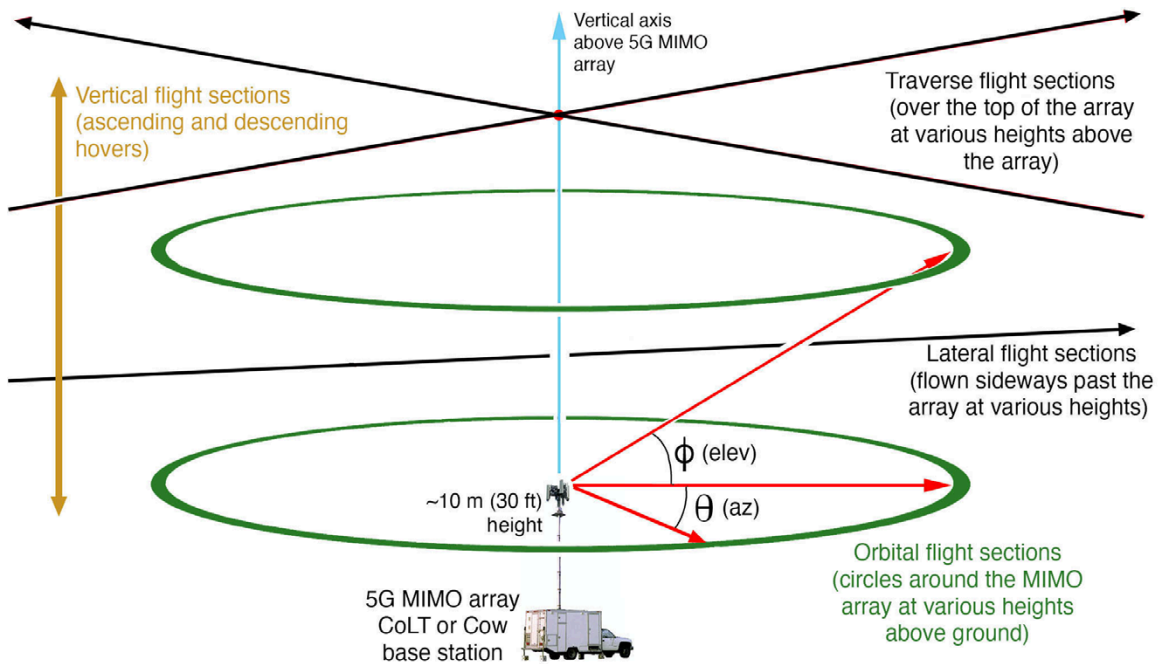


Figure 39. The four types of flight slices taken through the hemisphere around a MIMO array: orbital (circles), lateral (flyby), traverse (straight overhead) and vertical sections.

Appendix A shows a set of flight cards for specific sortie routes flown around the Radio 2 through four base stations. Appendix B shows flight cards for the sortie routes flown around the twin CoWs for Radio 1 at Table Mountain and later at Hill AFB.

⁶² A crewed helicopter currently, but we seek to build an automated uncrewed aerial vehicle (A-UAV) capability for these kinds of measurements in the future.

It is important to note that the *particular distances* from a MIMO array at which we fly (flew) these sections is not important, as long as we have sufficient received power at any given distance to obtain good power-measurement data points. This is because the raw data are ultimately, as described above and further below, reduced to radiated (EIRP) values that are being emitted from the array itself, as a function of angle around the array.

That analysis reduction will eliminate the parameter of distance itself from the final data set. But it will allow users of the final data to then compute, for themselves, *any* power at *any* distance from the array, in any given spatial direction from the array using the (EIRP, θ , ϕ) vectors in the provided data set.

8.3.2 Airborne Antennas

Since antenna patterns vary with spatial angle, the only ways to obtain data points at known measurement-antenna gains is to either hold a target transmitter within the main beam of a high-gain antenna, or else use a low-gain antenna that has nearly uniform gain throughout a broad solid-angle range. We took the second approach because it is simpler and less prone to errors, with airborne platforms, than operating narrow-beam, high-gain antennas. This is because aircraft bounce, roll, yaw, pitch, and vibrate in flight; keeping a high-gain beam steady on a target under those conditions requires dynamically stabilized mounts that can become a project in itself to procure and operate, not to mention presenting prohibitive size and mass problems. Figure 40 shows our solution to the airborne measurement-antenna challenge. Figures 41 through 43 show our implementation of this approach on the helicopters we used.

Table 10 lists the antennas that were used in the airborne measurements. One model of omnidirectional antenna (ETS Lindgren 3181 broadband biconical) was used for the Radio 1 measurements with a UH-60 Blackhawk helicopter. Another model of omni (Antenna Research Associates (ARA) VBC-1758-M broadband dipole) was used for the Radio 2 through 4 measurements taken with a R-44 Raven helicopter. The nominal uniform-gain elevation beamwidth of the omni antennas is specified as being at least $\pm 25^\circ$ (50° total) relative to the antennas' local horizontal plane.

This omni-antenna gain would be somewhat modified for high (above the horizon) elevation angles in the UH-60 belly mount. To check the belly-mounted gain characteristics, we built a metal-screen square (Figure 44) to simulate the center section of the UH-60 and mounted the omni antenna in the center of that frame. We oriented the frame so that the omni was pointed up, and then tipped the frame through a few angular degrees to simulate the banking of the helicopter in flight. The result of the gain measurement for small bank angles is shown in Table 11.

A single model of cavity-backed spiral (CBS) antenna (Tecom 201350) was used throughout the measurement series for all the base station radio measurements. CBS antennas are compact, rugged, wideband, and low gain. They have roughly 90-degree coverage at their antenna pattern half-power (-3 dB) points. They are widely used in many airborne electronic threat-warning systems, such as radar lock-on from adversaries (with a group of four CBSs on an airframe, two

at offset angles on the nose and two at offset angles on the tail). Their characteristics made them ideal for the vertical-axis measurements above the tops of the 5G MIMO arrays.

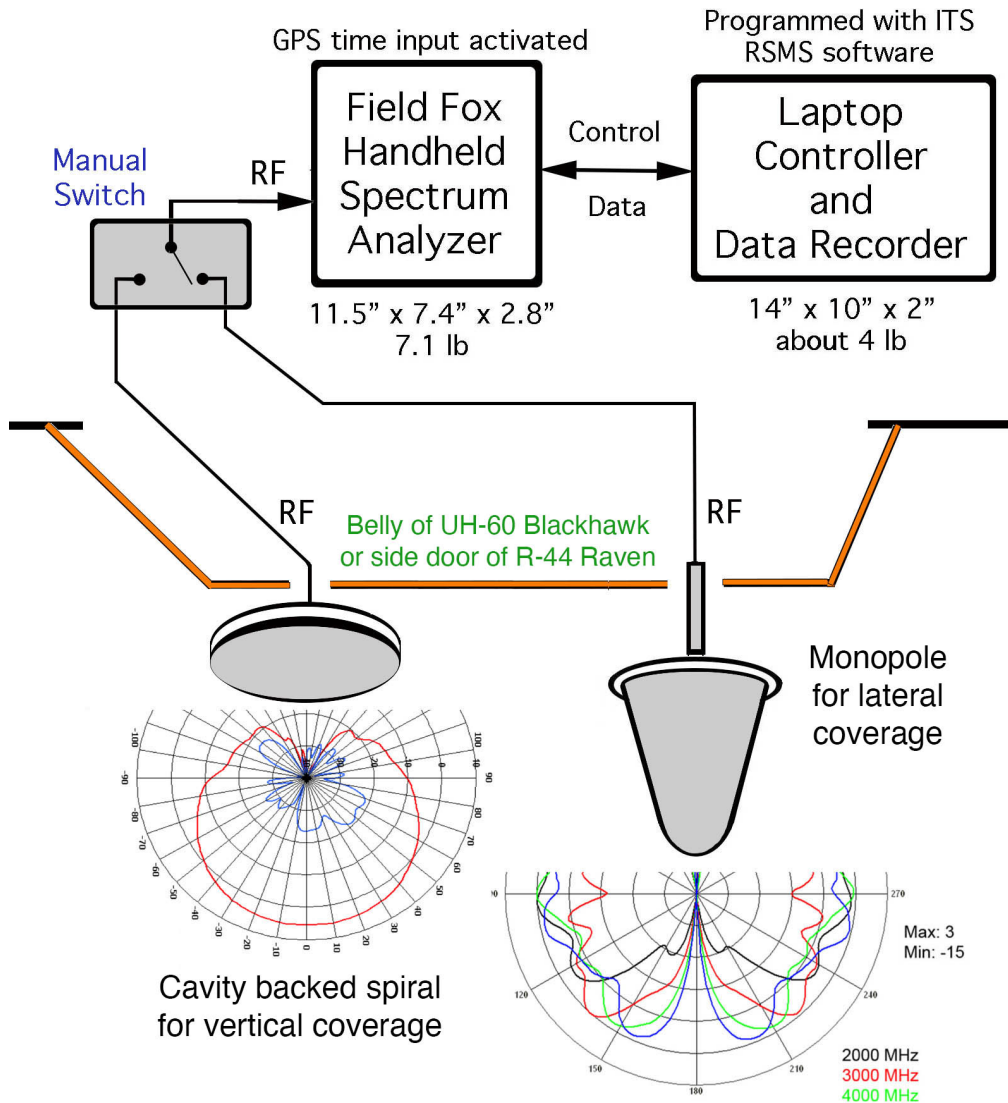


Figure 40. Dual low-gain antenna solution for the airborne 5G field strength collection challenge.

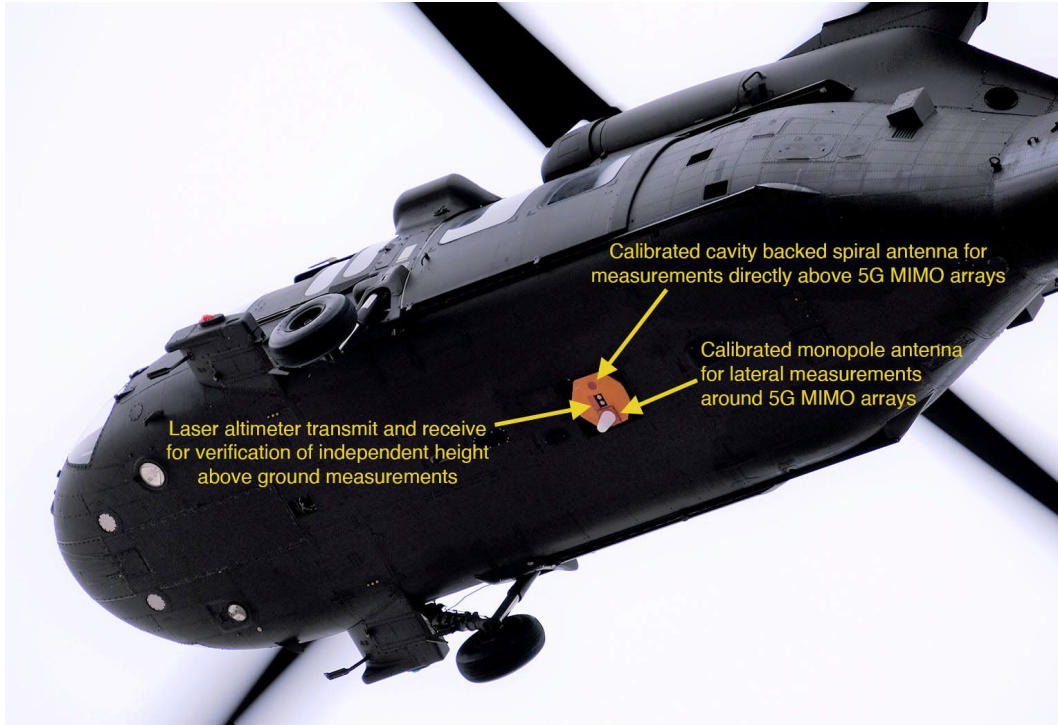


Figure 41. Measurement antenna configuration on UH-60 Blackhawk for 5G airborne field strength measurements on Radio 1 (lower C-band MIMO arrays).



Figure 42. Measurement antenna configuration on Raven R-44 for 5G airborne field strength measurements on Radios 2–4 (upper C-band MIMO arrays).

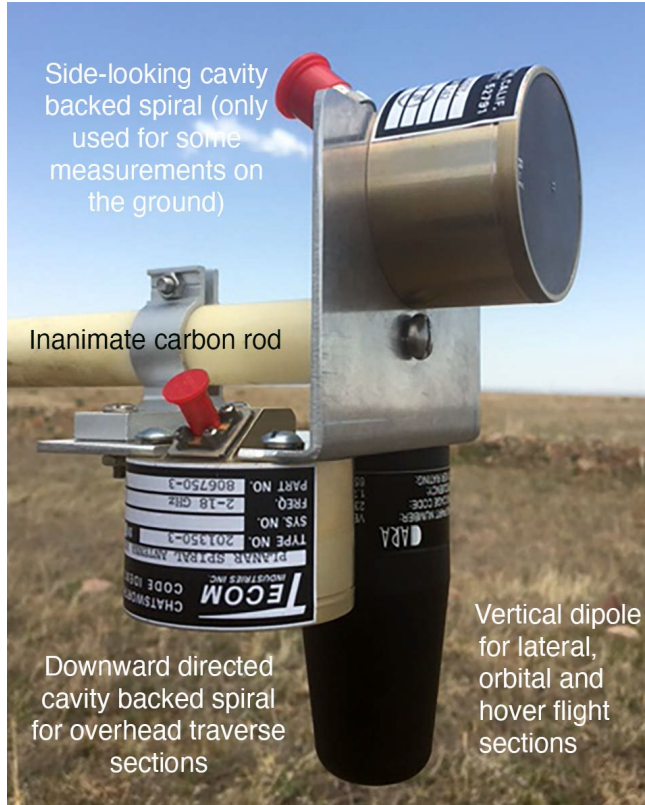


Figure 43. Details of boom-mounted antenna array (see Figure 42) used for airborne field strength measurements of upper C-band 5G MIMO Radios 2 through 4 on Raven R-44.



Figure 44. The 2.4 m (8 ft) square metal-screen plate used for calibration of the omni antenna gain at UH-60 ventral (belly) mount banked angles. Plate width matches center-fuselage width.



Figure 45. Airborne field strength measurement in progress with a 5G CoLT base station.

Table 10. Antennas used for airborne 5G field strength measurements.

Measurement	Antenna Mfr, Model & Type	Frequency Range & Polarization	Main Beam Gain
Radio 1 base station lower C-band at Table Mtn and pair of Radio 2's at Hill AFB	ETS Lindgren 3181 broadband biconical omni (on-board UH-60)	1–18 GHz Linear vertical	About +1 dBi (custom calibrated by the authors)
	Tecom 201350 cavity backed spiral (on-board UH-60)	2–18 GHz Circular	About +1 dBi (custom calibrated by the authors)
Radio 2 base station upper C-band	ARA VBC-1758-M broadband dipole omni (on-board Raven R-44)	1.7–8 GHz Linear vertical	About +1 dBi (custom calibrated by the authors)
	Tecom 201350 cavity backed spiral (on-board Raven R-44)	2–18 GHz Circular	About +1 dBi (custom calibrated by the authors)
Radio 3 base station upper C-band	ARA VBC-1758-M broadband dipole omni (on-board Raven R-44)	1.7–5.8 GHz Linear vertical	About +1 dBi (custom calibrated by the authors)
	Tecom 201350 cavity backed spiral (on-board Raven R-44)	2–18 GHz Circular	About +1 dBi (custom calibrated by the authors)

Measurement	Antenna Mfr, Model & Type	Frequency Range & Polarization	Main Beam Gain
Radio 4 base station upper C-band	ARA VBC-1758-M broadband dipole omni (on-board Raven R-44)	1.7–5.8 GHz Linear vertical	About +1 dBi (custom calibrated by the authors)
	Tecom 201350 cavity backed spiral (on-board Raven R-44)	2–18 GHz Circular	About +1 dBi (custom calibrated by the authors)

Table 11. Received-power offsets for UH-60 helicopter plate-section bank angles. Receiver-power offsets for helicopter plate-section bank angles.⁶³

UH-60 Simulated Belly Plate Bank Angle Condition	Relative Power Level of Incident CW Signal Originating from Horizon
No plate	0 dB
Plate at 0° bank (tilt) angle	+2 dB
Plate at 10° bank (tilt) angle	+1 dB
Plate at 20° bank (tilt) angle	+11 dB

The third antenna type used in the airborne measurements was an ARA Model VBC-1758-M omnidirectional broadband dipole. As shown in Figure 44, it was mounted vertically on the boom mount used for the Raven R-44 flights around 5G base station Radios 2 through 4 (all the upper C-band base stations).

In-flight, an on-board ITS engineer⁶⁴ operated the dual antennas as follows. As shown in Figure 41, the two antennas were connected to the rest of the measurement system through a manually operated single-pole two-throw (two position) RF switch. The ITS operator-engineer would mostly have the omni antenna selected via the RF switch. The CBS position was only selected in sortie legs where the helicopter was traversing directly above the MIMO array (see Figure 39). On those traverses, the CBS was switched in when the helicopter was within about 45° of the MIMO array’s zenith. The exact switch-over point was manifested in the collected data by a slight discontinuity in the data trace.

Note, in Figure 41, the presence of a laser altimeter on the UH-60 at Table Mountain. This altimeter provided a stand-alone, direct height above-ground-level (AGL) measurement that was used to validate the extent to which GPS-based estimates of AGL height could be used in subsequent flight testing at Hill AFB and Majors Field as a reliable and accurate radalt-independent method for assessing true AGL height. The laser altimeter check-point at Table Mountain was needed because most test aircraft in the JI-FRAI QRT program would ordinarily

⁶³ Actual UH-60 helicopter bank angles were kept at, or less than, about 10 degrees during data collections. The impact of the helicopter banking is estimated to therefore have been less than ±2 dB relative to having had no bank angle.

⁶⁴ Messrs. Geoff Sanders, Adam Hicks, and Savio Tran operated the airborne measurement system on various sorties.

need to use GPS-based heights to compare to radalt heights. The laser altimeter data from Table Mountain showed that GPS-based heights AGL were indeed reliable and could be used as a check against radalt-indicated AGL heights in the subsequent flight test series.

8.3.3 Airborne Spectrum Analyzer Settings and Data Collection

8.3.3.1 Airborne Spectrum Analyzer Selection

Downstream from the measurement antennas and their manual RF switch was the remainder of the airborne measurement system, consisting of a Keysight N9914B FieldFox® spectrum analyzer and a controller laptop computer (Figure 40). The main drivers behind this equipment selection were size, weight, power consumption, battery life, and minimal complexity. The N9914 analyzer met Army flight-safety requirements for not carrying overly heavy or bulky gear, addressing concerns about gear coming loose and hitting anyone in the event of an in-flight turbulence emergency or a hard landing. Power consumption and battery life had to be low enough and high enough, respectively, to keep the equipment running throughout a multi-hour flight. Minimal complexity was achieved by running all measurements in an automated, pre-programmed mode with RSMS V5 software and recording data automatically in-flight.

8.3.3.2 Airborne Strip Chart Flattens Data to a Single 5G Frequency

Measuring 5G field strength as a function of location in space required data collection through the dimension of time as the helicopter moved through time and space. We needed the equivalent of an analog strip-chart recording of measured 5G power as the helicopter moved through time and space. To get this flattened output, we had to flatten the dimension of frequency in our data collection. Since 5G channels operate with a fairly uniform frequency-power distribution (see Figure 14 for example), we took power data on *only the center frequency*,⁶⁵ *in a zero hertz frequency span*, of the 5G base station's operative channel.

8.3.3.3 Airborne Resolution Bandwidth

The collection bandwidth could not approach the 5G channel bandwidth of 60 MHz or 100 MHz (depending on the Radio model). The same 1 MHz resolution bandwidth was used for the airborne data collections as for the on-the-ground spectrum measurements, for the same reasons (see 7.1.2.2, above). Power in this bandwidth can be extrapolated to power in any other bandwidth by multiplying the ratio of 1 MHz to any other bandwidth (equivalent to taking 10-log of the bandwidth ratio for decibel computations).

⁶⁵ Except for Radio 4. Its control software tended to cluster its power at the low-frequency end of the channel, as we observed before we flew. Therefore we tuned the Radio 4 measurement to the center of that observed activity, in the low-frequency end of its channel.

8.3.3.4 Airborne Detector Selection

As discussed earlier for 5G signal characteristics versus measurement detection mode, the most straightforward and fool-proof detection mode to use for 5G signals is positive peak (see Section 4.4), with a sufficiently slow time domain sweep-rate as to ensure that a maximum-power peak-detected data point is collected for each analyzer screen display bin. Since the 3GPP standard, and most EMC analyses, use RMS average instead of peak power, a correction factor of either 10 or 11.5 dB (see Figure 16 and the related peak versus average power discussion, above) would be invoked during post-collection data analysis.⁶⁶

8.3.3.5 Spectrum Analyzer Data Bins Trace Sweep Time

The N9914 spectrum analyzer data traces (zero hertz span on the nominal 5G channel center frequency) were 600 seconds (10 minutes) long, with 10,001 data point per trace. Each data point thus represented 60 milliseconds, which is about 12 TDD cycles.

8.3.4 Airborne Data Analysis and Reduction to a Usable Product

As discussed above, the raw time-domain (zero hertz span) data collected in a 1 MHz bandwidth at the center frequency of each 5G channel, having been collected through specific paths in space, needs to be converted to EIRP vectors. This conversion makes the data usable for *any* point in space, at *any* distance from the array.

The conversion of raw field strength data to EIRP vectors is done as follows:

- 1) Data are collected against a GPS time base (from multiple independent sources) in the helicopter.
- 2) The helicopter's three-dimensional position in space is also collected, during the flight, against a GPS time base (multiple independent sources).
- 3) The common time base of the helicopter position and the recorded incident 5G power levels is used to create a new file having the recorded power levels as a function of three-dimensional location in space.
- 4) The power levels as a function of spatial position are reduced to power levels as a function of three-dimensional distance and direction from the MIMO array (using the array's known latitude, longitude, and height above ground). These pairings of incident, measured 5G power level with direction from the array are the initial vector set of antenna radiation pattern data.

⁶⁶ We used the 3GPP TDD = ON criterion for RMS average power in our analysis; we subtracted only 10 dB from our peak-detected power measurements to obtain 5G RMS average power.

- 5) The peak-detected power levels are converted to RMS average by subtracting 10 dB (consistent with the 3GPP definition of RMS average power during TDD ON).⁶⁷
- 6) This gives us a set of (EIRP/MHz, θ , ϕ) vectors where the power is a spectrum density, per megahertz.
- 7) We make a second vector set where we change the EIRP per megahertz levels to total EIRP. This is done by taking $10 \cdot \log(\text{full channel width}/1 \text{ MHz})$ against the original data collected in 1 MHz. For example, for a 100 MHz 5G channel width, we add 20 dB to the values that were collected in 1 MHz.
- 8) We make *both* sets of vectors, one with EIRP per megahertz and the second with total EIRP, available in files that are accessible to readers of this report.
- 9) We also make a set of files available that show so-called heat maps of power as a function of location along the flown flight paths.

8.3.5 Notes on the Final Data Products

The following things need to be understood about the final data sets:

- The azimuthal orientation (θ) of the graphs is relative to true north. The elevation angle (ϕ) of the graphs is relative to local horizontal. See Figure 39.
- The (EIRP, θ , ϕ) vectors in the final, processed data sets are in *two* flavors:
 - EIRP as RMS average-detected power spectrum density *per megahertz*;
 - EIRP as *total* RMS average-detected power for the *entire* 5G channel.
- The antenna radiation pattern vectors are made available in the final product files as *two-dimensional slices* (two-dimensional graphs) taken through the three-dimensional space around the MIMO arrays.

The graphs are clearly marked as *either* EIRP per megahertz *or else* as total channel EIRP.

Readers must pay attention to *which* EIRP they are looking at and referencing on any given graph, because there is a 20 dB difference between these values for a 100 MHz channel width.⁶⁸

Recognizing the potential for confusion in providing EIRP in both units, we nevertheless provide *both* versions of EIRP, as a density and as a total-power value, because of variation in analysts'

⁶⁷ An alternative conversion would take into account TDD 70 percent duty cycle by subtracting 11.5 dB, as discussed above. Our conversion of only a 10 dB difference makes the average value conservative, toward the high side.

⁶⁸ Radio 4 could only operate with a 60 MHz channel width. The EIRP conversion from 1 MHz to 60 MHz is $20 \cdot \log(60) = 17.8$ dB.

needs. We have observed that 5G power per megahertz is a commonly used metric for bench testing, while (in contrast) total radiated channel power might need to be assessed by regulators. Therefore, we have produced both EIRP values, even though we recognize the potential for confusion in having these two different values available in our data sets.

8.3.6 Access to the 5G Airborne EIRP Data Files

Because of the sheer volume of the 5G airborne EIRP data files, they are not included as figures in this report. They are available to the public as electronically downloadable files from the 5G_Aerial_RF_Radiation_Data repo at github.com/NTIA — [DOI:10.5281/zenodo.7150540](https://doi.org/10.5281/zenodo.7150540).

9. 5G MIMO BASE STATION TRANSMITTER EMISSION SPECTRUM MEASUREMENT RESULTS

Figures 46 through 48 show the measured emission spectra of upper C-band Radios 2 through 4.

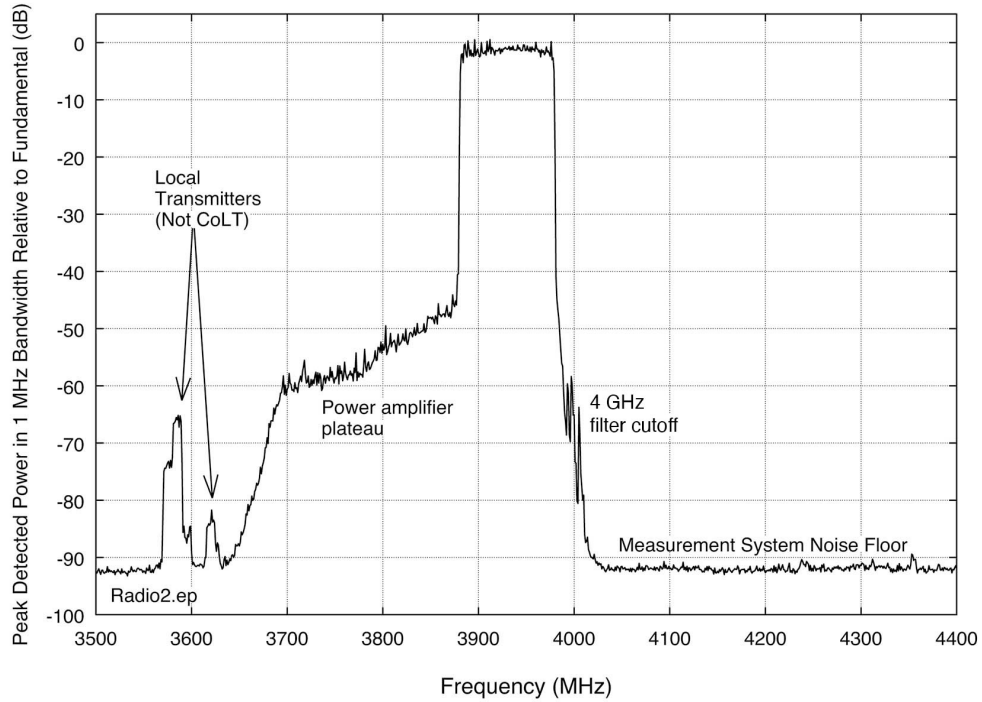


Figure 46. Measured emission spectrum of 5G base station transmitter Radio 2.

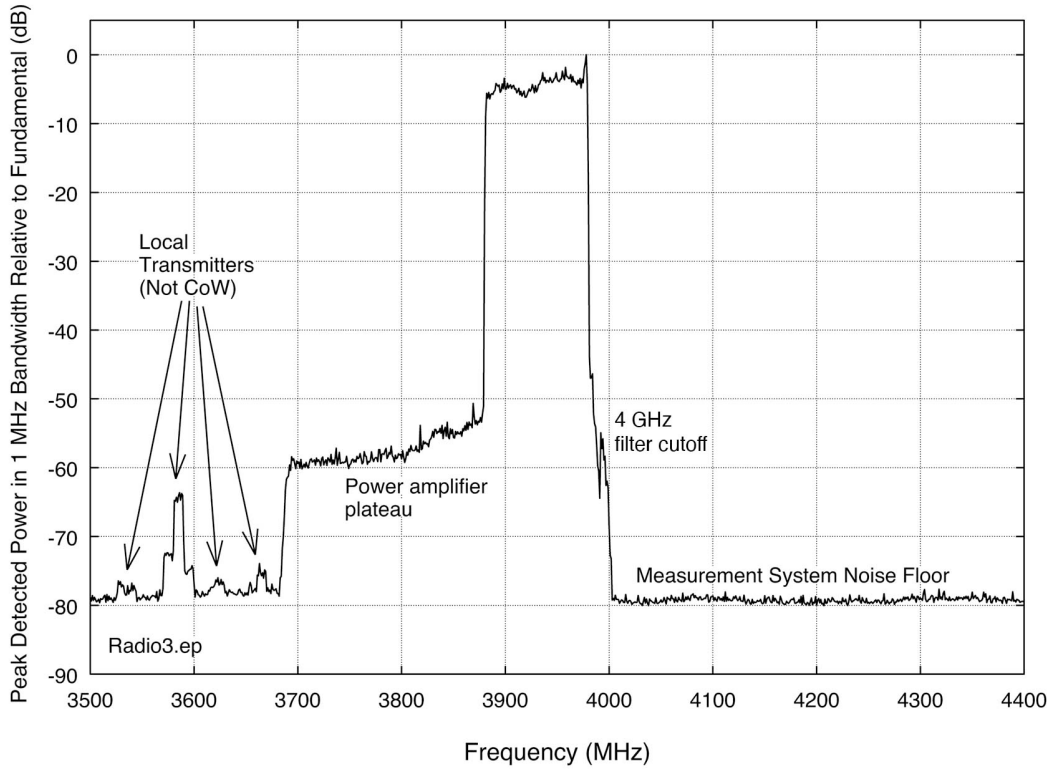


Figure 47. Measured emission spectrum of 5G base station transmitter Radio 3.

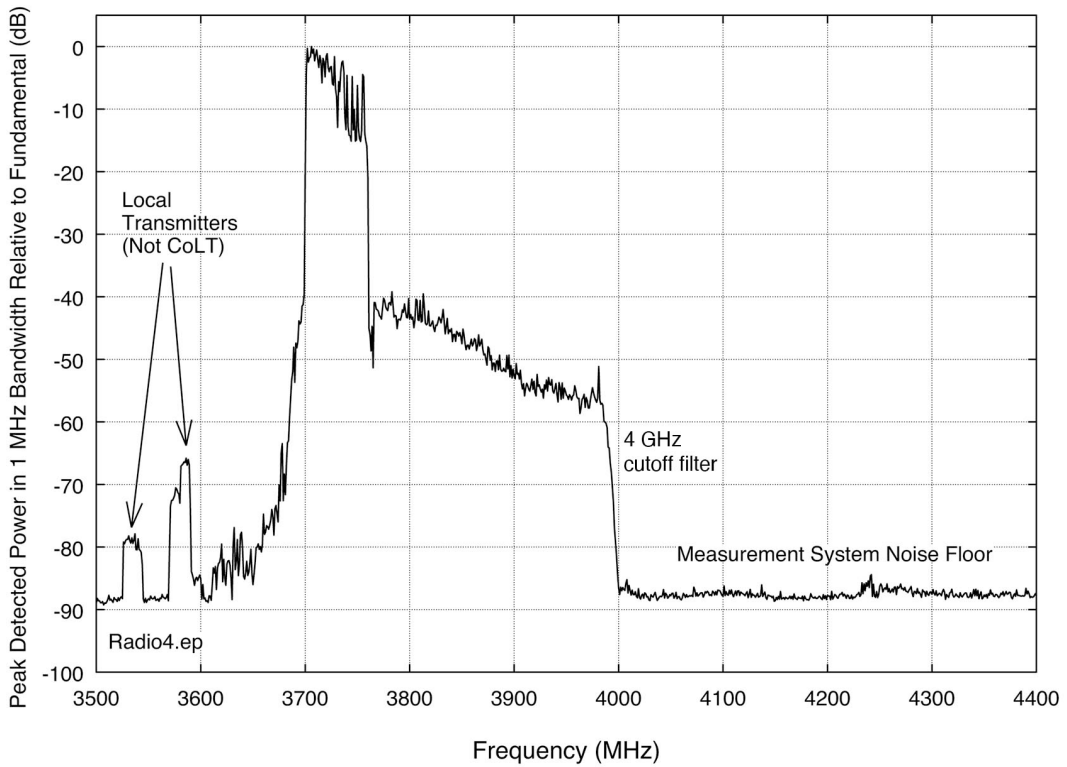


Figure 48. Measured emission spectrum of 5G base station transmitter Radio 4.

Note: Radio 4’s manufacturer has locked out the use of frequencies above 3800 MHz for units sold in the US. The manufacturer only provides for a single channel bandwidth of 60 MHz. Therefore, this radio was measured with its only available channel and bandwidth in the US, namely 3700–3760 MHz. The other two radios were measured with 100 MHz channels tuned to 3800–3980 MHz, at the top of the allocated US 5G n77 band.

Further Note: Measured emission spectra of one of the 5G Radio 1 base stations are shown in Appendix C. They are in an Appendix because they are n78-band radios (lower C-band, 3300–3600 MHz) and are therefore not directly applicable to the JI-FRAI QRT work program. They do however show the same overall structure as the high C-band, n77 band base stations, including wideband PA plateaus across their entire assigned band and bandpass filtering at the edges of the assigned n78 band.

9.1 Structure of 5G Base Station Transmitter Emission Spectra

The measured 5G base station emission spectra show strong morphological similarities to WiMAX and Long Term Evolution (LTE) emission base station transmitter spectra (see morphologically similar spectra for these two types of transmitters in [13] and [29]). The visible, unique structural components are: 1) a wideband power plateau that stretches across the transmitters’ entire band; 2) a sharply channelized desired-signal emission superimposed on that plateau; 3) a fast roll-off of spectrum emissions at the designated band edges.

9.1.1 Wideband Plateau Structure of the 5G Base Station Transmitters

The wideband plateaus are believed to originate in the transmitters’ final-stage PAs. This power should be present whenever the transmitters are powered. It should be present even if the intentionally modulated emissions were to be turned off. It is inherent in the operation of any amplifier circuit.

9.1.2 Channelized Desired-Signal Emission of the 5G Base Station Transmitters

The channelized desired-signal emission is produced by intentional modulation of the emitted signal. It features a very sharp, steep drop-off at its edges, to the PA power plateau. The drop-off ranges between 40 dB and 50 dB for the measured base station transmitters.

9.1.3 Steep Band-Edge Roll-Offs of the 5G Base Station Transmitters

A very fast, steep spectrum roll-off is seen for all the 5G base station transmitters’ emissions. Given the inherently wideband nature of the PA plateaus, the steep drop-offs seen at the exact frequencies of the administratively allocated band edges are surely not accidental. The measured base station transmitters all appear to incorporate effective bandpass filtering for their engineered band of 3700–3980 MHz.

Given that the radio transmitters include effective cutoff filtering at frequencies above 4 GHz, including the radalt band of 4200–4400 MHz, the next question to be answered is: How far down in power are the 5G unwanted emissions in the radalt band, compared to the 5G desired-emission (on-tuned) power?

9.2 Measurement Dynamic Ranges

The graphed dynamic ranges of the three transmitters are 91 dB, 80 dB and 89 dB, respectively. The limit for dynamic range in these results was how much power we could obtain from each transmitter. The outlier among the three, at 80 dB, was Radio 3. Although this radio was nominally specified as having the same maximum EIRP as the other transmitters, it in fact transmitted about 10 dB less.

We do not know why the Radio 3 transmitter power was relatively low compared to the other two transmitters. The carrier who brought it to Table Mountain also funded three of the manufacturer's engineers to be on-site to set up the base station and operate it. If anyone in the world knew how to make that transmitter perform at full power, it was the manufacturer's own engineers. What we do know is that the manufacturer's engineers were certain that the transmitter was being operated at the maximum available EIRP that could be obtained from it. Apparently, it does not operate at the maximum effective radiated power (ERP) listed in its nominal specifications.

9.2.1 Dynamic Range Relative to Measurement System Noise Floor

Spectrum (and signal) analyzers operate on the full input power in their selected resolution (IF) bandwidths. This means that they add their own, internal thermal-electron receiver noise to whatever additional power arrives via the RF input port. When we arrive at a segment of measured spectrum where we see *only* the analyzer's own, internal noise, with not even a single decibel of additional power being seen from the input signal, we can use this information to infer a *maximum* possible input signal power level within that spectrum segment. Take the measurement system's noise level as an arbitrary reference of 0 dB: if any additional power is present within the analyzer's resolution bandwidth from an input signal, then that additional signal power will add linearly to the analyzer's noise level. The way this addition works in decibel-math units is shown in Figure 49.

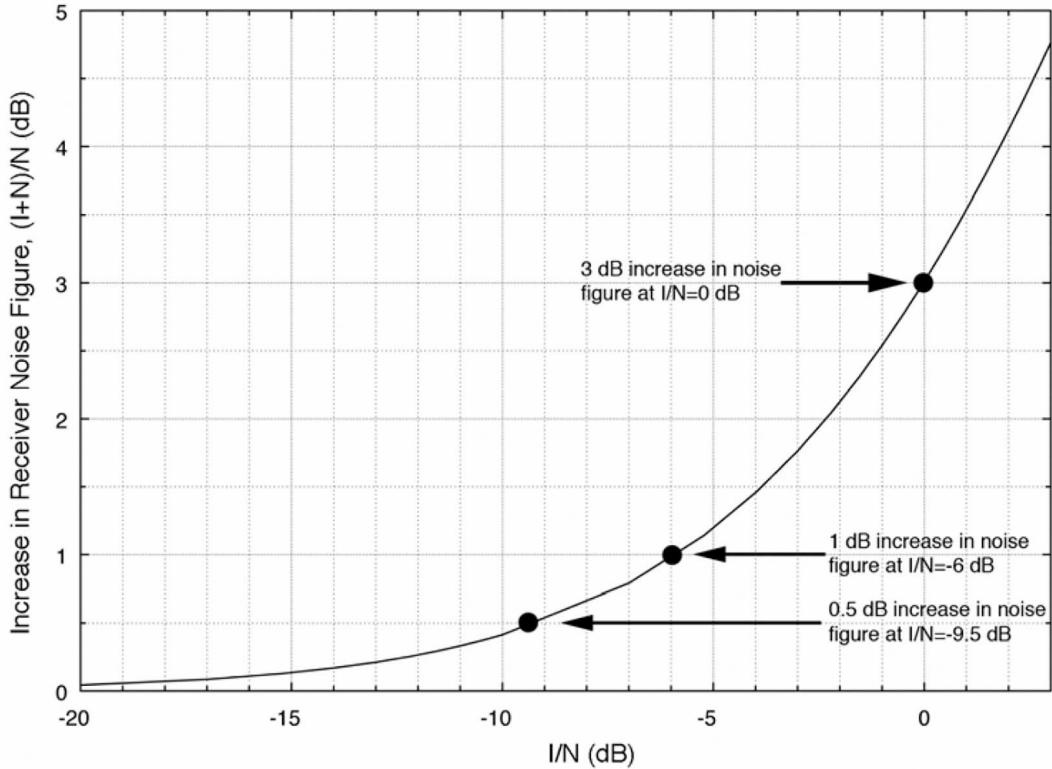


Figure 49. Decibel-math addition graph (from [30], pg. 9).

When we took the spectrum data, we observed the measurement system’s noise, in the time domain, at every frequency measurement step (per Section 7.2 and the example of Figure 15). We could observe, in the time domain at each measurement step, whether any perceptible 5G signal power was present.

9.2.2 Measurement-Based Maximum Possible 5G Unwanted Power in the Radalt Band

Across the frequency range of 4200–4400 MHz, we never saw any perceptible power from 5G emissions in the 100 ms time domain scans at each frequency step. We could visually see an impact of as little as 1/10 of a decibel above the analyzer’s noise. If such an emission had been present, we would have seen the very distinct TDD ON/OFF cycling every 5 ms. In effect, we would have seen “ripples” every 5 ms which would have been the “tops” of the TDD cycles shown in Figure 15.⁶⁹

Because $(-15 \text{ dB} + 0 \text{ dB}) = 0.1 \text{ dB}$ (see Figure 49), this *lack* of having seen even that much impact in any of the 100 ms time-domain dwell intervals of the spectrum measurement in the

⁶⁹ As each time-domain sweep for each dwell cycle is recorded during the spectrum measurement, we can provide the recorded sweeps to third parties if they wish to review them for any visible impact from 5G.

radalt band means that the 5G emissions across 4200–4400 MHz from each of the measured 5G base station transmitters must have been at least 15 dB below the analyzer’s noise floor.

This -15 dB maximum-level impact relative to our measurement system’s noise floor across the radalt band gives the upper-limit 5G power that could have occurred for each of Radios 2 through 4 shown in Table 12, if they were radiating at the regulatory limit of +62 dBm/MHz for urban area deployments.

Table 12. Minimum suppression of measured 5G base station power in the radalt band of 4200–4400 MHz.

Base Station Radio Model	Minimum Radalt-Band Suppression Relative to 5G Intentional Emission Power	Max Radalt-Band (4300 MHz) 5G Power Relative to +62 dBm/MHz Max Allowed 5G EIRP in its Allocated Band
2	(-91 dB–15 dB) = -106 dB	+62 dBm/MHz–106 dB = -44 dBm/MHz
3	(-80 dB–15 dB) = -95 dB	+62 dBm/MHz–95 dB = -33 dBm/MHz
4	(-89 dB–15 dB) = -104 dB	+62 dBm/MHz–104 dB = -42 dBm/MHz

From Table 12, suppression of 5G signals transmitted by base stations is as much as 106 dB (one quarter of one tenth of one billionth of the 5G intentional-radiation power) in the radalt band; it is always at least 95 dB, for certain. Suppression measured for the other two radios might have been similar, given the similar 4 GHz filtering seen in all three emission spectra—the ability to see further suppression for the other two radios was impeded by not having more radiated power available for the spectrum measurements.

Note that the total available 5G MIMO array EIRPs are +77.5 dBm (= +53 dBm maximum transmitter power plus 24.5 dBi maximum antenna gain). Running in 100 MHz channel bandwidth, the maximum power spectrum density that could be radiated during our measurements was (+77.5 dBm/MHz–20 dB) = +57.5 dBm/MHz for Radios 2 and 4. In a 60 MHz bandwidth for Radio 4, this would be +59.7 dBm/MHz. Table 13 shows 5G out-of-band levels relative to these numbers.

Table 13. Maximum 5G base station power in the radalt band of 4200–4400 MHz.⁷⁰

Base Station Radio Model	Max Radalt-Band (4300 MHz) 5G Power Relative to Actual 5G Radio Power Spectrum Density in 5G Allocated Band
2	+57.5 dBm/MHz–106 dB = -48.5 dBm/MHz
3	+57.5 dBm/MHz–95 dB = -37.5 dBm/MHz
4	+59.7 dBm/MHz–104 dB = -44.3 dBm/MHz

⁷⁰ These are *radiated* OoB levels, in contrast to regulatory OoB limits that are often specified as *conducted* levels.

10. THREE DIMENSIONAL 5G RADIATION PATTERN MEASUREMENT RESULTS

Examples of measured airborne 5G MIMO-array radiation patterns are shown in Figures 50 through 55.⁷¹

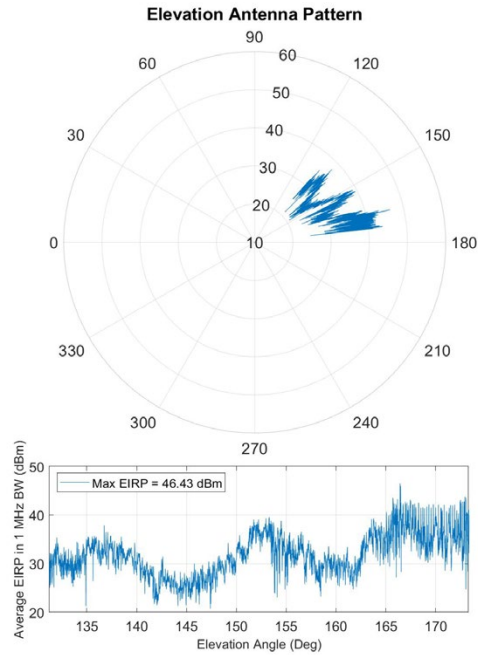


Figure 50. An ascending-hover section through Radio 4 radiation pattern.

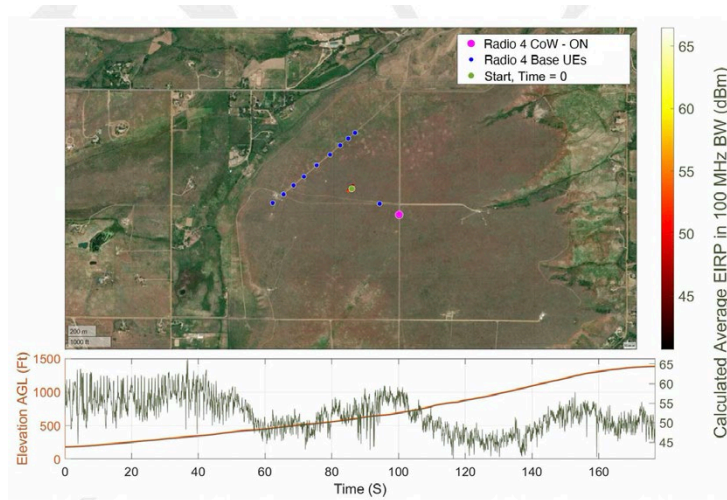


Figure 51. Corresponding ascending-hover heat map of Radio 4. Imagery data ©2021 Google.

⁷¹ The same EIRP data are plotted in the matching (corresponding) polar and rectangular axis graphs. The EIRPs are as measured with the polarization of the airborne collection antenna, as described in Table 10.

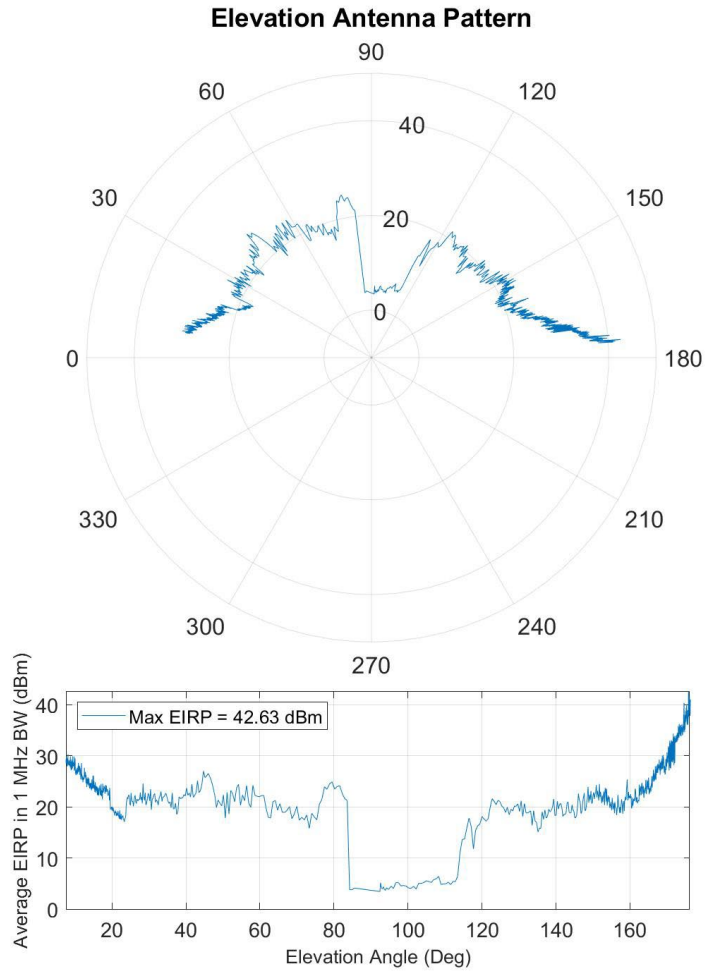


Figure 52. NE to SW overhead traverse at 200 ft AGL radiation pattern for Radio 2.

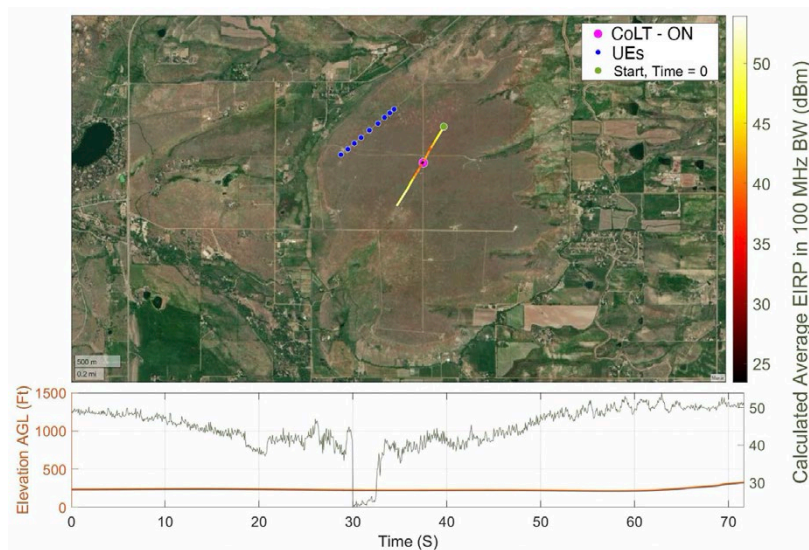


Figure 53. Corresponding NE to SW traverse heat map of Radio 2. Imagery data ©2021 Google.

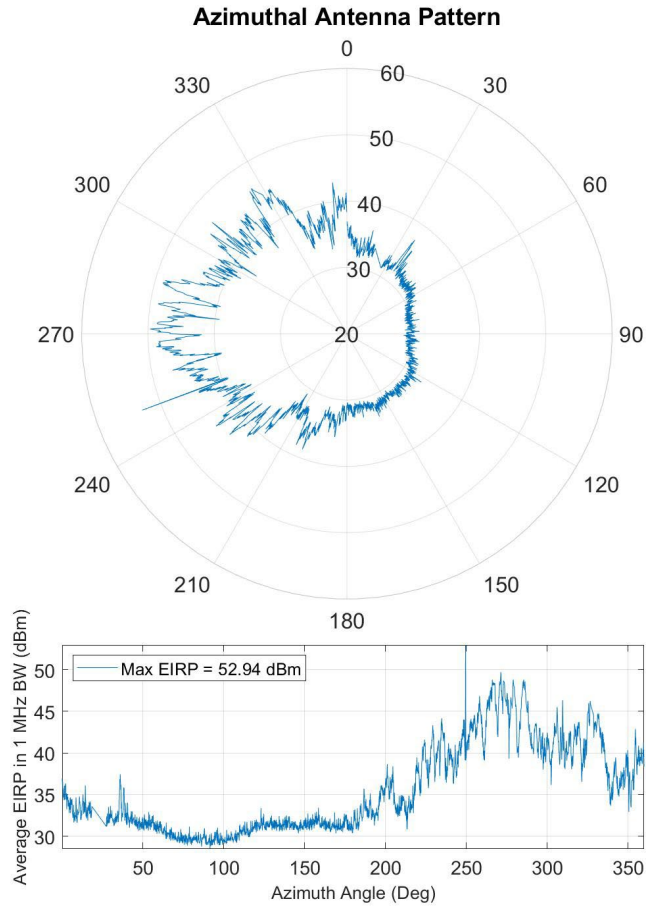


Figure 54. Orbital (circle-around) radiation pattern around Radio 2 at 200 ft AGL.

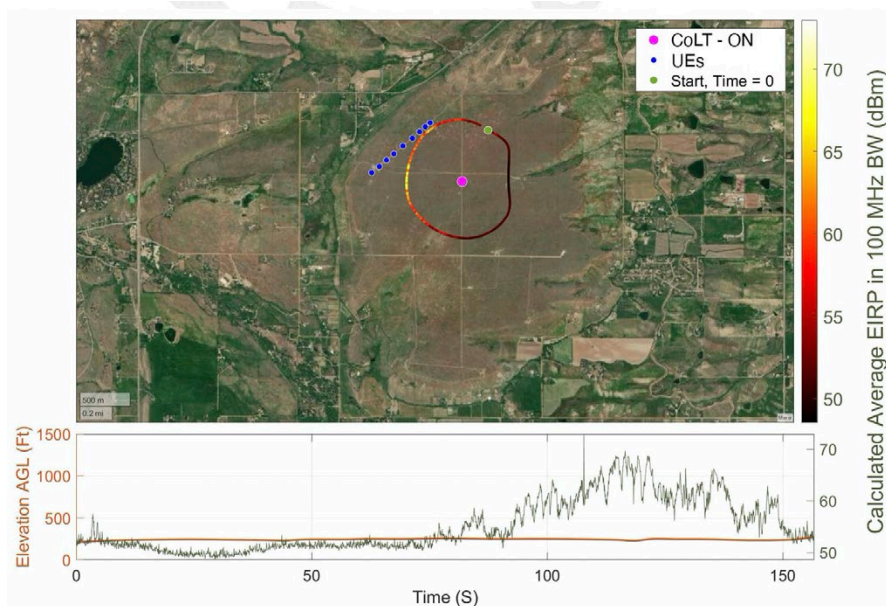


Figure 55. Corresponding orbital heat map of Radio 2. Imagery data ©2021 Google.

10.1 The Four Airborne 5G Radiation Pattern EIRP-Measurement Graph Types

For each helicopter flight section, there are four different graphs. These are:

- A circular-plane section, either azimuth angles or elevation angles (as titled on each graph). Coordinates are polar, (EIRP, θ) or else (EIRP, φ), depending on whether it is showing azimuth or elevation data, respectively. Power units are RMS average-detected power in *EIRP per megahertz*.
- A matching rectangular section showing the same data as the polar graph but graphed in (x, y) coordinates for either (EIRP, θ) or else (EIRP, φ), depending on whether the data are azimuthal or elevational. Power units are RMS average-detected power in *EIRP per megahertz*.
- An overhead-satellite view of the test site (either Table Mountain or Hill AFB) with the ground coordinates of the flight section superimposed. That path is color-coded for the EIRP being directed toward the path at each measured point. Power units are RMS average-detected power in *EIRP for the total power in the channel*.⁷²
- A matching rectangular section showing two curves: The AGL height of the collection platform (the helicopter), shown as a brown curve with the height scale on the left; and the power as function of time along that flight curve, shown a black curve with its power scales on the left. Power units are RMS average-detected power in *EIRP for the total power in the channel*.

10.2 Reading the Graphs

- The polar graphs show angles referenced either from zero degrees at true north (azimuth-angle graphs) or from zero degrees at the local horizontal (elevation-angle graphs). Note that the true-north referenced azimuth angles of the Table Mountain base station MIMO arrays toward the associated UEs ranged from 275° to 318°.
- The same notes apply to the corresponding x-y graphs. The data in these graphs are the same as in the polar plots; only the graph style is changed, from polar to rectangular.
- The overhead satellite view shows the GPS-based ground coordinates of the given flight sections. The colors' scale is adjusted for the dynamic range of the power data. The measured (GPS) locations of the base station MIMO arrays and associated UEs are graphed as magenta and blue dots, respectively.
- The matching rectangular graph shows heights above ground (AGL) as derived from on-board GPS data in the helicopter (which are relative to mean sea level (MSL)). Those points

⁷² For hover sections (ascending or descending), the ground-mapped flight section is of course only a single dot above the hover point.

have then been corrected to AGL by subtracting the known MSL altitude of the test site at each point along the flight path. The power curve on that graph shows EIRP in total channel bandwidth as read through time during that flight section.

10.3 Note on Isolated Data Points in the Airborne Data

In some of the airborne data sets, such as for instance in Figures 54 and 55 at 250° azimuth, isolated data points occur. These outlier points are characterized by their sharp discontinuity from the overall data trace and a large power-excursion size, 10 dB or more from the adjacent data points. They occur rarely. We do not know their origin, but we do not believe that they represent emissions from the transmitters we were measuring. This is because the targeted radio transmitters were themselves running at constant power output throughout the airborne data collections, as verified by our on-the-ground monitoring throughout every airborne measurement (see Section 7.2).

10.4 Airborne Radiation Levels Compared to Main Beam Levels

When examining the measured radiation patterns in the sky, one may want or need to compare these airborne levels to the EIRPs that were emitted in the base stations’ main beams (downtilted toward the UEs as shown in Figures 32 and 33). We therefore note here that the *maximum main-beam* RMS average-detected EIRP levels being emitted *from the base station MIMO arrays toward the UEs* during the data collection flights are as shown in Table 14.

Table 14. 5G MIMO base station main-beam power during the airborne measurements.

Base Station Radio Model	5G Full-Channel Transmitted EIRP	5G Power Density (per Megahertz) Transmitted EIRP
2	+77.5 dBm (max specified)	+77.5 dBm–20 dB = +57.5 dBm/MHz
3	+67.5 dBm ⁷³	+67.5 dBm–20 dB = +47.5 dBm/MHz
4	+77.5 dBm (max specified)	+77.5 dBm–17.8 dB ⁷⁴ = +59.7 dBm/MHz

Running in 100 MHz channel bandwidth, the maximum power spectrum density that could be radiated toward the UEs on the ground during our measurements was (+77.5 dB–20 dB) = +57.5 dBm/MHz for Radios 2 and 4. In a 60 MHz bandwidth for Radio 4, this would be +59.7 dBm/MHz, as shown in Table 14. Radio 3 was always at 10 dB lower power than its specified maximum, but the manufacturer’s on-site engineers were certain that the radio was in fact running at the maximum available power that could be obtained from the transmitter.

⁷³ -10 dB down from max specified, but this was the maximum power that the manufacturer’s three on-site engineers could obtain from the transmitter. We believe that the base station was operating at all its available EIRP when we measured it.

⁷⁴ Radio 4 channel was 60 MHz wide; $20 \cdot \log(1/60 \text{ MHz}) = -17.8 \text{ dB}$.

10.5 Airborne Radiation Patterns at Zenith Angles Above 5G MIMO Arrays

A frequently raised topic is: How much power do 5G MIMO arrays radiate toward radalts that are flying overhead? As our readers will observe when they examine the airborne 5G EIRP data sets (see Section 8.3.6), the MIMO arrays show broad, lower-level EIRPs around their overhead (zenith) angles. An example of this behavior is shown in

Figure 56.

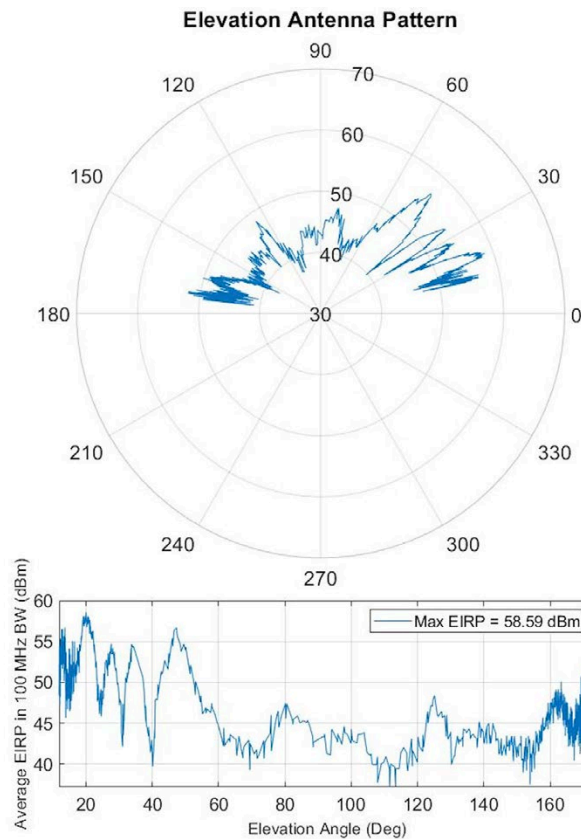


Figure 56. Overhead section of a 5G MIMO array, west-to-east. Note that power is in the full 100 MHz of the 5G channel (which was itself at +77.5 dBm EIRP in its main beam).⁷⁵

In measured airborne sections like this one, the maximum radiation pattern power is often around 20 dB lower than the main beam EIRP. (In this particular example, that level of +58.6 dBm is 18.9 dB below the main beam power of +77.5 dBm in the full-channel bandwidth.)

⁷⁵ The +58.59 dBm max EIRP on the graph is the maximum power shown in the graphed points, not the maximum of the base station.

We note, too, that the measured MIMO array radiation patterns typically show broad, somewhat deep radiation-pattern nulls⁷⁶ for angles at and near the arrays' zeniths. In the example of

Figure 56, this null is around $\pm 30^\circ$ (between elevation angles of $+60^\circ$ to $+120^\circ$) of the array's zenith. Its 100 MHz EIRP level is conservatively at about +45 dBm, which is 32.5 dB below the main beam, full-bandwidth EIRP (+77.5 dBm) of the transmitter. These measured levels in our airborne data sections can be used to analyze the responses of radalt receivers when their flight paths carry them directly above MIMO arrays.

10.6 Near-Far Effect for Radiation from Pairs of CoWs and CoLTs

Another frequently raised topic is: What if large numbers of 5G MIMO base stations are deployed across an area? How much will they add together, as opposed to these measurements that have been performed on a single MIMO array at a time, or else just two 5G CoWs?

An ancillary question is: Do we not need to deploy dozens or hundreds of 5G MIMO base stations for the types of power-in-the-sky measurements that are provided in the JI-FRAI QRT work program that we have described in this report?

These questions can to some extent be addressed by modeling, simulation, and analysis. In contrast, the sheer logistics of setting up and operating one or two 5G base stations at a time are significant. The resources required for setting up a dozen or more such base stations in a calibrated, controlled testing environment are unlikely to ever be available.

We have however examined the data obtained from the airborne collections with the twin CoWs at Table Mountain and with the two CoLTs at Hill AFB. These data show that there is a pronounced *near-far effect* when even only two base station transmitters are deployed side-by-side (at ~ 900 m = 3000 ft separation). The effect is this: The radiation from the nearest base station is always dominant, with the radiation from the farther base station rapidly becoming insignificant as we approach the nearer transmitter. The only location where this effect is not seen is when we are on the spatial cusp between the two transmitters, and they contribute equal amounts of power to our measurement system. That equality-cusp is a narrow zone.

The issue reduces to this, based on our measurement results: If there is a nearer base station with one or more distant transmitters, then the nearer transmitter's emissions will be dominant in a receiver. This effect will only be mitigated in cases where two or more transmitters are simultaneously nearly equidistant from the receiver.

Aggregates of base stations may be significant when there is not *any* single, dominant close-by base station transmitter. This condition of *no* dominant, closest base station would require separate analysis that we cannot provide here.

⁷⁶ Radiation pattern nulls are *lower* power, not *zero* power.

11. APPLYING THE DATA IN THIS REPORT

This report's data sets are intended to be applied to general analyses of 5G transmitted signal electromagnetic compatibility with radalt receivers. This is why the measured emission spectra have been graphed with a zero-decibel reference at their maximum emission power in their operational channels, rather than simply as the power received in our measurement circuits at a given location on the ground. And it is why the airborne radiation patterns have been graphed in terms of power radiated from the MIMO arrays, rather than as the particular power that we measured at specific points in space. In this section we provide the reader with examples of the application of data in this report to 5G transmitter and radalt receiver EMC coexistence math problems.

In providing these examples, we are *not* implying that the particular numbers that we use in each example are themselves representative of the overall EMC solutions to the overall engineering compatibility questions about coexisting 5G base station transmitters and radalt receivers. Our examples are rather meant to guide the reader in understanding *how* to apply the data in this report to the larger EMC question that JI-FRAI has addressed. We hope that this report's data will be used by independent, third-party analysts as a reference that can be applied to these larger issues and questions.

Note on polarization-dependent offsets in measured power levels: As described in Table 10, the airborne measurement antennas had vertical-linear and circular polarizations. The transmitted 5G base station signals are cross-polarized. The power offset introduced between linear or circular and cross-polarized will be 3 dB. Off-boresight polarization is strongly antenna- and angle-dependent, and even varies within the main beam for some antennas.⁷⁷ Lacking exact MIMO array design details and full-wave simulations or supplemental measurements, we do not know how the 5G MIMO array base station signal polarization behaves (varies) as a function of off-boresight (outside the 5G intentional main beam) angles in the sky around, above, and behind the MIMO array. We can only say that it is possible that our measured power levels in the sky could be *as much as* 3 dB lower than the power that would have been coupled into matched-polarized (cross-polarized) measurement antennas.

11.1 Applicable EMC Equations

The overall spectrum compatibility question addressed by the JI-FRAI program and examined in other studies involves, ultimately, understanding and being able to compute the amount of power that couples into radio receiver circuits from spatial power fields. A useful reference for these computations, where all needed spatial-field equations are explicitly derived, is [31].

Fundamentally, the needed equations must tell us two things: how much power exists in space at a given distance from a transmitter that has a given brightness (EIRP); and how much of that power in space will be coupled into a receiver circuit at such points, given that the receiver's

⁷⁷ Private communication, Dr. Charles Dietlein, NTIA.

antenna coupling factor to space (its gain) is either known or can be estimated. From [31], the needed equations are:

$$(FS, dBmV/m) = (EIRP, dBm) + 104.7 - 20\log(d, meters) \quad (1)$$

$$(P_{rx}, dBm) = \left(FS, \frac{dBmV}{m} \right) - 77.2 + (G_{rx}, dBi) - 20\log(f, MHz) \quad (2)$$

$$(P_{rx}, dBm) = (EIRP, dBm) + (G_{rx}, dBi) + 27.5 - 20\log(f, MHz) - 20\log(d, meters) \quad (3)$$

where:

FS = field strength in space in units of decibels relative to a microvolt per meter;

$EIRP$ = a transmitter's effective isotropic radiated power in decibels relative to a milliwatt;

f = radio frequency in megahertz;

P_{rx} = power coupled into a receiver's circuitry in decibels relative to a milliwatt;

G_{rx} = gain of the receiver's antenna in a given direction at frequency f , in decibels relative to isotropic;

d = distance between the transmitter and the receiver in meters.

- The first equation gives power in space (field strength) as a function of distance from a transmitter of a given brightness (EIRP).
- The second equation gives power in a receiver circuit produced by that spatial field strength.
- The third equation gives power in a receiver circuit as a function of a transmitter's brightness (EIRP) and distance.⁷⁸

11.1.1 Propagation Assumption

We take radio propagation to be free-space, $1/r^2$. This is justified by the relatively short distances over which 5G/radalt EMC coexistence math problems must be analyzed.

⁷⁸ This set of equations is over-specified; they are derivable from each other and are not independent. They are given here for the reader's convenience in picking whichever one is needed for a given problem.

11.1.2 Out-of-Band, Off-Axis Radalt Antenna Gains

The gains of the radalt receiver antennas need to be used *at the frequency* and *in the direction of* a 5G signal. If this frequency is a 5G unwanted emission at 4300 MHz, and the direction is in the radalt's main beam below the aircraft, then the radalt receiver's nominal specified antenna gain would suffice for the computation.

However, if the 5G emission in question is fundamental-frequency radiation below 4 GHz (at, e.g., 3900 MHz), and/or the direction from the 5G MIMO array to the radalt receiver antenna is not within the radalt's ordinary main-beam coverage (e.g., the 5G array is off to the side of the aircraft), then it may be inadequate engineering to simply use the radalt's ordinary on-tuned main-beam gain. An example of some out-of-band, off-axis radalt antenna gain patterns is shown in Figure 13. We believe that more such out-of-band, off-axis radalt antenna pattern data are needed for studies of the 5G/radalt EMC coexistence challenge.

11.2 Types of Applications

Some obvious applications of these data include:

- Determining 5G field strength in space as a function of distance from a 5G MIMO array in a given direction.
- Combining the measured emission spectra with 5G bench testing results for on-tuned (to radalt receivers, within their allocated band) versus out-of-band (to radalt receivers, on 5G intentional-radiation channels) interference, to determine the relative distances where 5G interference will occur for each mechanism.
- Determining distances where some pre-defined or pre-conditioned field strength threshold will occur around a 5G MIMO array.
- Connecting bench-testing results with measured EIRPs to determine the distances from a 5G MIMO array at which a given EIRP level will be expected to reach a given interference-power level in a radalt receiver.

Examples of each of these four applications are given here. Solutions are provided in 13.Appendix D.

As noted above, we emphasize that the *numbers used in these problems are for example only*. They are provided here only for *illustrative purposes*, to help readers understand how these problems are analyzed using available data.

Example 1. Analyzing an Airborne Data Plot

Referring to Figures 54 and 55, the maximum 5G EIRP that occurred in a circular orbit at 200 feet AGL around the 5G MIMO array of Radio 2, at 275° azimuth (roughly co-linear with the main beam power that was directed downward, below the orbit, toward the south end of the

line of UEs) was +48 dBm/MHz (per Figure 54) and +68 dBm in the channel's full bandwidth (per Figure 55, consistent with the radio's 100 MHz channel width).

- How far down, in decibels, are those measured power levels relative to the 5G MIMO main-beam power levels? (Use Table 14.)
- What was the elevation angle, from the MIMO array, of that circular orbit?
- Generate a graphical plot of the field strength in space, as a function of distance (10 m to 10 km), along that circular orbit elevation-angle vector for:
 - Field strength in power density ($\text{dB}\mu\text{V}/\text{m}$ per megahertz), and
 - In total channel power ($\text{dB}\mu\text{V}/\text{m}$).

Example 2. Applying Airborne Data to Measured Spectrum and Bench Testing Results

For this example, suppose the following results have been obtained from bench testing of a given hypothetical radalt model and its receiver antenna:

- The bench-testing threshold for out-of-band (to the radalt receiver = 5G intentional) radiation at 3950 MHz has been measured at -35 dBm/MHz.
- The hypothetical radalt receiver antenna characteristics at 3950 MHz are as shown in Figure 13.
- The bench-testing threshold for in-band (to the radalt receiver = 4300 MHz) has been measured at -85 dBm/MHz.
- The radalt receiver antenna characteristics at 4300 MHz are as shown in Figure 12.
- Use the measured 5G EIRP at 3950 MHz, at 45° above the MIMO array's horizon, of +35 dBm/MHz (from Figure 50).
- For simplification, assume that the relative 5G emission spectrum of Figure 46 would look the same (would have the same shape) anywhere/everywhere in space around the MIMO array.

Using the measured emission spectrum for Radio 2 (Figure 46), analyze:

- The *relative* distance (distance ratio) where 5G unwanted power in-band to a radalt receiver would occur, compared to the distance where 5G intentional radiation would cause interference.
- The absolute distance at which 5G intentional emissions would reach the hypothetical radalt receiver bench-test interference threshold of +35 dBm/MHz. This is where the 5G MIMO array would be 45° away from the radalt's local nadir (i.e., is 45° off of the direct vertical line beneath the airplane).

- The absolute distance at which 5G intentional emissions at the urban regulatory limit of +62 dBm/MHz would reach the interference threshold. Use the out-of-band -5 dBi radalt antenna gain for shallow angles that is observed in the example antenna patterns of Figure 12.

Example 3. Computing a Coordination Distance Based on a Field Strength Limit

Suppose that a spatial interference threshold power of +75 dB μ V/m has been determined for 5G power at 3900 MHz. Referring to the MIMO array measured in Figure 52, at what distance would this power level be encountered at 30° above the MIMO array's local horizon?

Example 4. Computing Coordination Distances Based on Airborne Data and Bench Testing Results

A hypothetical radalt receiver develops harmful interference effects at -43 dBm/MHz at 3900 MHz during bench testing. For the maximum 5G MIMO array EIRP output of +46 dBm/MHz at 13° above the horizon in Figure 50, and for radalt antenna characteristics at 3900 MHz that (for instance) look like Figure 13,

- At what distance from the MIMO array will that interference threshold occur?
- What will the distance be if an additional -6 dB of interference margin is included?
- What if that margin is extended by another 4 dB, for a total of -10 dB of interference margin on top of the bench-test result?

12. SUMMARY AND CONCLUSIONS

12.1 Summary

In this report, we have summarized the JI-FRAI QRT work program and the background against which it has been developed. We have provided, as concisely but as informatively as possible, technical aspects of the 5G/radalt EMC coexistence question that readers might find to be informative. These include the spectrum history of the 3700–4400 spectrum range in the US; the background and history of radalt development; and technical characteristics of radalts and of 5G radio signals in the 3 to 4 GHz portion of the spectrum.

We have described the two types of RF interference that could conceivably occur between 5G transmitters and radalt receivers, and have explained the importance of effective RF filtering on transmitters and/or receivers, depending on circumstances.

Within the context of this background, we have described the overall JI-FRAI QRT work program and the *how* and *why* of where the work described in this report fits into that bigger picture. That work, described in detail in this report, has been to establish two key EMC technical factors via measurements of 5G MIMO-array base station transmitters.

The first of these are measurements of the wideband, wide dynamic range emission spectra of all three models of 5G base station transmitters that are being deployed in the US 5G n77 radio band (3700–3980 MHz). The radiated spectra have been measured for all three known 5G base station transmitters across 3500 MHz to 4400 MHz with an effective dynamic range for the maximum limits of 5G unwanted power within the radalt band being as much as 106 dB below the radios' intentional emission power at 4 GHz. As described in more detail in Table 13, the 5G unwanted-emission power levels in the radalt band are upper-bounded by our results as being between -37.5 dBm/MHz (for the radio on which we achieved the smallest measurement dynamic range) and -48.5 dBm/MHz (for the radio model for which we achieved the largest measurement dynamic range). These being upper bounds, the actual unwanted emission levels may have been lower than these numbers—how much lower, we do not know.

The second major output has been exhaustive three-dimensional airborne measurements of actual radiation patterns of 5G MIMO arrays for those same radio models, plus a fourth model that operates in slightly lower frequency spectrum. Those measurements have been performed up in the sky, where airplanes fly. That is, from the local horizons of the 5G MIMO arrays all the way through the arrays' zenith angles.

The spectrum data that were collected have been analyzed and are provided in this report. The airborne data, because of their sheer volume, are provided via GitHub, as described in Section 8.3.6.

12.2 Conclusions

We have written this report to provide spectrum and airborne radiated power data to assist researchers in their quest to create safe, successful, and effective coexistence between 5G

terrestrial base station transmitters and airborne radalt receivers. It is our hope and expectation that those researchers will be able to fruitfully apply our data to their own EMC analyses, not the least of these being results of radalt-receiver bench testing.

We do offer some immediate conclusions. These are based on the data we have collected and analyzed.

The first conclusion regards the amount of suppression of 5G unwanted emissions within the allocated radalt spectrum band. As just noted, three models of 5G base station that are being deployed in the US 5G n77 band show distinctly visible, effective RF bandpass filtering in their emission spectra. The 5G transmitter high-frequency filter cut-offs are all at 4 GHz; above 4 GHz (i.e., within the radalt band of 4200–4400 MHz) these radios' spectrum emissions are as much as 106 decibels lower than their on-tuned intentional-radiation power in the 5G frequency band 3700–3980 MHz.

As described in more detail in Table 13, the 5G unwanted-emission power levels in the radalt band are upper-bounded by our results as being between -37.5 dBm/MHz (for the radio on which we achieved the smallest measurement dynamic range) and -48.5 dBm/MHz (for the radio model for which we achieved the largest measurement dynamic range). These being upper bounds, the actual unwanted emission levels may have been lower than these numbers—how much lower, we do not know. This low level of unwanted 5G emissions within the radalt spectrum band reduces the potential for a 5G-to-radalt harmful interference scenario which would be due to 5G unwanted emissions on radalt receiver frequencies. The FCC might seek to examine unwanted emissions from future 5G base station radios to see if they remain similarly low.

This measurement-based observation increases the likelihood that, to the extent EMC problem arise between 5G transmitters and adjacent-band radalt receivers, the technical solution to such a problem might be installation or retrofitting of more-effective RF power-rejection filters on radalt receivers for frequencies below 4200 MHz.

The second conclusion is that airborne radiation patterns show measurably, significantly less power than is found in 5G base station main antenna beams directed toward UEs at ground level. The amount of power reduction in the sky is variable and needs to be examined by researchers in detail, using the collected data that we have made available.

We note however that our airborne field strength data show that all the 5G MIMO arrays have distinct nulls (not zero power, but significantly reduced power relative to the main antenna-beam levels) at the skyward zeniths above the arrays. These radiated-power nulls will reduce vertical height separations between 5G towers and aircraft where any given power level will be encountered by radalt receivers passing through the sky above the 5G MIMO arrays. This observation, and the data that we have collected that show this effect should be addressed for the EMC cases of radalt receivers whose flight paths carry them directly above 5G base station transmitter arrays.

A third conclusion is that we have observed a distinct near-far effect in our airborne measurements on pairs of CoWs. This effect causes the nearer base station transmitters' emissions to be dominant in a receiver, with more-distant transmitters' contributions rapidly

fading to insignificance. This effect implies that aggregates of 5G base station transmitters might be most usefully analyzed for EMC cases in which there are *no* individual, nearby transmitters. Otherwise, when a single 5G transmitter is near a receiver, that single transmitter's emitted power will tend to be dominant over the cumulative, aggregated emissions from more-distant groupings of 5G transmitters.

13. REFERENCES

- [1] Federal Communications Commission Fact Sheet: “Expanding Flexible Use of the 3.7 to 4.2 GHz Band, Report and Order and Order of Proposed Modification - GN Docket No. 18-122, Feb. 7, 2020; Doc 362358A1.pdf <https://www.fcc.gov/document/fcc-expands-flexible-use-C-band-5g-0>
- [2] Radio Technical Commission for Aeronautics (RTCA), “Assessment of C-band Mobile Telecommunications Interference on Low Range Radar Altimeter Operations,” RTCA Paper No. 274-20/PMC-2073, Oct. 7, 2020. https://www.rtca.org/wp-content/uploads/2020/10/SC-239-5G-Interference-Assessment-Report_274-20-PMC-2073_accepted_changes.pdf
- [3] Redman, D. and C. Barber, and AFE 76s2 Project Members, “Derivation of Radar Altimeter Interference Tolerance Masks, Vol. I: Introduction, Test Procedures, and Fundamental Test Results,” Aerospace Vehicle Systems Institute (AVSI), Dec. 6, 2021. <https://avsi.aero/wp-content/uploads/2021/12/AVSI-AFE76s2-Report-ITMs-Vol-I-PUBLIC.pdf>
- [4] Barber, C. and D. Redman, and AFE 76s2 Project Members, “Derivation of Radar Altimeter Interference Tolerance Masks, Vol. II: Spurious Test Results,” Aerospace Vehicle Systems Institute (AVSI), Dec. 22, 2021. <https://avsi.aero/wp-content/uploads/2021/12/AVSI-AFE76s2-Report-ITMs-Vol-II-PUBLIC.pdf>
- [5] Aerospace Vehicle Systems Institute (AVSI), “AVSI Publishes Report Cataloging Out-of-Band Interference to Radar Altimeters,” Dec. 6, 2021. <https://avsi.aero/afe76s2-report/>
- [6] Garfield, B., *The Thousand Mile War*, Doubleday Oct. 1969, reprinted by Bantam Books Aug. 1988.
- [7] Sheehan, S., *A Missing Plane*, Penguin Publishing, 1986.
- [8] AN/APN-1 entry in United States Radar Equipment Handbook, MIL-HDBK-162B, Vol. 1, US Department of Defense, Dec. 15, 1973, pp. 17-20.
- [9] Sinsheimer, R. L., “Altitude Determination” in *Radar Aids to Navigation*, J. S. Hall, ed., Vol. II of the MIT Radiation Laboratory Radar Series, Office of Scientific Research and Development, National Defense Research Committee, 1947, Sec. 4.3, pp. 131-142.
- [10] AN/APN-22 entry in “United States Radar Equipment Handbook,” MIL-HDBK-162B, Vol. 1, US Department of Defense, Dec. 15, 1973, pp. 35-36.
- [11] National Telecommunications and Information Administration, “Manual of Regulations and Procedures for Federal Radio Frequency Management,” U.S. Department of Commerce, January 2021 edition. <https://www.ntia.doc.gov/page/2011/manual-regulations-and-procedures-federal-radio-frequency-management-redbook>

- [12] Sanders, G. A., J. E. Carroll, F. H. Sanders, R. L. Sole and R. J. Achatz, “Emission Spectrum Measurements of a 3.5 GHz LTE Hotspot,” NTIA Technical Report TR-15-512, U.S. Dept. of Commerce, Feb. 2015. <https://its.ntia.gov/publications/2790.aspx>
- [13] Frey, M., G. A. Sanders, J. Splett, J. Ladbury, F. H. Sanders, A. Kord and R. Jacobs, “Measured Emission Spectra of Selected AWS-3 LTE Transmitters,” NTIA Technical Report TR-18-528, U.S. Dept. of Commerce, Dec. 2017. <https://its.ntia.gov/publications/3189.aspx>
- [14] Sanders, F. and V. S. Lawrence, 1995, “Broadband Spectrum Survey at Denver, Colorado,” NTIA Report 95-321, U.S. Dept. of Commerce, Sep. 1995. <https://its.ntia.gov/publications/2353.aspx>
- [15] Sanders, F., B. Ramsey and V. S. Lawrence, 1995, “Broadband Spectrum Survey at San Diego, California,” NTIA Report 95-321, U.S. Dept. of Commerce, Sep. 1995. <https://its.ntia.gov/publications/2366.aspx>
- [16] Sanders, F., B. Ramsey and V. S. Lawrence, 1995, “Broadband Spectrum Survey at Los Angeles, California,” NTIA Report 95-321, U.S. Dept. of Commerce, Sep. 1995. <https://its.ntia.gov/publications/2368.aspx>
- [17] Sanders, F., B. Ramsey and V. S. Lawrence, 1995, “Broadband Spectrum Survey at San Francisco, California May-June 1995,” NTIA Report 95-321, U.S. Dept. of Commerce, Sep. 1995. <https://its.ntia.gov/publications/2398.aspx>
- [18] Sanders, F., R. Hinkle and B. Ramsey, “Analysis of Electromagnetic Compatibility Between Radar Stations and 4 GHz Fixed-Satellite Earth Stations,” NTIA Report 94-313, U.S. Dept. of Commerce, Jul. 1994. <https://its.ntia.gov/publications/2340.aspx>
- [19] Skolnik, M. I., *Introduction to Radar Systems*, McGraw-Hill, 1980, pp. 84–87.
- [20] Skolnik, M. I., *Radar Handbook 2nd ed.*, McGraw-Hill, 1990, Section 14.18 (pp. 14.34–14.36).
- [21] Frick, S., (Senior Radar Systems Engineer, Honeywell), “Radar Altimeters: Overview of Operation, Design, and Performance,” Briefing by Honeywell, Nov. 8, 2021. <https://avsi.aero/wp-content/uploads/2021/12/Radar-Altitude-Overview-of-Design-and-Performance.pdf>
- [22] Kayton, M. (TRW) and W. R. Fried (Autonetics), eds., *Avionics Navigation Systems*, John Wiley & Sons, 1969, Sections 14.4.7 and 14.4.8 (pp. 540–548).
- [23] G. W. Stimson, *Introduction to Airborne Radar 2nd ed.*, SciTech Publishing, Inc., 1998, pp. 37–38.
- [24] Radio Technical Commission for Aeronautics, “Minimum Performance Standards for Airborne Low-Range Radar Altimeters,” RTCA DO-155, 1150 18th NW, Suite 910, Washington, DC 20036. <https://standards.globalspec.com/std/940029/RTCA%20DO-155>

- [25] European Telecommunications Standards Institute (ETSI), Technical Specification for 5G NR Base Station (BS) Radio Transmission and Reception, 3GPP TS 38.104, Version 16.4.0, Release 16, August 2020, ETSI Reference RTS/TSGR-0438104vG40. https://www.etsi.org/deliver/etsi_ts/138100_138199/138104/16.04.00_60/ts_138104v160400p.pdf
- [26] Part 47 of the Code of Federal Regulations (47 CFR), Ch. 1, § 27.50: “Power Limits and Duty Cycle.” October 2010. <https://www.govinfo.gov/app/details/CFR-2010-title47-vol2/CFR-2010-title47-vol2-sec27-50>
- [27] Nadeem, Q-U-A, A. Kammoun and M-S. Alouini, “Elevation Beamforming with Full Dimension MIMO Architectures in 5G Systems: A Tutorial,” *IEEE Communications Surveys & Tutorials*, pp (99): 1-1, July 2019. <https://arxiv.org/pdf/1805.00225.pdf>
- [28] 5G Americas, “Advanced Antenna Systems for 5G,” 5G Americas White Paper, August 2019. https://www.5gamericas.org/wp-content/uploads/2019/08/5G-Americas_Advanced-Antenna-Systems-for-5G-White-Paper.pdf
- [29] Sanders, F. H., R. L. Sole, J. E. Carroll, G. S. Secrest and T. L. Allmon, “Analysis and Resolution of RF Interference to Radars Operating in the Band 2700–2900 MHz from Broadband Communication Transmitters,” NTIA Technical Report TR-13-490, U.S. Dept. of Commerce, Oct. 2012. <https://its.ntia.gov/publications/2684.aspx>
- [30] Sanders, F., R. Sole, B. Bedford, D. Franc and T. Pawlowitz, “Effects of Interference on Radar Receivers, NTIA Report TR-06-444, U.S. Dept. of Commerce, Sep. 2006. <https://its.ntia.gov/publications/2481.aspx>
- [31] Sanders, F. H., “Derivations of Relationships Among Field Strength, Power in Transmitter-Receiver Circuits and Radiation Hazard Limits,” NTIA Technical Memorandum TM-10-469, U.S. Dept. of Commerce, Jun. 2010. <https://its.ntia.gov/publications/2507.aspx>

ACKNOWLEDGEMENTS

The work described in this report has required intensive ongoing support from many organizations and individuals. Here we wish to recognize these people and organizations, and their significant contributions.

We would not have had the opportunity to be part of JI-FRAI's work program without the initiative and support of Dr. Jonathan Ashdown of the US Air Force. He was instrumental in bringing us into the JI-FRAI program as part of broader work for the ongoing Hill AFB 5G Project.

Within JI-FRAI, Mr. Alan Burke of the US Air Force provided initial JI-FRAI leadership that was crucially important to starting the entire program down a useful track while avoiding unnecessary distractions. After he moved on to the Missile Defense Agency, his successor, CDR Stephen Simpson of the US Coast Guard, provided continuing strong leadership and management of the entire effort, including our part of it.

Other DoD JI-FRAI members who have played especially significant roles and made important contributions to this work have included Lt. Col. Dylan McDermott (USAF), Mr. Linwood Knox, Mr. Dockery (Doc) Lambert, Mr. Jeff Zemke, Mr. Mark Fiebrandt, and Mr. Mike Mather.

Within the US Army, we could not have performed the initial Table Mountain airborne data collections and subsequent collections at Hill AFB without the tremendous support of the U.S. Army Redstone Test Center, Aviation Flight Test Directorate, Instrumentation Data Acquisition and Processing Division (TERT-ATG). Individuals there whom we wish to especially thank for their outstanding support include Ms. Angela Jones, who unfailingly and very professionally kept us all organized as we planned for the first Risk Reduction flights; and Mr. Dennis Shipley, the Lead Instrumentation Engineer who converted our approximate ideas about flight instrumentation into concrete results. This included getting our calibrated antennas properly mounted on the UH-60 and helping us to properly plan and execute our entire airborne measurement system. On the flight side, we very much thank the two Army Experimental Test Pilots (XPs), CW3 Brian McCormick and CW4 Todd Wolfe, who flew their specially instrumented UH-60 exactly as needed for the test series. This included providing expert control and navigation in-close to the 5G MIMO array towers under sometimes less-than-optimal weather conditions.

MITRE has provided ongoing, important assistance to the JI-FRAI effort. Two people there who have been especially helpful to us have been Mr. Jeff Correia and Dr. Steven Best.

The 5G carrier companies have contributed very substantial resources to our part of the JI-FRAI effort. We could not have completed the work described in this report without that support. We especially wish to thank Mr. Pete Tenerelli and Mr. Christopher Sheppard of Verizon for the outstanding level of support that they have given us. This has included intensive planning and execution of on-site 5G base station deployments at Table Mountain and at Hill AFB, and then finally for another base station in a second round of Table Mountain measurements. Other members of the Verizon team who made critically important contributions to setting up and operating the 5G base stations were Mr. Mark Skelton and Mr. Jay Rushing.

Another 5G carrier that made a large contribution was AT&T. We wish to thank Mr. Kory Lippolis of that organization, along with his entire team, for the major effort that they made to get their 5G base station deployed and to keep it running during our measurement series on that base station transmitter.

Among the 5G radio manufacturers, we obtained especially critically needed support from Nokia. That company provided information and on-site assistance that we could not have done without. We especially wish to recognize Mr. Bart Hardesty of Nokia Naperville, Illinois. A contractor, MasTec, provided crucially important on-site construction and operational support.

The Colorado Heli-Ops company provided the helicopters we used for three of our collections. They were very capable and flexible in assisting us with preparing our flights with the side-boom arm. Their pilots very expertly flew the routes we needed during the airborne collection sorties.

On the spectrum management side of things, we could not have (really, legally could not have) performed these measurements without Special Temporary Authorizations (STAs) allowing us to operate the 5G base stations, including at locations not that far from Denver International Airport and Salt Lake City Airport. Obtaining those STAs was a sometimes-almost-harrowing intersection of bureaucratic necessity with fundamental engineering-and-safety analyses. People who were crucially important to getting the STAs processed, analyzed and granted included Mr. Mike Chang of ITS, Mr. Rodney Murphy of the FAA, Mr. James Aviles of the FAA, Mr. Jerry Sullivan of the Department of Commerce Frequency Assignment Committee (NOAA), and Mr. Michael Brown of the Frequency Assignment Branch, NTIA.

Our in-house data collection engineers were Mr. Geoff Sanders, Mr. Adam Hicks, and Mr. Savio Tran. They flew their missions and collected their airborne data flawlessly.

Other important ITS engineering support staff included Mr. John Carroll (Acting Chief of the ITS Measurement Division), Mr. John Ewan, Mr. Ken Brewster, Mr. Eric Nelson (Acting Director of ITS), and Mr. Steve Shockome. Messrs Ewan and Brewster performed the tilt-axis antenna gain measurements for the measurement antenna mounted on the simulated UH-60 belly plate.

At NTIA's Office of Spectrum Management (OSM), Mr. Charles Cooper provided important assistance in a variety of roles, including interfacing with other agencies as we planned and implemented the work program. Likewise, Mr. Bob Pavlak at the FCC was of considerable assistance in helping us to get started with our work and carrying it through.

Lastly, we thank the many people, including numerous subject matter experts, who carefully reviewed the original draft of this report and who submitted well-considered comments and recommendations. Those reviews substantially improved the draft, converting it from a relatively rough document to a polished finished product. If this report has shortcomings, they are not attributable to any lack of well-considered inputs from our reviewers.

APPENDIX A: FLIGHT CARDS FOR AIRBORNE SORTIES AROUND 5G BASE
STATION RADIOS 2 THROUGH 4 AT TABLE MOUNTAIN

CoW Aerial Measurements Overviews and Draft Flight Cards

Version 1

Ken Calahan
(2 June 2022)

CoW Aerial Measurements Overview

- Objectives:
 - Make similar airborne measurements as were made in the JI-FRAI RRE.
 - RF Environment: [CoW ON with 10 UEs spread somewhat evenly between 270 and 330 degrees azimuth \(rel. True North\)](#)
- Overview:
 - Helicopter Altitude will be based on Pressure Altimeter set for JeffCo Airport altitude on take-off
 - Measure RF signals radiating from CoW at various altitudes
 - Ground Speed: 20 to 40 knots (pilot's discretion)
 - **Pattern A:** *Straight and level "Azimuthal" back-and-forth pattern on 300/120 headings, four (4) altitudes (6900, 6100, 5800, and 5700 ft MSL)*
 - **Pattern E:** *Overhead "Traverse" back-and-forth pattern over the top of CoW on 210/030 heading, four (4) altitudes (5700, 5800, 6100, and 6900 ft MSL)*
 - **Pattern B:** *Straight and level "Runway" back-and-forth pattern on 210/030 headings, four (4) altitudes (6900, 6100, 5800, and 5700 ft MSL)*
 - **Pattern C:** *Helicopter "Hover" over a fixed-point, Constant-Rate Ascent with large-radius descending loop to return to hover point for next ascent, 5700 ft MSL to 6900 ft MSL*
 - **Pattern D:** *Full Circle (Radius from a Fixed Point) around each CoW; radius = 500 meters, five altitudes (6900, 6100, 5800, 5700, and 5660 ft MSL) starting 350 feet west of hover point*

Aerial Measurement Systems

- GPS recorder (Garmin)
- RSMS Laptop
- Keysight Field Fox (6 GHz version)
- Antenna Switch
- Three 3-foot low-loss cables with N-type connectors
- MATLAB
- RSMS Fifth Generation acquisition program – **Swept, 0-Hz span**
- Boom-mounted omni and CBS antenna on Raven R-44 helicopter

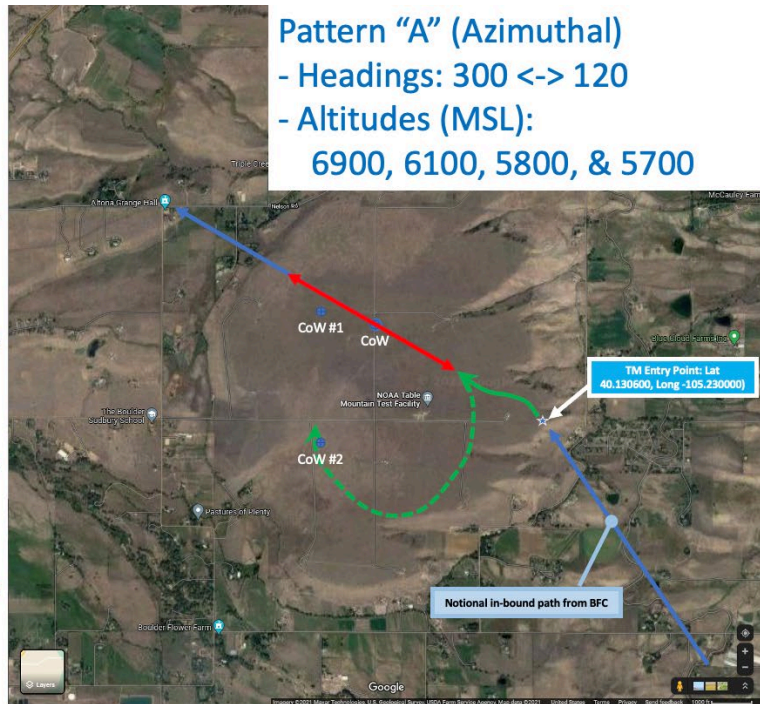
Take-off Configuration

- GPS recorder (Garmin): Settings – New track, max resolution, running, anchored in front left footwell
- Laptop: ON
- Laptop GPS time-sync: Done
- Field Fox: ON/Standby
- Antenna Switch: Position #1 (Down-looking CBS antenna)
- MATLAB: Open and Running
- MATLAB Command Line: Load **“Swept”**
- Configure measurement fields
- Start measurement at take-off or enroute

Pattern A Azimuthal Straight & Level “Back & Forth” (300/120 headings, Across the top of the CoW)

- Enter Table Mountain (TM) at the southern end of 55th St. at 6900 MSL
- TM Entry Waypoint: Lat 40.130600, Long -105.230000
- Line up on CoW, establish heading of 300 degrees True
- CoW Waypoint: Lat 40.137320, Long -105.244540
- Fly to NW edge of TM (Waypoint: Lat 40.141000, Long -105.252540)
- Near NW edge of TM, slow and reverse course, heading 120 degrees True
- Fly to SE edge of TM (near entry point)
- Near SE edge of TM, slow and reverse course, heading 300 degrees True
- Descend to 6100 MSL
- Fly to NW edge of TM
- Near NW edge of TM, slow and reverse course, heading 120 degrees True
- Fly to SE edge of TM (near entry point)
- Near SE edge of TM, slow and reverse course, heading 300 degrees True
- Descend to 5800 MSL
- Fly to NW edge of TM
- Near NW edge of TM, slow and reverse course, heading 120 degrees True
- Fly to SE edge of TM (near entry point)
- Near SE edge of TM, slow and reverse course, heading 300 degrees True
- Descend to 5700 MSL
- Fly to NW edge of TM
- Near NW edge of TM, slow and reverse course, heading 120 degrees True
- Fly toward SE edge of TM (near entry point)
- About half-way to previous SE turn-around points, initiate a large-radius right turn to reposition for entry into Over-flight (030/210) pattern

Pattern “A” (Azimuthal)
- Headings: 300 <-> 120
- Altitudes (MSL):
6900, 6100, 5800, & 5700



Pattern E
Over-flight Straight & Level "Back and Forth"
(030/210 headings, Across the top of the CoW)

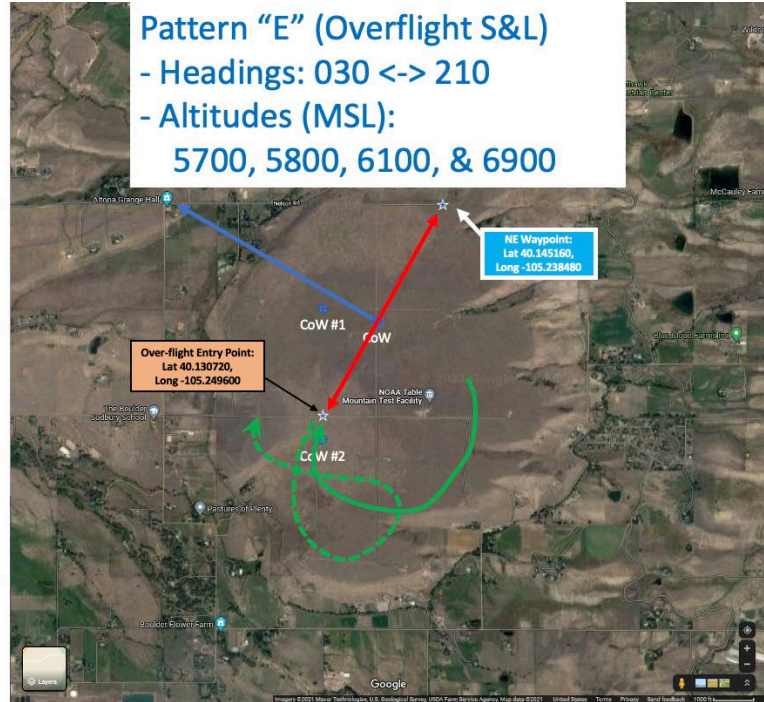
- Enter pattern from just west of CoW #2 at 5700 MSL, heading: 030 degrees true
- Over-flight Entry Waypoint: Lat 40.130720, Long -105.249600
- Fly to matching NE Waypoint (Lat 40.145160, Long -105.238480)
- Beyond NE Waypoint, slow and reverse course, heading 210 degrees True
- Fly to and beyond Over-flight Entry Waypoint, then slow and reverse course, heading 030 degrees True

- Ascend to 5800 MSL, align on Over-flight pattern entry point
- Fly to NE Waypoint
- Beyond NE Waypoint, slow and reverse course, heading 210 degrees True
- Fly to and beyond Over-flight Entry Waypoint, then slow and reverse course, heading 030 degrees True

- Ascend to 6100 MSL
- Fly to NE Waypoint
- Beyond NE Waypoint, slow and reverse course, heading 210 degrees True
- Fly to and beyond Over-flight Entry Waypoint, then slow and reverse course, heading 030 degrees True

- Ascend to 6900 MSL
- Fly to NE Waypoint
- Beyond NE Waypoint, slow and reverse course, heading 210 degrees True
- Fly to and beyond Over-flight Entry Waypoint

- Circle left to re-position for NW (030) entry into Pattern B



Pattern E to Pattern B Transition

- **Antenna Switch:**
 - Call for switch toggle from Position #1 (Down-looking CBS antenna) to Position #2 (Omni antenna)
 - Confirm switch toggle
 - Note "Switching done" and Clock Time in "Measurement Notes" field

Pattern B
Runway Straight & Level "Back and Forth"
(030/210 headings, broadside to CoW)

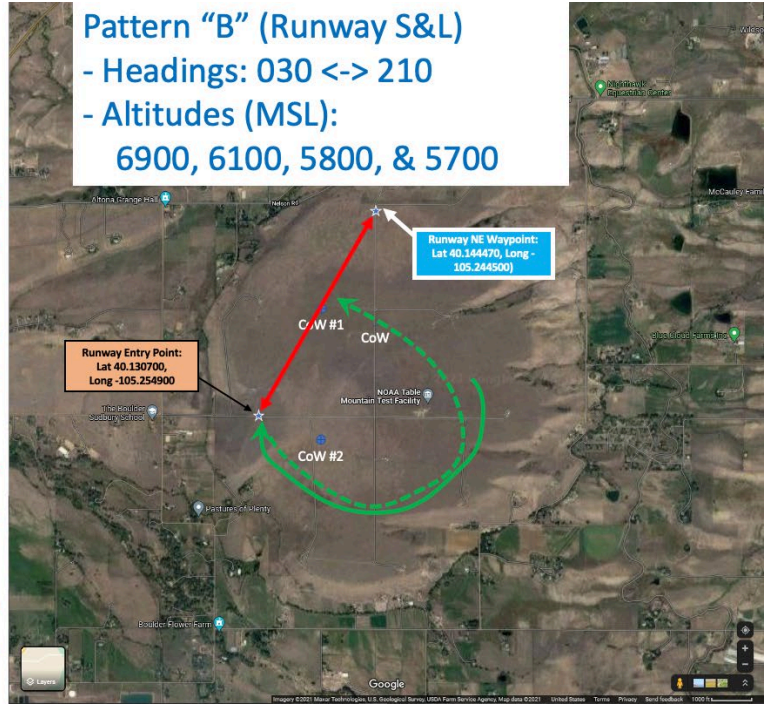
- Enter pattern from SW over west edge & Plateau Road at 6900 MSL, heading: 030 degrees true
- Runway (030/210) Entry Waypoint: Lat 40.130700, Long -105.254900
- Fly to Runway NE Waypoint (Lat 40.144470, Long -105.244500)
- Beyond NE Waypoint, slow and reverse course, heading 210 degrees True
- Fly to SW edge of TM (beyond pattern entry point)
- Near SW edge of TM, slow and reverse course, heading 030 degrees True

- Descend to 6100 MSL, align on SW pattern entry point
- Fly to NE Waypoint
- Beyond NE Waypoint, slow and reverse course, heading 210 degrees True
- Fly to SW edge of TM (beyond pattern entry point)
- Near SW edge of TM, slow and reverse course, heading 030 degrees True

- Descend to 5800 MSL
- Fly to NE Waypoint
- Beyond NE Waypoint, slow and reverse course, heading 210 degrees True
- Fly to SW edge of TM (beyond pattern entry point)
- Near SW edge of TM, slow and reverse course, heading 030 degrees True

- Descend to 5700 MSL
- Fly to NE Waypoint
- Beyond NE Waypoint, slow and reverse course, heading 210 degrees True
- Fly to SW edge of TM (beyond pattern entry point)
- Near SW edge of TM, slow and reverse course, heading 030 degrees True

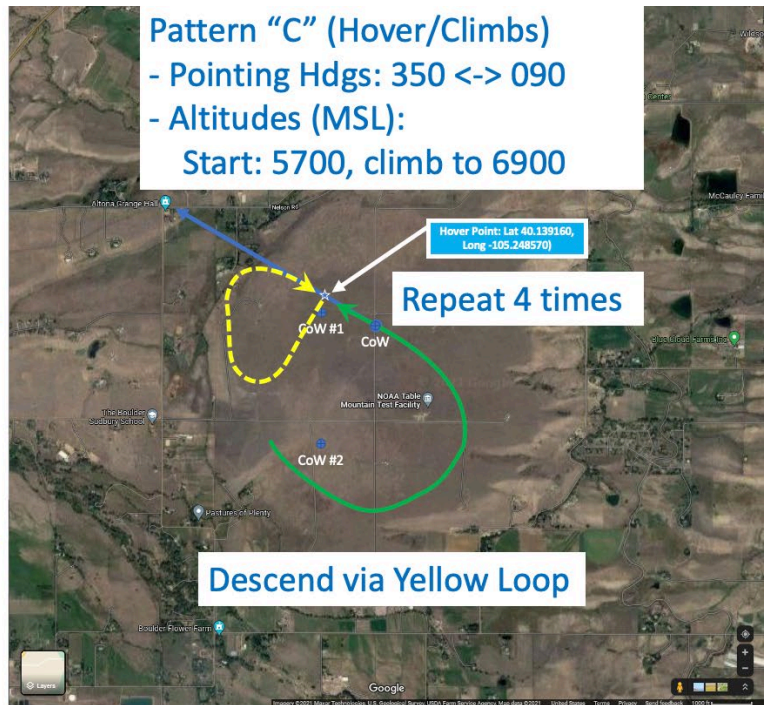
- Circle left (large radius) to reposition at Hover point; Climb to 6900 MSL



Pattern C
Hover
(1300 feet "down beam" of CoW)

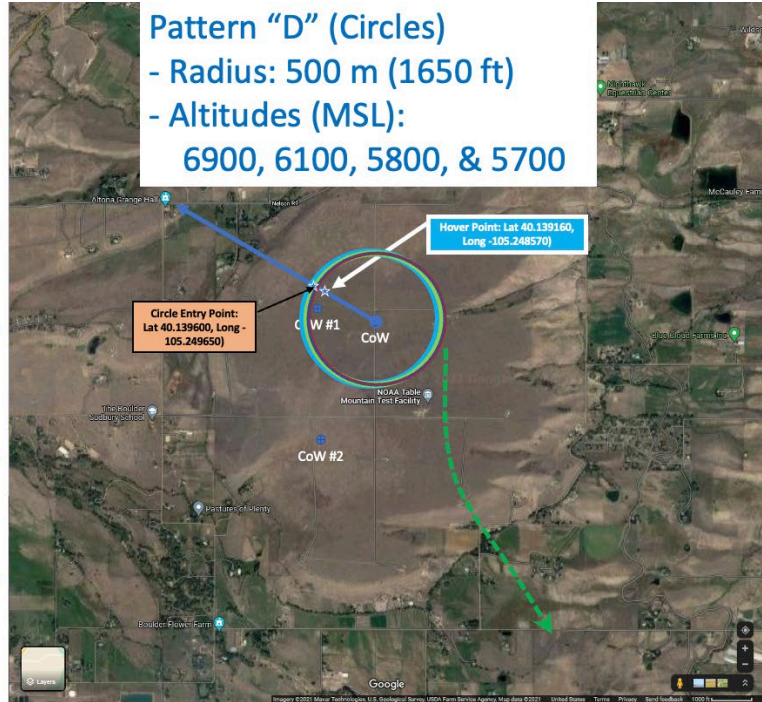
- Approach CoW from SE on heading of 300 degrees at 5700 MSL
- CoW Waypoint: Lat 40.137320, Long -105.244540
- Fly to Hover Point 1300 feet NW of CoW
- Hover Waypoint: Lat 40.139160, Long -105.248570
- Upon reaching Hover Point, orient facing NE (Ground speed: 0 knots)
- Stabilize at 5700 feet MSL for 30 seconds
- Ascend at 200 feet/minute to 6900 feet MSL
- Rotate to Heading 210
- Begin descent along 210 at 20 knots ground speed
- During descent, perform long radius right turn back around to Hover Pt.
- Stabilize at 5700 feet MSL for 30 seconds
- Ascend at 200 feet/minute to 6900 feet MSL
- Rotate to Heading 210
- Begin descent along 210 at 20 knots ground speed
- During descent, perform long radius right turn back around to Hover Pt.
- Stabilize at 5700 feet MSL for 30 seconds
- Ascend at 200 feet/minute to 6900 feet MSL
- Rotate to Heading 210
- Begin descent along 210 at 20 knots ground speed
- During descent, perform long radius right turn back around to Hover Pt.
- Stabilize at 5700 feet MSL for 30 seconds
- Ascend at 200 feet/minute to 6900 feet MSL
- Stabilize at 6900 feet MSL for 30 seconds

- After returning to 6900 feet MSL, maintain orientation and "slide" NW about 350 feet to Lat 40.139600, Long -105.249650 (Circle Entry Point)



Pattern D
Radius about a Fixed Point (the CoW)
(500 meters radius)

- Pointing NE, accelerate to 20 knots and begin flying a "radius from a fixed point" clockwise around the CoW. (Red Circle)
- Begin right-hand (CCW) "radius to a fixed point" at 500 meters radius around the CoW (Lat 40.137320, Long -105.244540). Complete 360 degrees (at 6900 feet MSL) following a clockwise path. Continue around another 180 degrees to the 120-degree azimuth relative to the CoW.
- Descend to 6100 MSL over the next 90 degrees of the circle. Continue right-hand (CW) "radius to a fixed point" at 500 meters radius around the CoW (Lat 40.137320, Long -105.244540). Complete 360 degrees (at 6100 feet MSL) following a clockwise path.
- Upon arriving at the 120-degree azimuth relative to the CoW location, descend to 5800 MSL over the next 90 degrees of the circle. Continue right-hand (CW) "radius to a fixed point" at 500 meters radius around the CoW (Lat 40.137320, Long -105.244540). Complete 360 degrees (at 5800 feet MSL) following a clockwise path.
- Upon arriving at the 120-degree azimuth relative to the CoW location, descend to 5700 MSL over the next 90 degrees of the circle. Continue right-hand (CW) "radius to a fixed point" at 500 meters radius around the CoW (Lat 40.137320, Long -105.244540). Complete 360 degrees (at 5700 feet MSL) following a clockwise path.
- Complete circle to 090 (south-bound), straighten out, mission complete
- Return to BJC



Pattern "D" (Circles)
 - Radius: 500 m (1650 ft)
 - Altitudes (MSL):
 6900, 6100, 5800, & 5700

Return-to-Base/Post-Landing Configuration

- Click on **"Stop"** and let **"Swept"** finish current run
- Laptop: Stays ON
- Field Fox: Stays ON
- Antenna Switch: Confirm switch in Position #2 (Monopole antenna)
- MATLAB: Confirm "Swept" is stopped (Start button back to "green")
- MATLAB: Confirm data is in file folder
- GPS time-sync: N/A
- GPS recorder (Garmin): Let run until back to Ken
- Once all processes have finished, power down equipment and dismantle

Latitude and Longitude Coordinates

- CoW
- *Runway (030/120) Entry and NE Waypoints*

CoW and Waypoint Coordinates

CoW #1:

- Degrees & Decimal Minutes (DMM): N 40 08.284, W 105 14.957
- Decimal Degrees (DD): Lat 40.138062, Long -105.249290

CoW #2:

- Degrees & Decimal Minutes (DMM): N 40 07.802, W 105 14.957
- Decimal Degrees (DD): Lat 40.130027, Long -105.249290

NRD (North end of N/S Road):

- Degrees & Decimal Minutes (DMM): N 40 08.284, W 105 14.672
- Decimal Degrees (DD): Lat 40.145006, Long -105.244530

SRD (South end of N/S Road):

- DMM: N 40 07.253, W105 14.672
- DD: Lat 40.120880, Long -105.244530

SOF (South End of S/N "over-flight" path):

- DMM: N 40 07.253, W105 14.957
- DD: Lat 40.120880, Long -105.249290

NOF (North End of S/N "over-flight" path):

- DMM: N 40 08.284, W105 14.957
- DD: Lat 40.145006, Long -105.249290

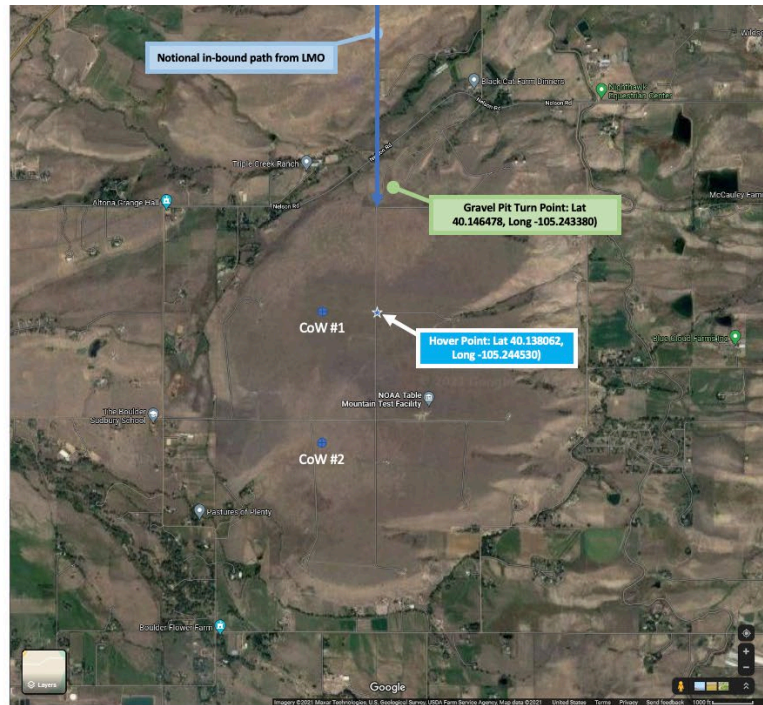
HOV (Hover point 1300 feet due east of CoW #1):

- DMM: N 40° 08.284', W 105° 14.672
- DD: Lat: 40.138062, Long: -105.244530

ENT8 (Entry Point to start the Figure 8s; ~350 feet east of HOV)

- DMM: N 40° 08.284', W 105° 14.543
- DD: Lat: 40.138062, Long: -105.243280

(Use Gravel Pit Turn Point (Lat 40.146478, Long -105.243380) as a waypoint)



APPENDIX B: FLIGHT CARDS FOR AIRBORNE SORTIES AROUND 5G RADIO 1 BASE STATIONS AT TABLE MOUNTAIN AND HILL AFB

Sortie Overview

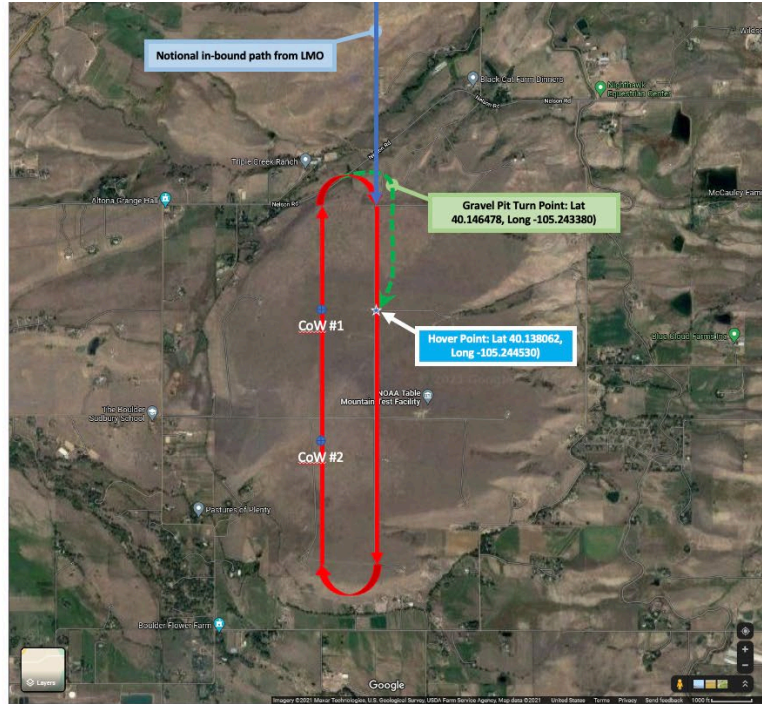
- **Objectives:**
 - Pilots: Sorted on flight paths as shown in following slides
 - ITS Flight Crew: Measurements with both CoW's RF turned ON
 - Risk Reduction Environment: Both CoWs ON, Freq: 3500–3600 MHz, BW: 100 MHz
 - Sortie summary is on next four slides
 - Complete success was achieved on all elements (summarized below and on next four slides)
- **Overview:**
 - Confirmed that altimeters (RADALT, Lidar Altimeter, and WAAS) worked as expected
 - Measured "RF-ON" signals (composite signal both CoWs radiating)
 - Straight and level at four (4) altitudes AGL (100, 200, 500, and 1300 feet AGL)
 - Helicopter hover over a fixed-point, stepped descent/ascent through nine (9) altitudes AGL
 - 'Figure 8' Flight Path = "Radius from a Fixed Point" around each CoW; radius = 500 meters, four altitudes (60, 100, 200, and 500 feet AGL)
 - Overhead "Traverse" Flight Path = South-to-North Flight over the top of both CoWs

Other Sortie Data Collected

- **Objectives:**
 - Pilots: Repeat Previous Flight Paths
 - ITS Flight Crew: Measurements of 3-dimensional 5G field strength
 - Both CoWs ON, Freq: 3500–3600 MHz
 - Vertical "slices" of CoW #1 beam pattern azimuthal angles (e.g., – bore-sight 10o, 20o, 30o, 50o, etc.)
 - Complete success was achieved on all elements (summarized below and on next four slides)
- **Overview:**
 - Confirmed altimeters (RADALT, Lidar Altimeter, and WAAS) worked as expected
 - Measurements TBD; Placeholder is to fly same patterns, or subset of patterns
 - Flew a set of vertical and horizontal cuts through the CoW radiation patterns, from 10 feet AGL to 1300 AGL
 - Completed exhaustive, aggressive probing of CoW patterns

North/South Straight & Level "Racetrack" (3rd Config, Both CoWs RF-ON, ~35 minutes)

- Enter Table Mountain (TM) from the north (Altitude: 5650 ft MSL)
- Align with TM's North/South (N/S) Road
- Enter pattern at the north end of the N/S road at 100 feet AGL
- N. End of N/S road: Lat 40.145006, Long -105.244530
- Fly south directly over N/S Road to south end.
- S. End of N/S Road: Lat 40.120880, Long -105.244530
- Execute right turn (west) to return north, parallel to N/S road, at 100 feet AGL (directly over CoWs, ~1300 feet west of N/S road)
- S. End of S/N "over-flight" path: (Lat 40.120880, Long -105.249290)
- N. End of S/N "over-flight" path: (Lat 40.145006, Long -105.249290) (Ground speed: 30 knots)
- Transition to 200 feet AGL at entry point north of N/S road
- Fly south directly over N/S Road to south end.
- Execute right turn (west) to return north, parallel to N/S road, at 200 feet AGL (directly over CoWs) (Ground speed: 30 knots)
- Transition to 500 feet AGL at entry point north of N/S road
- Fly south directly over N/S Road to south end.
- Execute right turn (west) to return north, parallel to N/S road, at 500 feet AGL (directly over CoWs) (Ground speed: 30 knots)
- Transition to 1300 feet AGL at entry point north of N/S road
- Fly south directly over N/S Road to south end.
- Execute right turn (west) to return north, parallel to N/S road, at 500 feet AGL (directly over CoWs) (Ground speed: 30 knots)
- After clearing north end of 1300 feet AGL run, right turn (east), looping 180 degrees clockwise to relocated to next pattern - a hover point (Lat: 40.138062, Long: -105.244530) 1300 feet east of CoW #1. (Dashed Green Line/Arrow). (Use Gravel Pit Turn Point (Lat 40.146478, Long -105.243380) as a waypoint)



Hover over a Fixed Point (1st Config, Baseline, RF-off, ~10 minutes)

- Continue south from Gravel Pit Turn Point to Hover Point (Green Line/Arrow)
- Maintain altitude at 1300 feet AGL (approx. 6800 feet MSL)
- Upon reaching Hover Point, orient facing west (Ground speed: 0 knots)
- Hover Point: Lat 40.138062, Long -105.244530
- Hover at 1300 feet AGL for 30 seconds
- Descend to 500 Feet AGL, hover at 500 feet AGL for 30 seconds
- Descend to 200 Feet AGL, hover at 200 feet AGL for 30 seconds
- Descend to 150 Feet AGL, hover at 150 feet AGL for 30 seconds
- Descend to 80 Feet AGL, hover at 80 feet AGL for 30 seconds
- Descend to 50 Feet AGL, hover at 50 feet AGL for 30 seconds
- Descend to 40 Feet AGL, hover at 40 feet AGL for 30 seconds
- Descend to 30 Feet AGL, hover at 30 feet AGL for 30 seconds
- Descend to 20 Feet AGL, hover at 20 feet AGL for 30 seconds
- Descend to 10 Feet AGL, hover at 10 feet AGL for 30 seconds
- Ascend to 20 Feet AGL, hover at 20 feet AGL for 30 seconds
- Ascend to 30 Feet AGL, hover at 30 feet AGL for 30 seconds
- Ascend to 40 Feet AGL, hover at 40 feet AGL for 30 seconds
- Ascend to 50 Feet AGL, hover at 50 feet AGL for 30 seconds
- Ascend to 80 Feet AGL, hover at 80 feet AGL for 30 seconds
- Ascend to 150 Feet AGL, hover at 150 feet AGL for 30 seconds
- Ascend to 200 Feet AGL, hover at 200 feet AGL for 30 seconds
- Ascend to 500 Feet AGL, hover at 500 feet AGL for 30 seconds
- After returning to 500 feet AGL, orient south and "slide" east 350 feet to Lat 40.138062, Long -105.243280
- Pointing south, accelerate to enter next pattern (radius from a fixed point) at east side of "Figure 8" patterns. (Dashed Green Line)

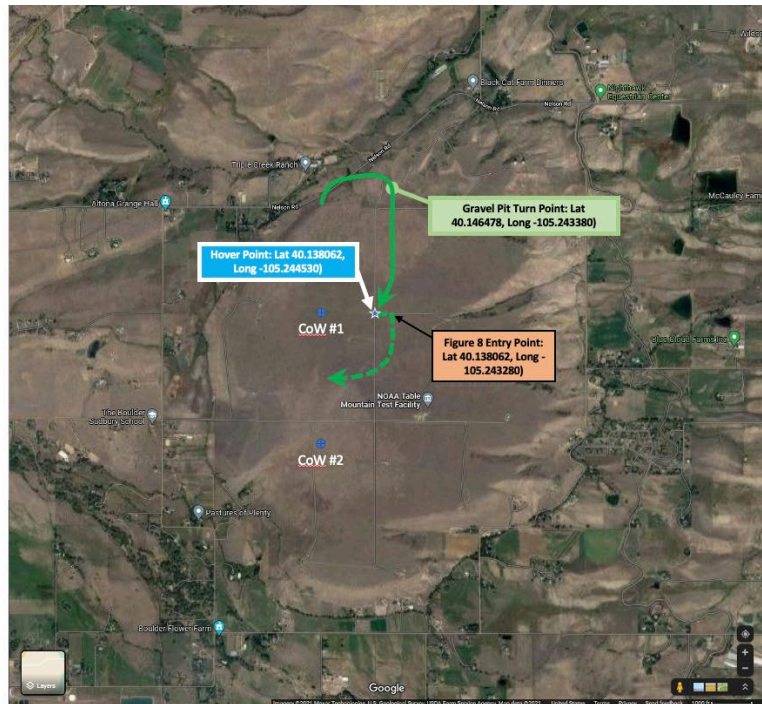


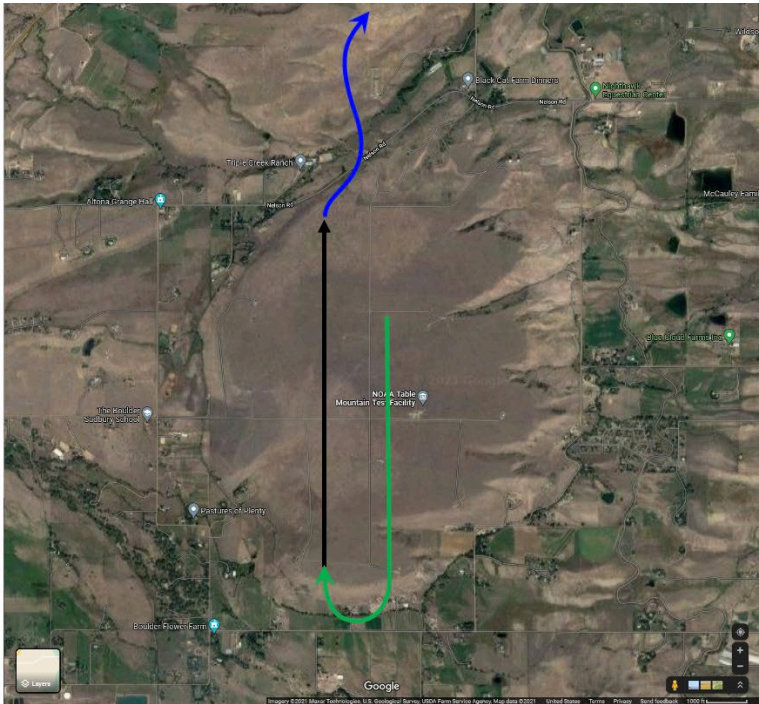
**Figure-8s around the CoWs
(3rd Config, Both CoWs RF-ON, ~45 minutes)**

- Starting point: hover over Lat 40.138062, Long -105.243280 (500 meters east of CoW#1) at 500 feet AGL, pointing south. Ground speed: 20 knots
- Begin right-hand (CCW) "radius to a fixed point" at 500 meters radius around north CoW (Lat 40.138062, Long -105.249290). Complete 360 degrees (at 500 feet AGL) following a clockwise path. Continue 450 degrees.
- When facing west, execute left turn (south) to fly "radius to a fixed point" at 500 meters radius around south CoW (Lat 40.130027, Long -105.249290). Complete 360 degrees (at 500 feet AGL).
- When facing west, execute right turn (north) to fly "radius to a fixed point" at 500 meters radius around north CoW (Lat 40.138062, Long -105.249290) AND descend to 200 feet AGL. Complete 360 degrees (at 200 feet AGL).
- When facing west, execute left turn (south) to fly "radius to a fixed point" at 500 meters radius around CoW #2 (Lat 40.130027, Long -105.249290). Complete 360 degrees (at 200 feet AGL).
- When facing west, execute right turn (north) to fly "radius to a fixed point" at 500 meters radius around south CoW (Lat 40.130027, Long -105.249290). Complete 360 degrees (at 100 feet AGL).
- When facing west, execute left turn (south) to fly "radius to a fixed point" at 500 meters radius around north CoW (Lat 40.138062, Long -105.249290) AND descend to 60 feet AGL. Complete 360 degrees (at 60 feet AGL).
- When facing west, execute left turn (south) to fly "radius to a fixed point" at 500 meters radius around south CoW (Lat 40.130027, Long -105.249290). Complete 360 degrees (at 60 feet AGL).
- When facing west, execute right turn (north) to fly "radius to a fixed point" at 500 meters radius around north CoW (Lat 40.138062, Long -105.249290). Complete 270 degrees (at 60 feet AGL).
- Exit pattern heading south (parallel to N/S Road), ascend to 200 feet AGL to south end of TM. Turn right (west) to a northbound over-flight of CoWs. (Green Dashed Line) Entry point (Lat 40.120880, Long -105.249290)



**Over-fly CoWs at 200 feet AGL
(3rd Config, Both CoWs RF-ON, ~5 minutes)**

- Enter pattern at 200 feet AGL from the south, going north. Entry point (Lat 40.120880, Long -105.249290)
- Fly north directly over CoWs to the north end of TM at 200 feet AGL. (Black Line) (Ground speed: 20 knots)
- Depart TM for LMO (transition to preferred flight altitude)



APPENDIX C: Measured Emission Spectra of Lower C-band Base Stations (Radio 1)

The emission spectra of Radio 1 (5G n78 band) were measured the same way, and with the same measurement system, as the n77-band emission spectra of Radios 2 through 4 shown in Figures 46 through 48. The only differences for the Radio 1 measurements were the distance from the base station MIMO array to the RSMS (80 meters for Radio 1 instead of 161 meters for Radios 2 through 4); and that the Radio 1 base station had no associated 5G Core or UEs. Lacking a Core and UEs, the Radio 1 spectra were measured with the base station's MIMO array running in a pre-programmed maintenance mode. The two spectra shown here (Figures C-1 and C-2) were measured with base station antenna beams that were down-tilted directly into the RSMS' position. The two spectra differ in emission bandwidths (20 MHz versus 100 MHz). Structural comparison to the spectra of Figures 46 through 48 shows the notable observation that the lack of a Core and UEs had no apparent effect on the Radio 1 base station emission spectra.

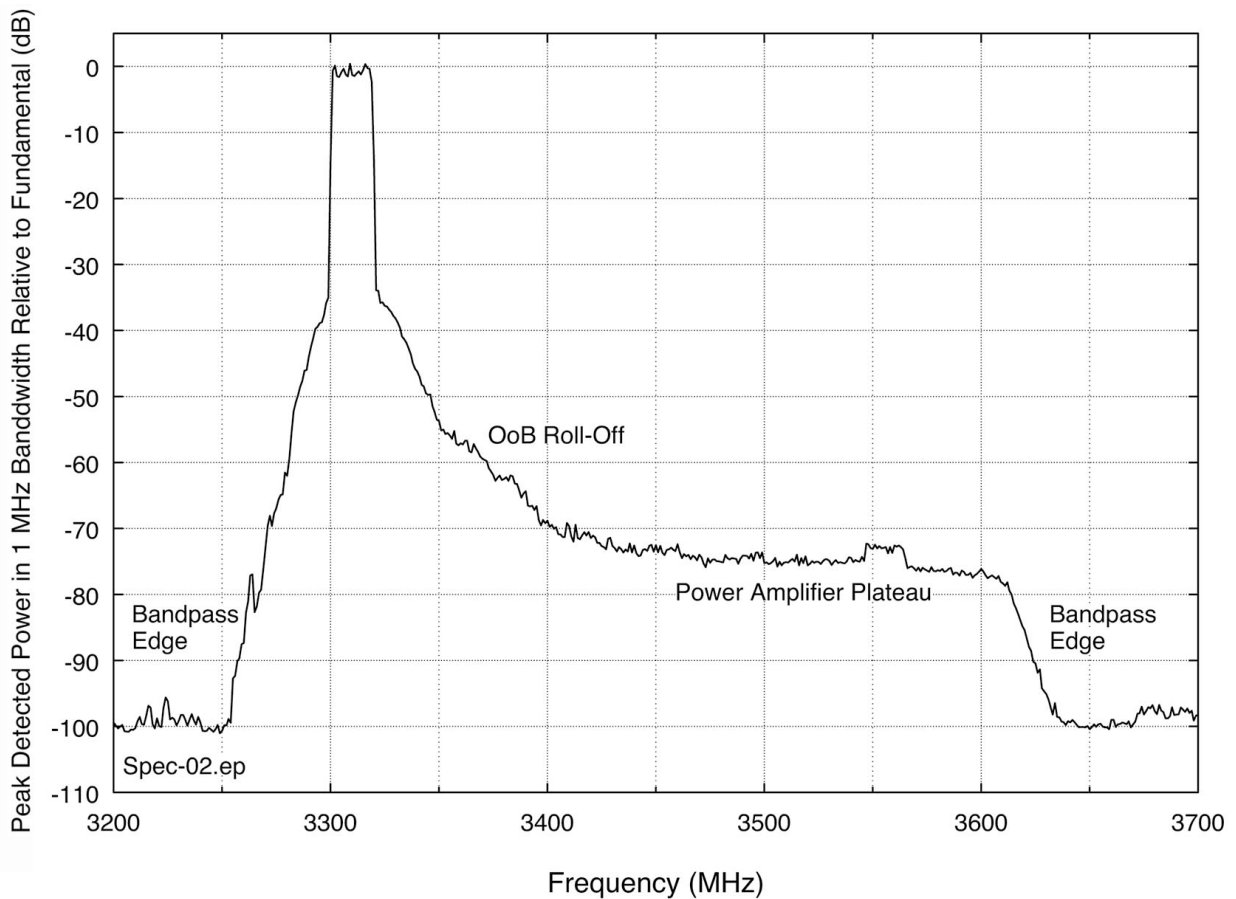


Figure C-1. Measured emission spectrum of lower C-band 5G base station transmitter Radio 1 running with a 20 MHz channel bandwidth. Note that power is plotted in 1 MHz measurement bandwidth, relative to the center-frequency emission level, which was itself at +77.5 dBm EIRP in its main beam.

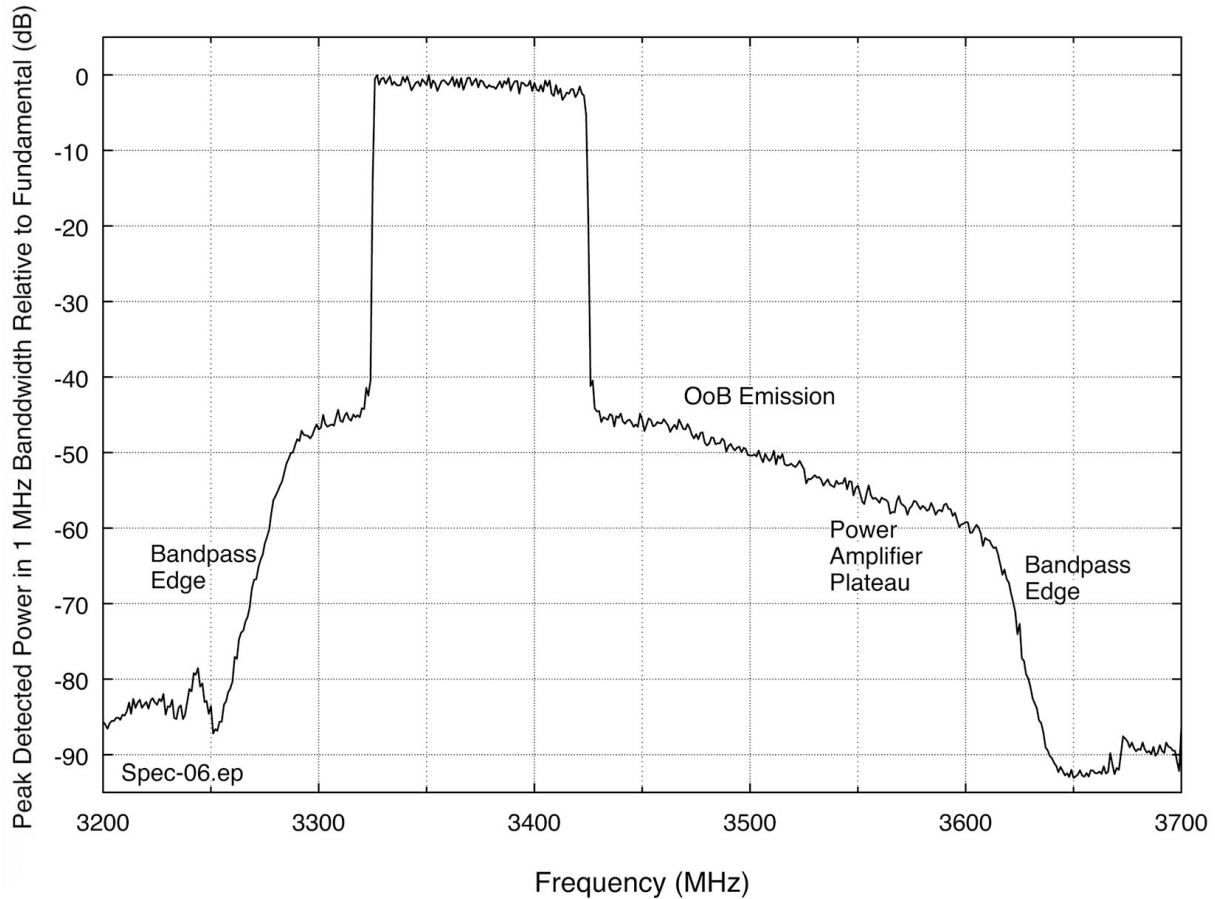


Figure C-2. Measured emission spectrum of lower C-band 5G base station transmitter Radio 1 running with a 100 MHz channel bandwidth. Power is plotted in 1 MHz measurement bandwidth, relative to the center-frequency emission level, which was itself at +77.5 dBm EIRP in its main beam.

Comparing these spectra to upper C-band Radios 2 through 4 (US 5G n77, Figures 46 through 48), the Radio 1 spectra have the same structural characteristics. These include: OoB emissions adjacent to the desired emission, rolling into a wideband transmitter PA, and a distinct pair of bandpass edges at the lower and upper ends of the assigned band.

We have found these characteristics to be held in common among WiMAX, LTE, and 5G base stations. See, for example, measured 2 GHz band and 3 GHz band LTE and WiMAX emission spectra in [13] and [29], respectively.

APPENDIX D: SOLUTIONS FOR EXAMPLE APPLICATIONS FROM SECTION 11

D.1 Example 1 Solution

Referring to Figures 54 and 55, the maximum 5G EIRP that occurred in a circular orbit at 200 feet AGL around the 5G MIMO array of Radio 2, at 275° azimuth (roughly co-linear with the main beam power that was directed downward, below the orbit, toward the south end of the line of UEs) was +48 dBm/MHz (per Figure 54) and +68 dBm in the channel's full bandwidth (per Figure 55, consistent with the radio's 100 MHz channel width).

For *Part (a)*, from Table 14, the full-channel transmitter EIRP of Radio 2 was +77.5 dBm. The radio's power per megahertz was 1/100 as much (because of a 100 MHz channel bandwidth), which was therefore +57.5 dBm. The maximum airborne power on that circular orbit was therefore **9.5 dB less than in the transmitter's main beam that was aimed toward the UEs on the ground** (in both units, because a decibel is a decibel).

For *Part (b)* the orbit height was 200 ft AGL = 61 m. The MIMO array's height AGL was 10 m, as mentioned in multiple places throughout this report. The orbital radius, from a quick check of Google Earth *vis a vis* Figure 55, was about 630 m. Therefore the elevation angle of the orbit from the MIMO array was $\tan^{-1} (61-10)/630 = 4.6^\circ$ **upward from the MIMO array**.

For *Part (c)* the operative equation is:

$$(FS, \text{dBmV/m}) = (EIRP, \text{dBm}) + 104.7 - 20\log(d, \text{meters})$$

where the EIRPs are +50 dBm/MHz and +70 dBm total power. The equation gives field strengths of +134.7 dBm/MHz at 10 m and +74.7 dBm/MHz at 10 km. The corresponding total-power levels are those numbers plus 20 dB. The graph looks like Figure D-1.

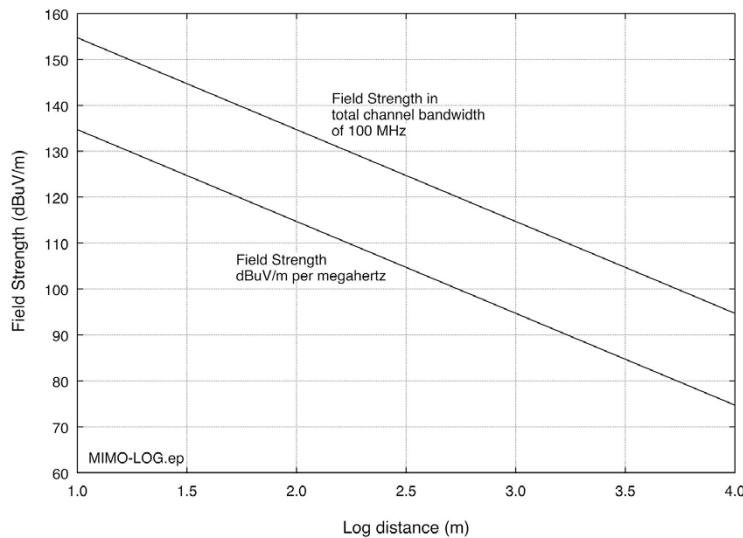


Figure D-1. Example graph of spatial field strength as a function of distance from a 5G transmitter antenna.

D.2 Example 2 Solution

For *Part (a)*, find the radalt receiver antenna gains at the appropriate frequencies and directions from Figures 12 and 13. These are +5 dBi at 45° at 4300 MHz and -5 dBi at 45° at 3950 MHz.

Next, note from Table 12 that the 5G emission level at 4300 MHz is at least -106 dB down from the intentional radiated power.

We are looking for the *relative distance ratio* between the 5G intentional-emissions interference case and the 5G unwanted-emissions interference case. Arithmetical differences between decibel (log) quantities are ratios. So we solve this ratio problem by taking decibel differences.

The decibel difference between the 5G on-tuned power interference threshold and the 5G unwanted-power interference threshold is between the stated bench test levels of -35 dBm/MHz and -85 dBm/MHz. This difference is 50 dB, in favor of a *larger* limiting distance for the 5G unwanted emissions at 4300 MHz (because the hypothetical receiver is more sensitive to 5G emissions on its tuned frequency than it is to 5G intentional emissions outside its allocated band).

The decibel antenna gains in the two different bands are +5 dBi at 4300 MHz versus -5 dBi at 3950 MHz, for a total gain difference of 10 dB. This difference is also in favor of a *larger* limiting distance at 4300 MHz (because that's where the radalt receiver antenna performs better).

The total, overall difference is: -106 dB (for spectrum) + 50 dB (for the relative difference in radalt receiver sensitivity to interference in the two bands) + 10 dB (for the better radalt receiver antenna gain performance at 4300 MHz). This is an overall difference of -46 dB, the negative sign meaning that the overall result favors a *smaller* limiting distance being at 4300 MHz (because the -106 dB spectrum result at 4300 MHz has swamped the higher radalt receiver sensitivities and gains at 4300 MHz).

In free space, every distance-doubling equals -6 dB (by r^2), so the value of -46 dB equates to a distance ratio of $2^{-46/6} = 2^{-7.7} = 1/203$. That is, the 4300 MHz limiting distance for this hypothetical transmitter would be 1/203 of the limiting distance due to 5G emissions at 3950 MHz.

We conclude, based on this fictitious example, that the limiting EMC issue for this hypothetical radalt with its hypothetical antenna gain (but with the *real* measured Radio 2 spectrum) would be the *intentional* 5G emissions at 3950 MHz, and *not* the unwanted 5G emissions at 4200 to 4400 MHz. The intentional 5G emissions would in this case need to be de-coupled from the radalt receiver by installing more effective front-end RF filtering on the radalt receiver.

For *Part (b)* of the problem, the solution is obtained by solving the third equation for distance:

$$20\log(d, \text{meters}) = (EIRP, \text{dBm}) + (G_{rx}, \text{dBi}) + 27.5 - 20\log(f, \text{MHz}) - (P_{rx}, \text{dBm})$$

And then we insert the given numbers: $20\log(d) = +35 - 5 + 27.5 - 72 - (-35) = 20.5$.

Dividing by 20 and taking the antilog gives the distance at 3950 MHz at 45° above the horizon: 11 meters. We emphasize again that this is an artificially generated problem, only intended to show *how* this analysis can be done. (Distances would be larger in the 5G main beam.)

For Part (c), we repeat the Part (b) solution with the regulatory limit of EIRP = +62 dBm/MHz:

$$20\log(d) = +62 - 5 + 27.5 - 72 - (-35) = 47.5.$$

Dividing by 20 and taking the antilog gives us a distance of $d = 237$ meters (780 ft) for this hypothetical example case.

D.3 Example 3 Solution

From Figure 52, the EIRP at 30° above the MIMO array's horizon is +20 dBm/MHz. Solving the operative equation:

$$(FS, dBmV/m) = (EIRP, dBm) + 104.7 - 20\log(d, meters)$$

for distance and inserting the numbers gives $20\log(d) = 20 + 104.7 - 75 = 49.7$.

Dividing by 20 and taking the antilog gives a distance of 305 meters (1000 ft) in this made-up example computation.

D.4 Example 4 Solution

For Part (a): From Figure 13, the radalt receiver antenna gain at 30° below its horizon (corresponding to radiation at 30° above the MIMO array's horizontal) is about -3 dBi at 3900 MHz. Using the equation

$$20\log(d, meters) = (EIRP, dBm) + (G_{rx}, dBi) + 27.5 - 20\log(f, MHz) - (P_{rx}, dBm)$$

We get: $20\log(d) = +46 + (-5) + 27.5 - 71.8 - (-43) = 39.7$.

This gives $d = 97$ m (~320 ft) 30° above the MIMO array's horizontal.

For Part (b), the solution is double that distance, because a distance factor of two in free space equates to a decibel change of 6 dB. So with an additional 6 dB margin we get 194 m (~640 ft) at 30° above the MIMO array's horizontal.

For Part (c), the distance is longer than the original number by $2^{10/6} \cong 3.2$ times farther away. So the distance with the 10 dB margin becomes about 310 m (~1000 ft) at 30° above the MIMO array's horizontal.

BIBLIOGRAPHIC DATA SHEET

1. PUBLICATION NO. TR-22-562		2. Government Accession No.		3. Recipient's Accession No.	
4. TITLE AND SUBTITLE Measurements of 5G New Radio Spectral and Spatial Power Emissions for Radar Altimeter Interference Analysis				5. Publication Date October 2022	
				6. Performing Organization Code NTIA	
7. AUTHOR(S) Frank Sanders, Kenneth R. Calahan, Geoffrey A. Sanders, and Savio Tran				9. Project/Task/Work Unit No. 6942000-300	
8. PERFORMING ORGANIZATION NAME AND ADDRESS Institute for Telecommunication Sciences National Telecommunications & Information Administration U.S. Department of Commerce 325 Broadway Boulder, CO 80305				10. Contract/Grant Number.	
				12. Type of Report and Period Covered	
11. Sponsoring Organization Name and Address Office of the Secretary of Defense for Research and Engineering (OUSD/R&E) 3600 Defense Pentagon, Room 3B854 Washington DC 20301-3600					
14. SUPPLEMENTARY NOTES					
15. ABSTRACT (A 200-word or less factual summary of most significant information. If document includes a significant bibliography or literature survey, mention it here.) Introduction of Fifth Generation New Radio (5G NR) systems in the US between 3700 and 3980 MHz has raised concerns about electromagnetic compatibility with airborne radar altimeter (radalt) receivers operating between 4200 and 4400 MHz. This report describes work performed by the Department of Commerce's Institute for Telecommunication Sciences (ITS) for the Joint Interagency 5G Radar Altimeter Interference (JI-FRAI) Quick Reaction Testing (QRT) program to address these concerns. Two collected data sets are described: radiated wideband, wide dynamic range 5G base station emission spectra; and three-dimensional radiation patterns around 5G base station antennas. The emission spectra show effective filtering that reduces out-of-band (OoB) 5G emissions in the radalt band by as much as -106 dB below the 5G fundamental, for an upper-bounded OoB 5G power density not exceeding -48.5 dBm/MHz when maximum measurement range was achieved. The 5G radiation patterns show significantly less power in the sky than in 5G main beams directed groundward, especially at array zeniths. These data can be used for receivers whose flight paths carry them laterally past, and even directly above, 5G base stations. Finally, we have documented a near-far effect in airborne measurements on pairs of 5G transmitters. This causes the nearer transmitters' emissions to be dominant in receivers. When a single 5G transmitter is near a receiver, that single transmitter's emitted power will tend to dominate over the cumulative, aggregated emissions from more-distant, aggregated 5G transmitters.					
16. Key Words (Alphabetical order, separated by semicolons) 5G; 5G NR; 5G emissions; 5G electromagnetic compatibility; 5G EMC; 5G emission spectrum; 5G radiation; 5G spectrum; airborne radar altimeter interference; airborne radio altimeter interference; JI-FRAI; MIMO antenna radiation patterns; radar altimeters; radio altimeters; radalts; radalt electromagnetic compatibility; radalt EMC; radalt interference; radalt receiver interference; radalt spectrum					
17. AVAILABILITY STATEMENT <input checked="" type="checkbox"/> UNLIMITED. <input type="checkbox"/> FOR OFFICIAL DISTRIBUTION.		18. Security Class. (This report) Unclassified		20. Number of pages 151	
		19. Security Class. (This page) Unclassified		21. Price: n/a	

NTIA FORMAL PUBLICATION SERIES

NTIA MONOGRAPH (MG)

A scholarly, professionally oriented publication dealing with state-of-the-art research or an authoritative treatment of a broad area. Expected to have long-lasting value.

NTIA SPECIAL PUBLICATION (SP)

Conference proceedings, bibliographies, selected speeches, course and instructional materials, directories, and major studies mandated by Congress.

NTIA REPORT (TR)

Important contributions to existing knowledge of less breadth than a monograph, such as results of completed projects and major activities.

JOINT NTIA/OTHER-AGENCY REPORT (JR)

This report receives both local NTIA and other agency review. Both agencies' logos and report series numbering appear on the cover.

NTIA SOFTWARE & DATA PRODUCTS (SD)

Software such as programs, test data, and sound/video files. This series can be used to transfer technology to U.S. industry.

NTIA HANDBOOK (HB)

Information pertaining to technical procedures, reference and data guides, and formal user's manuals that are expected to be pertinent for a long time.

NTIA TECHNICAL MEMORANDUM (TM)

Technical information typically of less breadth than an NTIA Report. The series includes data, preliminary project results, and information for a specific, limited audience.

For information about NTIA publications, contact the NTIA/ITS Technical Publications Office at 325 Broadway, Boulder, CO, 80305 Tel. (303) 497-3572 or e-mail ITSinfo@ntia.gov.